1.0 Cover page

Solicitation and Call for Proposals

(AFC 518)

TECHNOLOGY DEVELOPMENT GRANTS

Alpha Foundation for The Improvement of Mine safety and Health

Final Technical Report

Project Title:	A Hybrid Geopolymer-Biopolymer Cementitious Material for Pumpable Roof Support
Grant Number:	AFC 518-24
Organization Name:	The University of Arizona
Principal Investigator:	Lianyang Zhang, Ph.D., P.E.
Graduate Student:	Arash Nikvar-Hassani
Contact Information:	Email: lyzhang@email.arizona.edu Phone: 520-626-0532
Period of Performance:	August 2017 – July 2019

Acknowledgement/Disclaimer
This study was sponsored by the Alpha Foundation for the Improvement of Mine Safety and Health, Inc. (ALPHA FOUNDATION). The views, opinions and recommendations expressed herein are solely those of the authors and do not imply any endorsement by the ALPHA FOUNDATION, its Directors and staff.

Table of Contents

2.0 Executive Summary

Effective roof support is critical to prevent ground falls and ground fall accidents. Among the different roof support techniques, pumpable roof supports have advantages over other roof support systems and have been increasingly used in underground mines. The major constituent of a pumpable roof support system is the cementitious material such as calcium-sulfo-aluminate (CSA) cement and Portland cement currently used in practice. However, these conventional cementitious materials cannot achieve the normally conflicting responses such as high stiffness, high peak strength and large yield strength required for effective roof support. To enhance the performance of pumpable roof supports, there is an urgent need to develop unconventional cementitious materials that possess such normally conflicting properties.

Therefore, this proof-of-concept project aims to develop an innovative hybrid geopolymer-biopolymer (GP-BP) cementitious material with high stiffness, high peak strength and large yield strength for effective pumpable roof support. For effective field applications, the new hybrid cementitious material is designed to be a mixture of two separate pumpable streams: stream 1 composed of class F fly ash (FA), cement kiln dust (CKD), superplasticizer (SP) and water, and stream 2 containing sodium hydroxide (SH), sodium silicate (SS), BP and water. The FA is the aluminosilicate source for the GP. The CKD and SP are for adjusting and controlling the setting time of the hybrid cementitious material and the pumpability of stream 1, respectively. The SH is the alkali activator for GP formation and the SS is for adjusting the Si/Al ratio and providing additional Na^+ cations for charge balancing. The BP (carrageenan, gellun gum or cellulose nanofibers) is used to enhance the mechanical behavior of the GP. When the two pumpable streams stay alone, they remain as a slurry and a solution, respectively, and can be easily handled and transported. When they are mixed together, a GP-BP composite cementitious material is formed.

The study systematically investigated the effect of the various factors on pumpability, stetting time, and mechanical properties of the hybrid cementitious material. In this regard, the two streams were designed and prepared so that hybrid cementitious material specimens at different water to solid (W/S) ratios and containing different amount of CKD, SP and BP were produced. A series of pumpability, setting time, unconfined compression and split tensile tests were conducted on the specimens at different conditions. SEM imaging and EDX and XRD analyses were also performed to study the microstructure and chemical composition of the specimens.

The results indicate that the W/S ratio and the amount of CKD, SP and BP all have important effect on the pumpability, setting time and/or mechanical properties of the hybrid cementitious material. By properly adjusting the relative amount of the various components, the new hybrid cementitious material can be tailored and used in practice at different conditions to achieve optimum performance. As a preliminary demonstration and validation, small (152.4 mm diameter and 304.8 mm height) bagged specimens were produced using polyester fabric and tested, which show much higher peak and residual strength than the currently used crib bagged pumpable roof supports.

With the systematic laboratory investigations and the small-scale demonstration and validation, the newly developed technology for producing hybrid cementitious material to enhance pumpable roof support is completely ready for prototype development. In this regard, a prototype development plan has been prepared to advance the proof-of-concept to a fully functional working prototype, including large-scale demonstration and validation tests at the University of Arizona (UA) and the NIOSH Mine Roof Simulator Laboratory, collaborations with Jennmar Corporation and mine companies, and working closely with the technology transfer department at UA.

3.0 Concept Formulation and Mission Statement

All underground mines can subject to ground falls, which imposes a significant hazard to underground mine workers. According to NIOSH (2017), ground fall accidents in underground mines cause 8 to 10 fatalities and more than 800 injuries per year, representing about 30% of the fatal accidents and 15% of the injuries that occur each year in underground mines. In addition, there are nearly 2000 reportable non-injury falls every year. Therefore, it is critical to build appropriate roof supports so that ground falls and ground fall accidents are prevented.

There are mainly two types of roof support systems, the intrinsic support systems and the standing support systems (Peng 2000; Mark and Barczak 2000; Esterhuizen and Berk 2016). Roof bolts are the best example of intrinsic supports. Roof bolts are loaded as the roof deforms, and they interact with the rock to reduce bed separation by confinement much as reinforcing steel does with concrete. Standing supports, such as cribs, posts, or longwall shields, develop loads in response to the convergence between the roof and floor.

Of the different standing roof support systems, the Can support is probably the most widely used in the United States for longwall tailgate applications. The Can provides a high-deformation support system and consistent loading through as much as 50% strain, thereby improving ground support in many applications. Despite the success of the Can support, it has some limitations. For example, the Can support must be topped off with something, usually timbers, to establish roof contact, which typically "softens" the support response due to the contact compatibility of the timbers with the uneven roof, requiring wedges or small pieces of wood to provide a tight fit and allowing roof convergence to occur with minimal resistance. Moreover, if multiple timber layers are placed on top of the Can, there may be hinge points that can also reduce the overall stability of the support system.

Pumpable roof supports have been increasingly used in mines to support the roof due to their advantages over other bulky standing roof support systems. As the name implies, a pumpable roof support is installed in place where roof support is required using a pumpable material, usually a cementitious grout. Typically, a two-component material is pumped from a remote location, generally, but not always, above ground, into a containment bag (crab bag) to form the support. The unfilled support bags are transported into the mine in a collapsed configuration, minimizing the transportation needs to the installation site. During installation, the bags are secured to the mine roof and then extended down to the floor. The solidified grout material captured by the containment bag provides a full support column between the mine roof and floor and thus eliminates the need for secondary materials such as wooden wedges to be installed to establish proper roof contact (Fig. 1). Pumpable roof supports minimize the underground material handling efforts, thereby reducing the risk of injuries historically associated with in-mine support construction. On-site fabrication also facilitates application of the pumpable roof support in areas that are inaccessible to transportation equipment such as scoops or rail cars, making it ideal for many bleeder applications.

Pumpable roof support systems have evolved during the last two decades, with improvements to bag design and several variations of cementitious material aiming to optimize the performance of the support system. Currently, there are two basic types of cementitious material used for construction of pumpable roof supports: calcium-sulfo-aluminate (CSA) cement and Portland cement. The CSA cement generally has a faster setup and strength gain through ettringite formation but is much more expensive (Barczak and Tadolini 2008; Cheng et al. 2015). It has also

been observed that some Portland cement-based materials severely decompose (lose structural integrity) when exposed to air (Batchler 2017).

Fig. 1: (a) Crib bag installed in a collapsed configuration to the mine roof; and (b) Crab bag after filling with cementitious material (from Jennmar 2013; NTI 2019)

To compare the differences between supports filled with the two different cements, NIOSH investigators have tested a large number of pumpable roof supports in the NIOSH Mine Roof Simulator Laboratory (Batchler 2017). The results show that the CSA cement is significantly stiffer compared to the Portland cement. The results also show that both types of cements decrease in strength and begin to crack as the load increases, which often occurs with brittle cements. Up to a point, the bag contains the cracking material and the support can still bear significant weight. Eventually, however, an increasing load will cause the surrounding bag to tear, which leads to a rapid decrease in the pumpable support's strength. Accordingly, the NIOSH investigators plan to study supports using less brittle materials than the two commonly used cements.

Considerable research has been done on the development of new cementitious materials in order to enhance the performance of pumpable roof supports and lower the related cost. For example, Hird (2011) developed a combined cementitious grout mixture consisting of two pumpable grout streams, one composed of ordinary Portland cement and water and the other containing pulverized fuel ash (PFA) (as the pozzalan material), an inorganic gelling agent and water. The two pumpable grout streams are transported separately and simultaneously along separate pipelines to a point of application wherein the separate grout streams are combined into a grout mixture. The overall water-to-solids ratio of the combined grout mixture is between 1:1 and 1:2 by weight. The ratio of Portland cement to PFA is between 1:1 and 1:2, and the gelling agent is 1%-8% by weight of the combined grout mixture.

Researchers have also developed high-water and fast-setting cement (HWFSC) composed of high bauxite cement with gypsum, lime, compounding retarder, retarding agents, and activators (Cheng et al. 2015). These compounds facilitate the mixture of HWFSC with large quantity of water. The HWFSC also has two pumpable grout streams (or parts). A single part just acts as a slurry and does not transform into a gel within 24 hours. When the two streams are combined together, however, they cure rapidly (within a few minutes).

Despite the considerable research conducted so far, the conventional cementitious materials currently used in practice still cannot achieve the normally conflicting properties of high load stiffness, high peak strength and large yield strength because they are produced based on essentially the same mechanisms (Barczak and Tadolini 2008; Cheng et al. 2015; Batchler 2017). To significantly enhance the performance of pumpable roof supports, an unconventional superior performance cementitious material should be developed based on different mechanisms.

Therefore, the overall **goal** of this research is to develop a novel hybrid cementitious material with superior performance through effective fusion of geopolymer and biopolymer. Geopolymer is a relatively new class of material produced by chemical dissolution and subsequent recondensation of aluminosilicates to form an amorphous three-dimensional framework structure (Davidovits 1988, 1991, 1994; Duxson et al. 2007; Dimas et al. 2009; Majidi 2009):

$$M_n[-(SiO_2)_z\text{-}AlO_2\text{-}]_n \quad (1)$$

where M is an alkali cation (Na^+ or K^+), n the degree of polymerization, and z the number of SiO_2 monomer units per AlO_2. Different raw materials that contain reactive or amorphous silica and alumina can be used for geopolymer production, including metakaolin, fly ash, mine waste, red mud, and blast furnace slag, among others. Noteworthy is that most of these raw materials are industrial wastes or byproducts, and hence significant environmental and economic benefits are expected if the waste-based geopolymer is used in practice.

Geopolymer not only possesses mechanical performance comparable to conventional Portland cement in many applications, but carries additional advantages such as rapid strength gain, high strength, low shrinkage, high thermal resistance, excellent acid resistance, and significantly reduced energy usage and greenhouse gas emissions. The unique characteristics of geopolymer render it an ideal alternative to conventional Portland cement for sustainable development. Therefore, geopolymer is selected as the starting material in this proof-of-concept project to develop a new cementitious material for pumpable roof supports.

However, geopolymer also exhibits brittle behavior with low tensile strength, ductility, and fracture toughness. To overcome the limitations, a variety of fibers made of steel, carbon, glass, polyvinyl alcohol (PVA), basalt, and wollastonite have been researched as reinforcement in geopolymer matrix. For example, Giancaspro et al. (2003) and Zhao et al. (2007) respectively studied geopolymer composites made by infiltrating coarse and fine stainless steel meshes with geopolymer resins, which showed metal-like tensile yield behavior (instead of abrupt brittle failure) with "yield strength" significantly higher than that of the pure geopolymer. Bernal et al. (2010) investigated the reinforcement of blast furnace slag-based geopolymer concrete using steel fibers, resulting in substantial improvement in both the tensile and flexural strengths but reduced the compressive strength. Carbon fibers have also been examined as a reinforcement extensively (Hammell et al. 1999; Comrie and Kriven 2004; Lin et al. 2008, 2009). Results showed that inclusion of carbon fibers significantly improves the resulting composite's tensile strength, ductility, and fracture toughness. Hammell et al. (1999) and Pernica et al. (2010) also studied glass fiber as a reinforcement and observed improvement in flexural strength. Zhang et al. (2006, 2008) used PVA fiber to reinforce fly ash/metakaolin-based geopolymer and achieved much improved flexural strength and reasonable toughness. Sun and Wu (2008) also used PVA fiber to modify the brittle properties of fly ash-based geopolymer. Dias and Thaumaturgo (2005) and Li and Xu (2009) investigated the mechanical properties of basalt fiber-improved geopolymer concrete.

Incorporation of different fibers into geopolymer can substantially improve the tensile strength, ductility, and fracture toughness, but decreases the compressive strength in many cases. These fibers usually have a cross-sectional dimension at the micro/macro-scale and can certainly increase the tensile strength, ductility, and fracture toughness by bridging micro/macro cracks, transferring loads, and delaying the development of micro/macro cracks. However, cracks initiate at nanoscale where micro/macro-fibers do not function effectively (Metaxa et al. 2010). Also, the micro/macro-fibers will adversely affect the constructability of the cementitious material for pumpable roof supports.

Reinforcement of geopolymer using nanofibers, such as carbon nanotubes (CNTs) and carbon nanofibers (CNFs), has also been investigated. For example, MacKenzie and Bolton (2009) investigated the effect of incorporating single-wall CNTs on the electrical and mechanical properties of geopolymer. Although nanofibers possess excellent physical and mechanical properties, such as exceptional high strength, stiffness, and aspect ratio, they have a major drawback for matrix reinforcement: poor dispersion, usually due to van der Waals attractions and other surface forces, resulting in a particular difficulty to produce uniformly dispersed fibers within the matrix (Xie et al. 2005; Moniruzzaman and Winey 2006; Ashton 2009; Yazdanbakhsh et al. 2010). To truly achieve nanoscale fiber reinforcement in a composite, it is critical to achieve uniform dispersion (i.e., no aggregation) of nanofibers within the matrix (Xie et al. 2005; Grobert 2007; Ashton 2009). Therefore, research is required to develop new methods for reinforcing geopolymer at the nanoscale.

Many naturally occurring materials, such as bone, tooth dentin, and nacre (abalone shell), although made of relatively weak constituents, exhibit superior mechanical properties: high compressive strength, fracture toughness, ductility, and flexibility (Mann 2001; Yu and Chen 2009; Espinosa et al. 2009; Dunlop and Fratzl 2010), owing to their distinct micro/nano structure organized in a hierarchical fashion and the inclusion of a small fraction of biopolymer. They are hybrid inorganic/organic composites formed via mineralization of the inorganic components mediated by organic biopolymer that bind inorganic micro/nano crystals and regulate their orientation and size. Such a nano-scale mediation is found to be the main reason why the naturally formed hybrid composites possess superior mechanical properties. For example, bone is made of inorganic carbonate hydroxyapatite crystals and organic collagen fibers with a hierarchical structure that leads to high fracture toughness and flexibility (Loong et al. 2000; Ritchie et al. 2009). Nacre, often called mother-of-pearl, despite containing 95 vol.% $CaCO_3$ in the form of aragonite, can have a work of fracture of up to 3,000 times greater than that of pure aragonite. This surprisingly high toughness results from the arrangement of the aragonite in staggered layers of interlocking platelets, each platelet being surrounded by the remaining 5 vol.% of protein biopolymer. When a crack travels through nacre, it has to pass around but not through the platelets. The much increased crack path length leads to an enhanced work of fracture (Jackson et al. 1986, 1990; Meyers et al. 2008; Pokroy et al. 2009). The porous shell of diatom is produced from silica precipitation of silicic acid and intracellular polymerization within a specialized vesicle onto a biopolymer matrix consisting of long-chain polyamines and polycationic polypeptides (Milligan and Morel 2002; Sumper 2002).

Recent years have also seen significant research on the fabrication of new composites by mimicking the bio-formation process in nature (Ortiz and Boyce 2008; Yu and Chen 2009; Espinosa et al. 2009; Dunlop and Fratzl 2010). For example, inspired by nacre, Tang et al. (2003) fabricated a multilayered composite by layering montmorillonite clay platelets (C) and poly

(diallydimethylammonium) chloride polyelectrolytes (P) through sequential layer-by-layer adsorption, resulting in a $(P/C)_n$ multilayer composite (n = the number of bilayers). Sen et al. (2007) synthesized a homogeneous composite consisting of carbonate apatite and chitosan in the presence of citric acid using an in-situ precipitation method. Their results show that the carbonate apatite particulates were distributed homogeneously within the chitosan hydrogel network and the resulting composite had excellent mechanical properties. Murugan and Ramakrishna (2004), Rusu et al. (2005), Zhang et al. (2005), and Cai et al. (2009) also used chitosan to produce inorganic/ organic composites.

Based on the discussion above, it can be concluded that geopolymer is an ideal starting material for producing cost effective and high-performance cementitious material for pumpable roof supports. Moreover, the geopolymer can be further enhanced with biopolymer by mimicking the unique bio-formation process in nature. Specifically, the interpenetrating cross-linked network of biopolymer macromolecules can serve as a binding and toughening agent in the geopolymer matrix, leading to improvement in mechanical properties of the geopolymer-biopolymer composite cementitious material. Therefore, this proof-of-concept project develops the nonconventional hybrid cementitious material through effective fusion of geopolymer and biopolymer.

Because the main source material for the geopolymer is fly ash, a waste from coal power plants, the new cementitious material is more cost effective than the existing ones used in practice. Utilization of fly ash as the source material also reduces the monetary and environmental costs related to disposal and management of fly ash. Moreover, geopolymer can be produced at ambient or slightly elevated temperatures and thus consumes much less energy and releases much less greenhouse gasses than the conventional Portland cement.

4.0 Proof-of-Concept Technology Components

A pumpable roof support contains the crib bag and the cured cementitious material pumped into it (see Fig. 1). For a pumpable roof support to provide effective and safe support to the roof, the key is to ensure that the support system, especially the cementitious material, to have high load stiffness, high peak strength and large yield strength. However, the conventional cementitious materials currently used in practice cannot achieve these normally conflicting properties because they are produced based on essentially the same mechanisms. To significantly enhance the performance of pumpable roof supports, an unconventional cementitious grout material that possesses the normally conflicting properties of high load stiffness, high peak strength and large yield strength needs to be developed.

Therefore, this proof-of-concept project focuses on the cementitious material with a design strategy to develop a completely new paradigm for producing an unconventional cementitious material. To do that, we do not use or simply modify the conventional cements. Instead, we develop the new cementitious material based on a novel cement called geopolymer. Geopolymer is a class of material that is formed by chemical dissolution and subsequent recondensation of aluminosilicates to form an amorphous three-dimensional framework structure. Geopolymer has many advantages compared to the conventional Portland cement, including rapid strength gain, high strength, low shrinkage, high thermal resistance, excellent acid resistance, and significantly reduced energy usage and greenhouse gas emissions. Like the conventional Portland cement, however, geopolymer also tends to be brittle with low tensile strength, ductility, and fracture toughness. Much research has been conducted to overcome these limitations by using various micro/macro fibers and even nanofibers such as carbon nanotubes to reinforce the geopolymer, and these techniques have achieved certain success in improving the geopolymer's mechanical performance. However, because cracks emanate at the nanoscale, the micro/macro fibers fail to restrain crack initiation effectively. Because of the difficulty in achieving uniform dispersion of insoluble nanofibers such as carbon nanotubes (CNTs) and carbon nanofibers (CNFs) in the geopolymer matrix, a promising nano-scale enhancement technique that does not use nanofibers but can hinder and suppress the initiation and propagation of cracks at the nano-scale at the very beginning phase has yet to be developed.

This proof-of-concept project develops an innovative hybrid composite cementitious material through effective fusion of geopolymer and biopolymer. The overall hypothesis is that the interpenetrating cross-linked network of biopolymer macromolecules will serve as a binding and toughening agent in the geopolymer matrix, leading to the improvement in mechanical properties. The hybrid geopolymer-biopolymer cementitious material not only inherits the many advantages of geopolymer itself but also shows enhanced mechanical properties such as higher tensile strength, fracture toughness and ductility due to the incorporation of biopolymer.

The new hybrid cementitious material is a mixture of two pumpable grout streams, stream 1 composed of class F fly ash and water, and stream 2 containing sodium hydroxide, sodium silicate, biopolymer and water. The fly ash is the aluminosilicate source for the geopolymer. The sodium hydroxide acts as the alkali activator required for geopolymer formation. The sodium silicate is used to adjust the Si/Al ratio and provide additional Na^+ cations for charge balancing. The biopolymer is used to enhance the mechanical behavior of geopolymer through formation of an interpenetrating cross-linked network binding and toughening the geopolymer matrix. Cement kiln dust (CKD) and superplasticizer are also included in stream 1 for adjusting and controlling the setting time of the hybrid cementitious material and the pumpability of stream 1, respectively.

When the two grout streams stay alone, they remain as a slurry and a solution, respectively, and can be easily handled and transported. When the two streams are mixed together and pumped into a crib bag (Fig. 2), a hybrid geopolymer-biopolymer cementitious material is formed. The new cementitious material can be tailored and used in practice at different conditions to achieve the optimum performance by simply adjusting the relative amount of the different components.

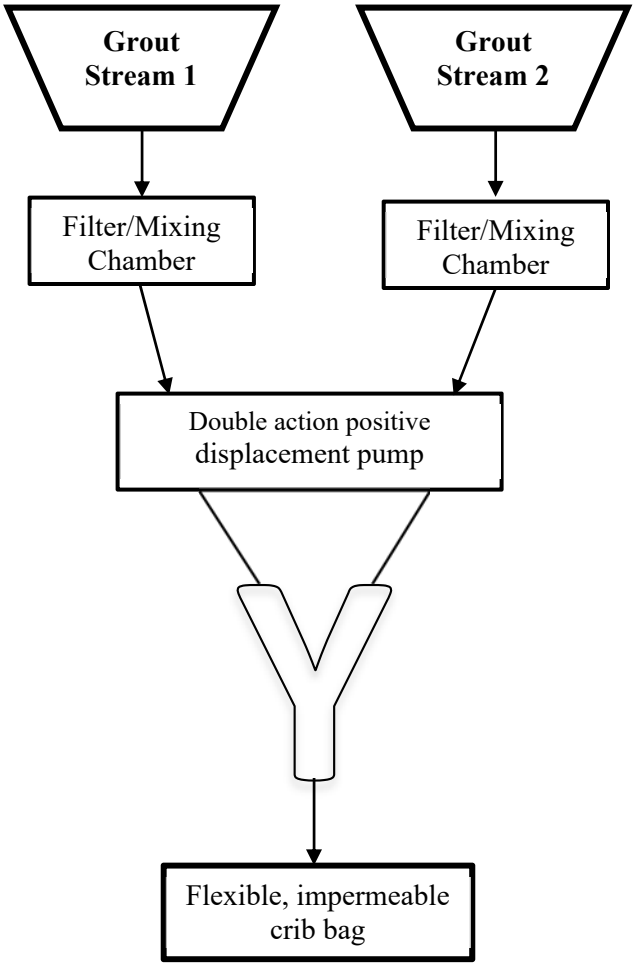

Fig. 2: Flow chart of two grout streams pumped to a crib bag to form pumpable roof support.

In summary, this proof-of-concept project is at the component level and focuses on the development of a hybrid geopolymer-biopolymer cementitious material with superior performance for effective pumpable roof support. To achieve the overall goal, a synergistic experimental program has been carried out to study the pumpability, setting time, mechanical properties, microstructure, and chemical composition of the hybrid cementitious material at different conditions.

5.0 Proof-of-Concept Evaluation

This section describes the proof-of-concept protocol for evaluating the hybrid cementitious material at different conditions in detail, including the source materials and supplements used in this study, the test configurations and conditions, and the detailed results.

5.1 Materials

The materials used in this investigation include class F fly ash (FA), cement kiln dust (CKD), reagent grade 98% sodium hydroxide (SH) (NaOH), sodium silicate (SS) (Na_2SiO_3) solution, superplasticizer (SP), biopolymer (BP), and de-ionized water. The FA is the aluminosilicate source for geopolymer and was provided by Salt River Materials Group (SRMG) in Phoenix, Arizona. The CKD is a high calcium content material selected as an accelerator to control the setting time of the hybrid cementitious material and was obtained from CalPortland company in Tucson, Arizona. Table 1 shows the chemical composition of the FA and CKD from XRF analysis. The FA contains mainly silica and alumina while the CKD contains mainly calcite and alumina. Fig. 3 shows the particle size distribution curves of the FA and CKD. The mean particle sizes of FA and CKD are respectively around 13.5 μm and 36.2 μm with 88.0% and 36.0% particles passing No. 200 (75 μm) sieve. Fig. 4 shows the SEM micrographs of the FA and CKD. The FA particles are spherical while the CKD particles have irregular shapes. Fig. 5 shows the XRD patterns of the FA and CKD powders. The FA is mainly constituted of crystalline materials including mullite and quartz. An amorphous phase with a broad band registered between about 15° and 40° is also clear. For CKD, the dominant crystalline phases are CaO, $CaCO_3$ and SiO_2. The peaks corresponding to $Ca(OH)_2$ are broad indicative of semi-crystalline structure of this phase. The NaOH is an alkali activator required for geopolymer formation and was purchased from Hill Brothers Chemical in Tucson, Arizona. The sodium silicate solution (SiO_2 = 29%, Na_2O = 8%, and H_2O = 63%) is for adjusting the Si/Al ratio and providing additional Na^+ cations for charge balancing, and was purchased from Fisher Scientific in Pittsburgh, Pennsylvania. The superplasticizer is for controlling the pumpability of the first stream and was supplied by Sika corporation, California. Three different biopolymers, carrageenan (CAR), gellun gum (GEL), and cellulose nanofibers (CNF), were selected in this project to enhance the mechanical behavior of geopolymer. CAR is a natural high molecular weight polysaccharide produced from seaweed plant (Li and Zhang 2016). GEL is a high molecular weight polysaccharide fermented from Sphingomonas elodea microbes (Chang et al. 2017). CNF is isolated from wood following a combined TEMPO oxidation and homogenization process (Bhalerao et al., 2015; Jiao et al., 2016; Sun et al., 2017). The CAR and GEL were obtained from TIC GUMS, Maryland and the CNF was obtained from Sappi company, Netherland.

Table 1 Chemical composition of FA and CKD.

Chemical compound	SiO_2	Al_2O_3	CaO	Fe_2O_3	MgO	Na_2O	SO_3	K_2O
FA (%)	57.50	29.30	6.00	2.95	1.36	2.60	NA	NA
CKD (%)	11.0	3.90	42.0	2.0	3.6	NA	NA	0.6

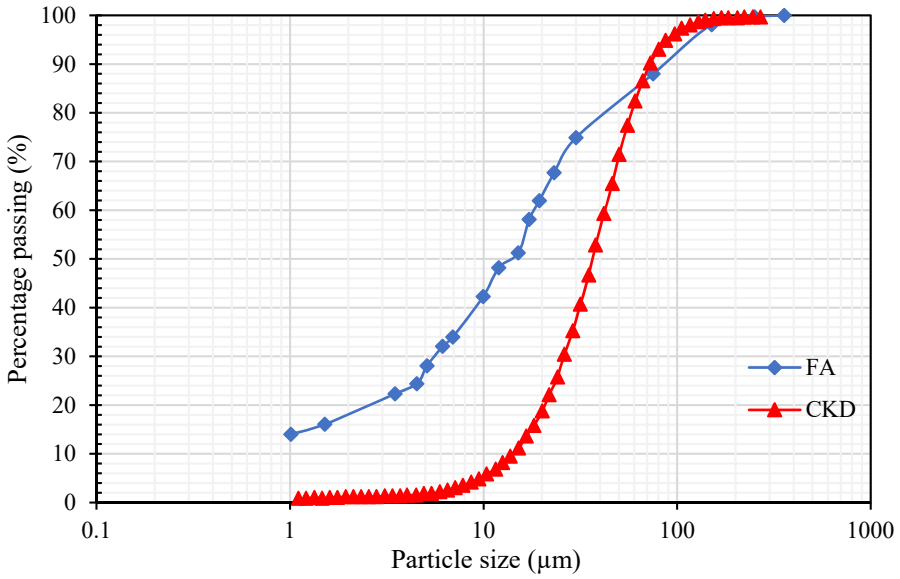

Fig. 3: Particle size distribution curves of FA and CKD.

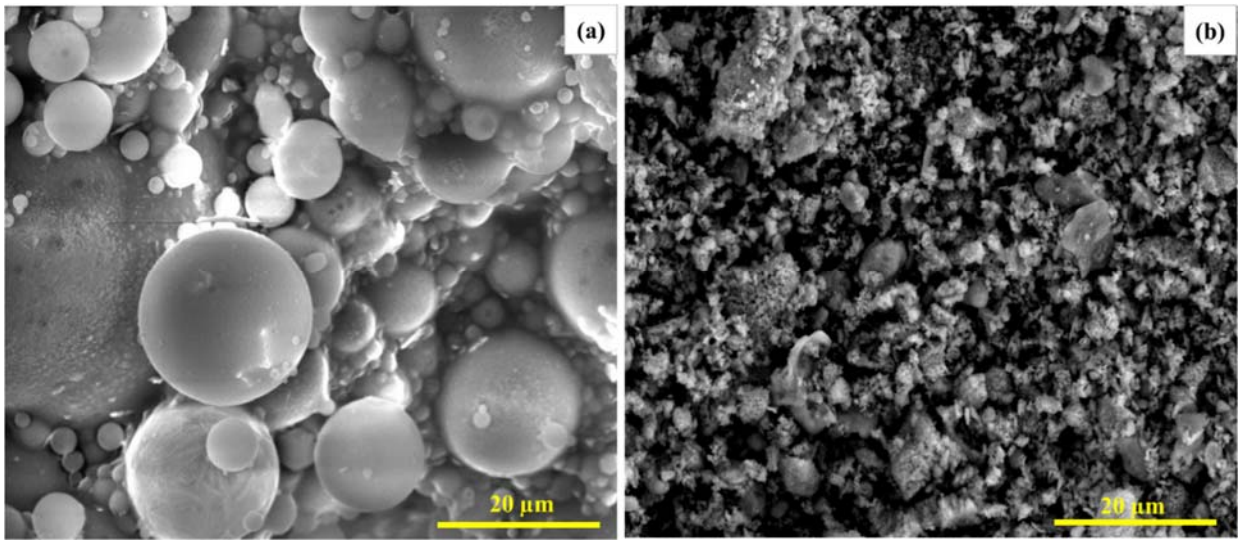

Fig. 4: SEM micrographs of (a) FA; and (b) CKD.

5.2 Methods

The hybrid geopolymer-biopolymer cementitious material is designed to be a mixture of two separate pumpable grout streams, stream 1 composed of class F fly ash and water, and stream 2 containing sodium hydroxide, sodium silicate, BP, and water. CKD and superplasticizer were also included in stream 1 to adjust and control the setting time of the hybrid cementitious material and the pumpability of stream 1, respectively. To prepare the first stream, FA and CKD were mixed for 5 min and then water and superplasticizer were added while mixing continued to obtain a homogeneous slurry. To prepare the second stream, NaOH pellets were dissolved in sodium silicate solution and water and left at room temperature to cool down and then BP was added and thoroughly mixed in the solution.

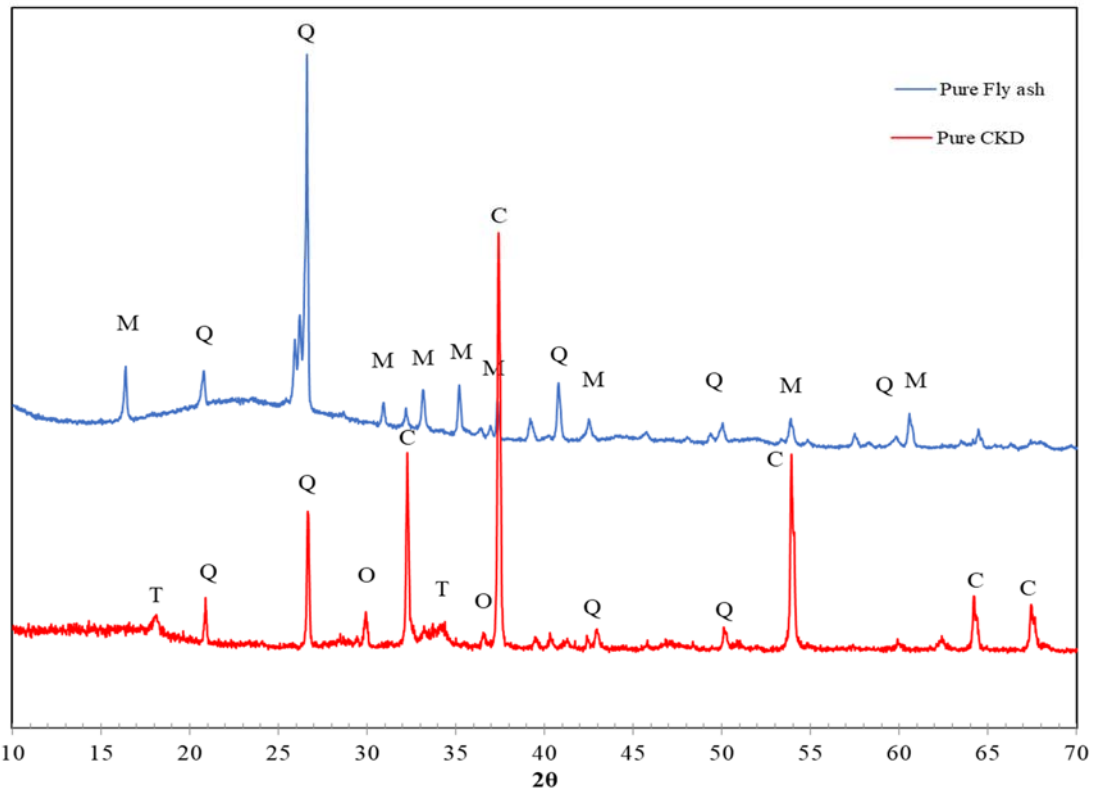

Fig. 5: XRD pattern of FA and CKD powders [M: $Al_{2.272}O_{4.864}Si_{0.728}$, Q: SiO_2, C: CaO, O: $CaCO_3$, T: $Ca(OH)_2$].

After both streams were ready, they were mixed and the fresh paste was cast into cylindrical molds (25.4 mm in diameter and 50.8 mm in height). The molds were then placed in an oven for curing at a specified temperature (25, 35, or 45 °C). After 24 hours, the specimens were removed from the molds, sealed with plastic bags and put back in the oven for curing until the test day.

The study systematically investigated the effect of the various factors on pumpability, setting time, and mechanical properties of the hybrid cementitious material. In this regard, the two streams were designed and prepared so that the final paste at different water to solid (W/S) ratios (0.50, 0.55, and 0.60) and containing different amount of CKD, superplasticizer and BP were produced. Specifically, the CKD was added in stream 1 at a dosage of 0, 10, 15, and 20 wt.% of FA, respectively. The superplasticizer was also included in stream 1 at a dosage of 1 and 2 wt.% of FA+CKD, respectively. The BP was included in stream 2 at a dosage of 0, 0.1, 0.2, 0.3, 0.4 and 0.5 wt.% of FA+CKD, respectively. Based on the previous studies on geopolymer in our laboratory, an SH concentration of 5 M and a SS/SH ratio of 1 were selected for stream 2.

The pumpability (rheological) tests on the two streams were performed using a coaxial cylinder viscometer Fann model 35A (Fig. 6). To this end, the slurry (stream 1) or solution (stream 2) is confined between two concentric cylinders with different radius and one of these cylinders rotates at a certain speed. In this model, the slurry or solution contained in the large radius recipient is sheared between the outer sleeve (rotor) and the inner cylinder (bob) which is attached to a torque measuring device. The torque required to rotate the bob is measured by the viscometer. By changing the rotational speed (3, 6, 100, 200, 300, and 600 rpm), several viscosity ranges can be

measured. This test was performed according to the instructions provided in API Spec 10 (API 1990). In this regard, the first torque reading was done after one minute of shearing the slurry or solution at the highest rotational speed and then the rotational speed was sequentially decreased to the lower rotational velocity and the corresponding torque reading was done after 20 seconds of rotation at each rotational speed. The equations and constants provided by the viscometer manufacturer were used for calculating the viscosity.

Fig. 6: Viscometer Fann model 35A.

The setting time tests were carried out on the hybrid cementitious material with a Vicat apparatus (Fig. 7) following ASTM C191 (2013). Specifically, the fresh paste after mixing the two streams was cast in Vicat molds and put in an oven at a specified temperature (25, 35, or 45 °C). The molds were taken out of the oven at an interval of 10 min and tested to measure the initial and final setting times. The initial setting time is defined as the period between the time when the two streams are mixed and the time at which the needle can just penetrate the paste to a depth of 25 mm. The final setting time is the period between the time when the two streams are mixed and the time at which the needle fails to make a complete circular impression on the paste surface.

The unconfined compressive tests were conducted following ASTM C39/C39M (2016) and using an ELE Tri Flex 2 loading machine (Fig. 8) at a constant loading rate of 0.1 mm/min to measure the peak unconfined compressive strength (UCS), residual UCS and Young's modulus of the hybrid cementitious material specimens at different conditions. The end surfaces of the specimens were polished to ascertain that they are flat and parallel. Three specimens were tested at each condition.

The split tensile tests (Fig. 9) were performed following ASTM D3967 (2008) and using the same ELE Tri Flex 2 loading machine (Fig. 8a) at a constant loading rate of 0.1 mm/min to measure the tensile strength of the hybrid cementitious material specimens at different conditions. Three specimens were tested at each condition.

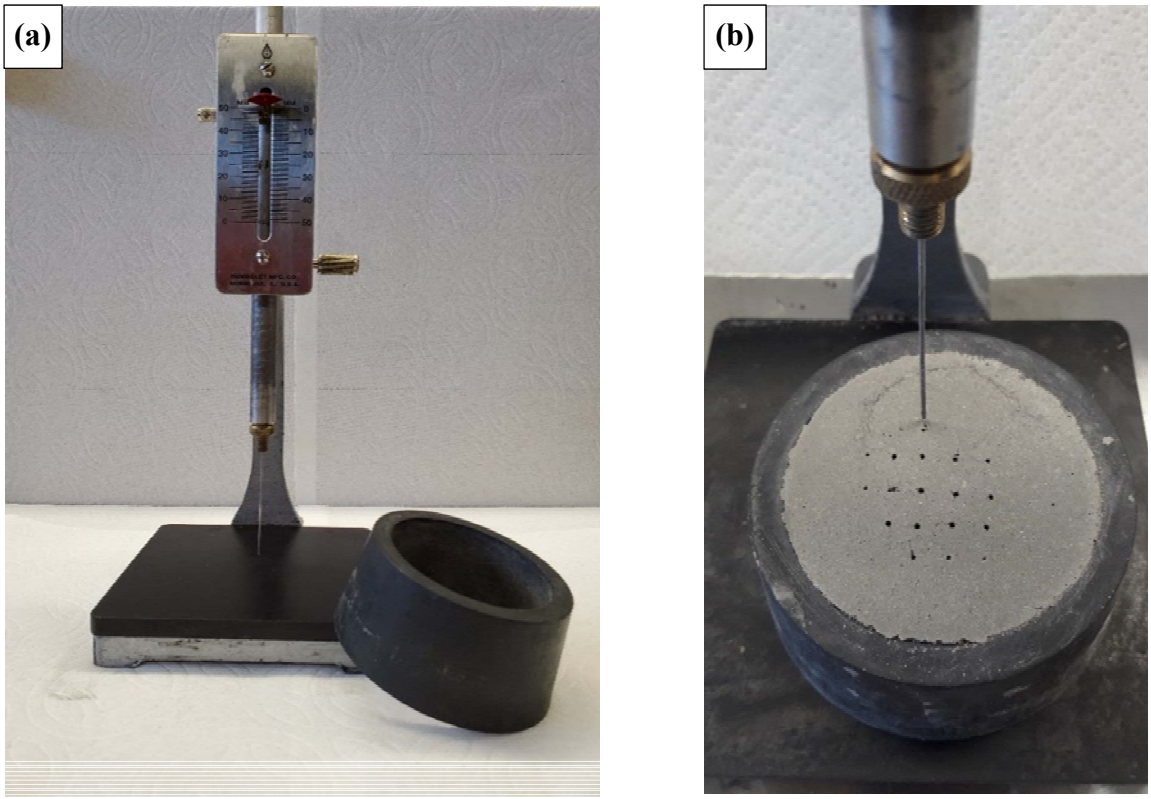

Fig. 7: (a) Vicat apparatus; and (b) Vicat mold filled with cementitious material paste after test.

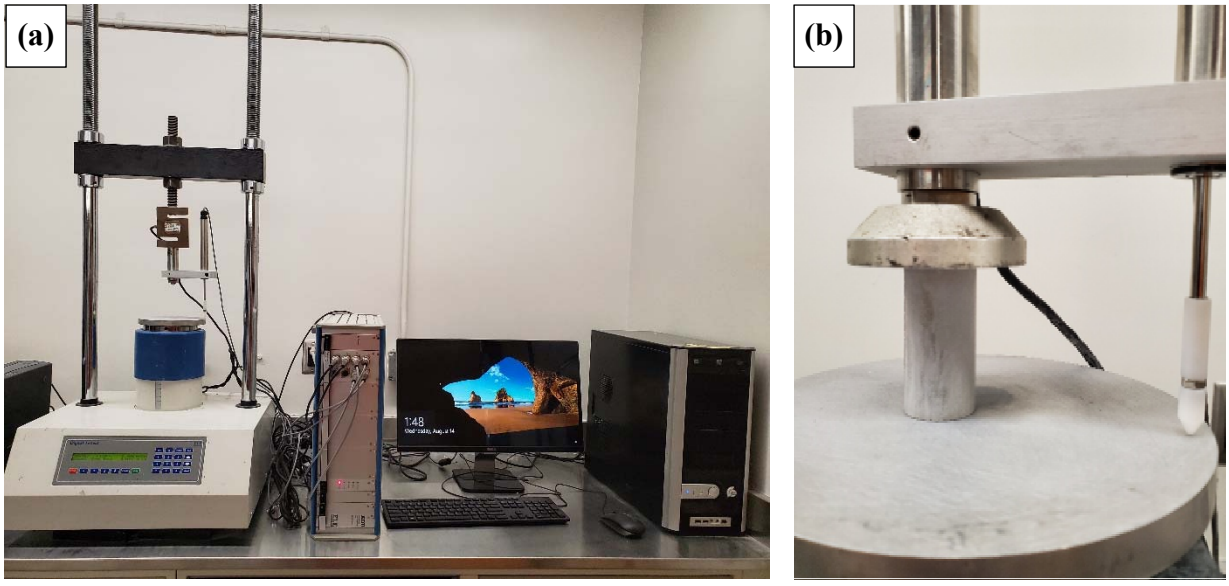

Fig. 8: (a) ELE Tri Flex 2 loading machine; and (b) Specimen under unconfined compressive loading.

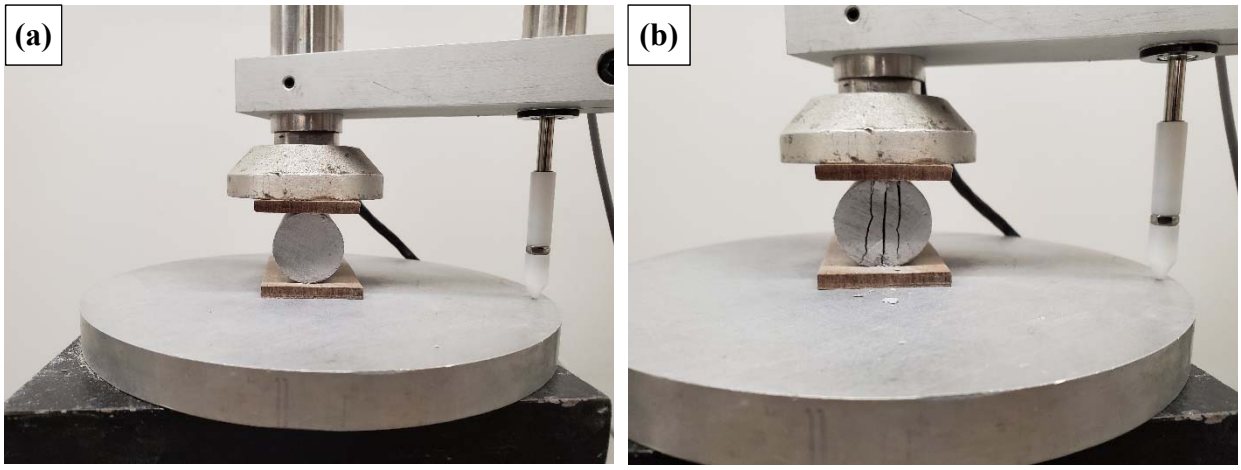

Fig. 9: Split tensile test performed on a specimen: (a) under loading; and (b) after failure.

SEM imaging was performed in the SE conventional mode using the FEI INSPEC-S50/Thermo-Fisher Noran 6 microscope to investigate the microstructure of the hybrid cementitious material at different conditions. The fresh surface of failed specimens from the unconfined compression tests, without polishing to keep the fractured surface "un-contaminated", were used for the SEM imaging. Along with the SEM, EDX was also conducted to evaluate the elemental composition of the different components in the hybrid cementitious material.

To study the phase composition of the starting materials and the changes occurred due to geopolymeric and pozzolanic reactions, XRD analysis was carried out. The XRD analysis was performed with a Scintag XDS 2000 PTS diffractometer using Cu Kα radiation, at 2.00° min ranging from 10.00° to 70.00° with 0.600 s count time.

5.3 Results and discussion

5.3.1 Pumpability

For field applications, the first and second streams need to be pumped within different pipes for a long distance to the underground mine site. Therefore, it is important to ensure that the two streams have good pumpability. Stream 1 as a slurry is a mixture of FA, CKD, SP and water. The pumpability of stream 1 was investigated through viscosity tests by considering W/S = 0.50, 0.55, and 0.60 and SP dosage of 0, 1 and 2 wt.% of FA+CKD, respectively. Only 20 wt.% CKD was considered for the viscosity test because this is the determined CKD content for ensuring required initial and final setting times (see Section 5.3.2 below). Stream 2 is simply an alkaline solution containing a very small amount of BP (at a dosage of 0, 0.1, 0.2, 0.3, 0.4, or 0.5 wt.% of FA+CKD) and thus can be easily pumped. Therefore, only a few viscosity tests were done on stream 2 for random check.

Fig. 10 shows the measured viscosity of stream 1 with 20 wt.% CKD at a time of 0, 1, and 2 hours after the two streams were mixed, respectively. It is noted that the viscosity decreases at a lower CKD content. The results at 0 wt.% SP are not shown in the figure because the viscosity was much higher than 300 cP at all conditions. The viscosity tends to increase with time. For instance, the viscosity at W/S = 0.50 and 1 wt.% SP increased from 300 cP right after mixing to 350 cp and 499 cP at 1 and 2 hours after mixing, respectively. As expected, the inclusion of SP and increase of W/S both decreased the viscosity of stream 1.

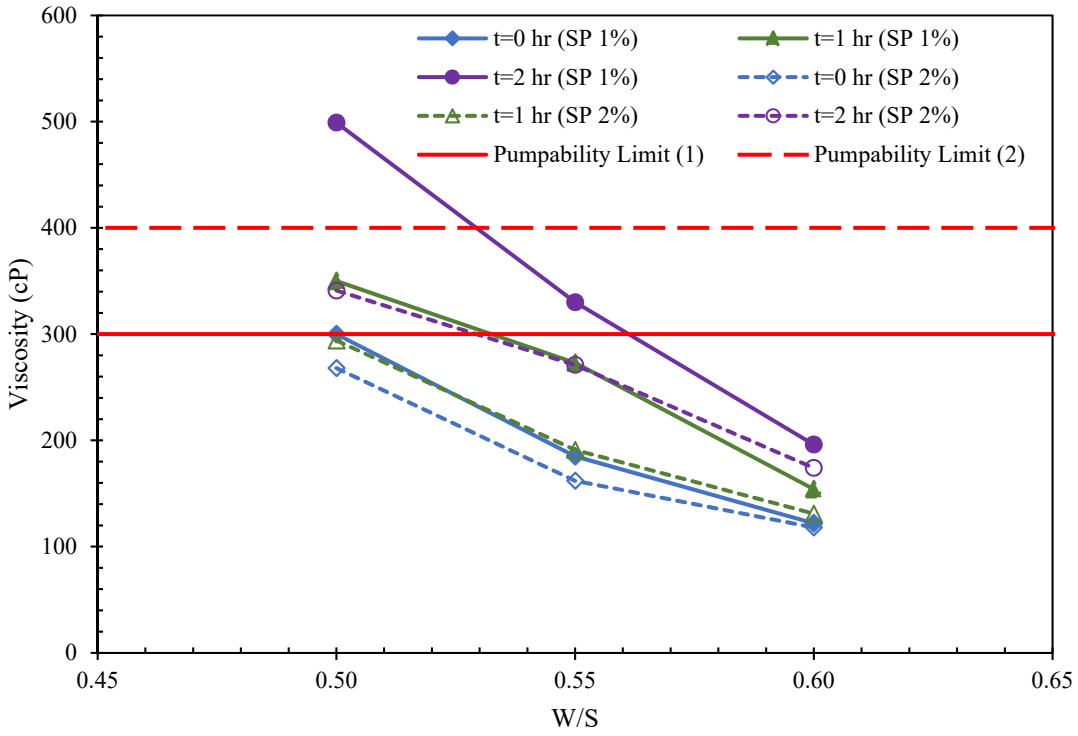

Fig. 10: Viscosity of stream 1 with 20 wt.% CKD.

Several viscosity limits are defined in the literature about the pumpability of cementitious materials. For instance, Porcherie et al. (2011) showed that a cementitious material is pumpable if the viscosity is less than 300 cP. On the other hand, Gong et al. (2019) demonstrated that a geopolymer cementitious material is pumpable if it has a viscosity less than 400 cP. For clear observation, both limits are shown in Fig. 10. If the conservative limit of 300 cP is considered, stream 1 can be designed to be pumpable within a certain period of time by simply selecting an appropriate W/S ratio and SP content. For example, if stream 1 is required to be pumpable within 2 hours after mixing, W/S of 0.60 and 1% SP, W/S of 0.6 and 2% SP, or W/S of 0.55 and 2% SP can be selected. The final selection of which combination will also be dependent on the required setting time and mechanical properties as discussed in next sections. Again, stream 2 is an alkaline solution containing SH, SS, and BP and always has a viscosity much smaller than 300 cP.

5.3.2 Setting time

For field applications, after the two streams are poured into the crib bag, the mixture needs to gain strength quickly. Therefore, the setting time of the hybrid cementitious material is of great importance.

Several studies were conducted to enhance the geopolymerization process and decrease the setting time of class F fly ash based geopolymer paste by addition of a supplemental material such as ordinary Portland cement (OPC), cement kiln dust (CKD), nano-silica, high-calcium slag, metakaolin, calcium chloride, and citric acid (Granizo et al. 2007; Zhang et al. 2011; Kusbiantoro et al. 2013; Deb et al. 2015; Nath and Sarker 2014, 2015, 2017; Nath et al. 2015). A summary of these studies is provided in Table 2. For example, Nath and Sarker (2015) conducted an experimental study to decrease the setting time of class F fly ash based geopolymer with 14 M

NaOH and SS/SH ratio of 2.5 at ambient temperature (21-23 °C). Addition of 5 and 12 wt.% of OPC reduced the initial setting time from > 24 hr to 309 and 40 min and the final setting time from > 24 hr to 470 and 120 min, respectively. Lee and Lee (2013) reduced the setting time of class F fly ash based geopolymer paste by addition of slag. For example, by using 20 wt.% slag, the geopolymer paste prepared with 8 M NaOH and SS/SH ratio of 0.5 cured at ambient temperature (~17 °C) reached an initial and final setting time of 10 and 50 min, respectively.

In this project, cement kiln dust (CKD) was selected to reduce the setting time of the hybrid cementitious material containing mainly the class F fly ash (FA) based geopolymer. Fig. 11 shows the measured initial and final setting time from Vicat tests for the hybrid cementitious material at different CKD contents (10, 15, and 20 wt.% of FA), for W/S = 0.50, 0.55, and 0.60, superplasticizer (SP) at 1 and 2 wt.% of FA+CKD, and a 35 °C curing temperature. The results at 0 wt.% CKD are not shown in the figure because even the initial setting time was longer than 12 hours.

As can be seen, the addition of CKD as a calcium source decreased the setting time significantly. For example, the initial and final setting times at 10, 15, and 20 wt.% of CKD with W/S = 0.50 and 1% SP were 153, 28, and 13 min and 366, 283, and 60 min, respectively. This is in agreement with the findings of previous researchers summarized in Table 2 who used high calcium content material like OPC to accelerate the curing of class F fly ash based geopolymer.

As expected, the increase of W/S from 0.50 to 0.55 and 0.60 delayed the setting time. For instance, the initial setting time increased from 13 min to 17 min and 37 min and the final setting time from 60 min to 170 min and 300 min for the cementitious material with 20 wt.% CKD and 1 wt.% SP, respectively. Moreover, the addition of SP increased the initial and final setting times. For example, increasing the SP content from 1 wt.% to 2 wt.% increased the initial setting time from 17 min to 26 min and the final setting time from 170 min to 202 min for the cementitious material with W/S = 0.50 and 20 wt.% CKD, respectively. Overall, the results show that CKD has a major effect on the setting time at different W/S ratios and SP contents.

Hird (2011) developed a cementitious grout for pumpable roof support by using pulverized fuel ash as a pozzolanic material, OPC as a hydraulically active cementitious component, sodium aluminate and aluminum sulfate as activator/gelling agent, and water. The combination of materials was seen to gel within 5 min and was self-supporting within 15 min. Regarding the results obtained through Vicat test in this study, 20 wt.% CKD provides comparable gelling and self-supporting times at different water contents for the cementitious material. Also, CKD is an industrial byproduct. Therefore, this project selects CKD as a supplemental material for adjusting setting of the hybrid cementitious material. Regarding the BP included in the second stream, it essentially has no effect on the setting time of the hybrid cementitious material due to the very low dosage used.

To study the effect of curing temperature on the setting time of the cementitious material, Vicat tests were performed at a curing temperature of 25, 35 and 45 °C, respectively, with W/S = 0.55 and 0.60, 1 and 2 wt.% SP, and 20 wt.% CKD. As can be seen in Fig. 12, higher curing temperature significantly reduced the setting time. For example, at W/S = 0.55 and 1 wt.% SP, increasing the curing temperature from 25 °C to 45 °C resulted in a decrease in initial and final setting times from 19 min to 11 min and from 214 min to 70 min, respectively. It can also be seen that the effect of curing temperature on the final setting time is much higher than that on the initial setting time. This is in agreement with the findings of Lee and Lee (2013).

Table 2 Summary of studies conducted to decrease setting time of the geopolymer.

Reference	Source Material	Additive	Water Content	NaOH (M)	SS/SH	Temp. (˚C)	Initial setting time	Final setting time
Nath and Sarker (2015)	Class F FA	-	W/S = 0.2	14	2.5	21-23	>24 hour	
	Class F FA	5% OPC		14	2.5	21-23	309 min	470 min
	Class F FA	12% OPC					40 min	120 min
Pangdaeng et al. (2014)	Class C FA	-	Alkaline Liquid / Binder = 0.4	10	0.67	23	124 min	144 min
	Class C FA	5% OPC					66 min	82 min
	Class C FA	10% OPC					39 min	53 min
	Class C FA	15% OPC					28 min	47 min
Deb et al. (2015)	Class F FA	1% NS	Alkaline Liquid / Binder = 0.4	8	2	20	13 h	19 h
	Class F FA	2% NS					11 h	18 h
	Class F FA	3% NS					10 h	16 h
	Class F FA	15% Slag + 3% NS					1.3 h	4 h
	Class F FA	10% OPC + 3% NS					35 min	60 min
Lee and Lee (2013)	Class F FA	20% Slag	Alkaline Liquid / Binder = 0.38	4	0.5	17	55 min	160 min
				6			50 min	114 min
				8			10 min	50 min
				4		28	25 min	60 min
				6			18 min	43 min
				8			Rapid setting	
Nath and Sarker (2014)	Class F FA	10% Slag	W/S = 0.2	14	2	21-23	290 min	540 min
		20% Slag					94 min	340 min
		30% Slag					41 min	100 min
Nath et al. (2015)	Class F FA	-	W/S = 0.2	14	2.5	23	>24 hour	
		10% Slag					208 min	336 min
		8% OPC					109 min	214 min
		2% $Ca(OH)_2$					609 min	905 min
Kumar et al. (2010)	Class F FA	-	Alkaline Liquid / Binder = 0.35	6	-	27	295 min	NA
		10% Slag					74 min	
		20% Slag					50 min	
		35% Slag					44 min	
		50% Slag					42 min	
Huseien et al. (2016)	Class F FA	74% Slag +10% POFA + 1% H.L.	Alkaline Liquid / Binder = 0.3	8	3	27	10 min	15 min
		70% Slag +10% POFA + 6% H.L. + 4% Gyp					6 min	10 min
		70% Slag +10% Gyp					6 min	12 min

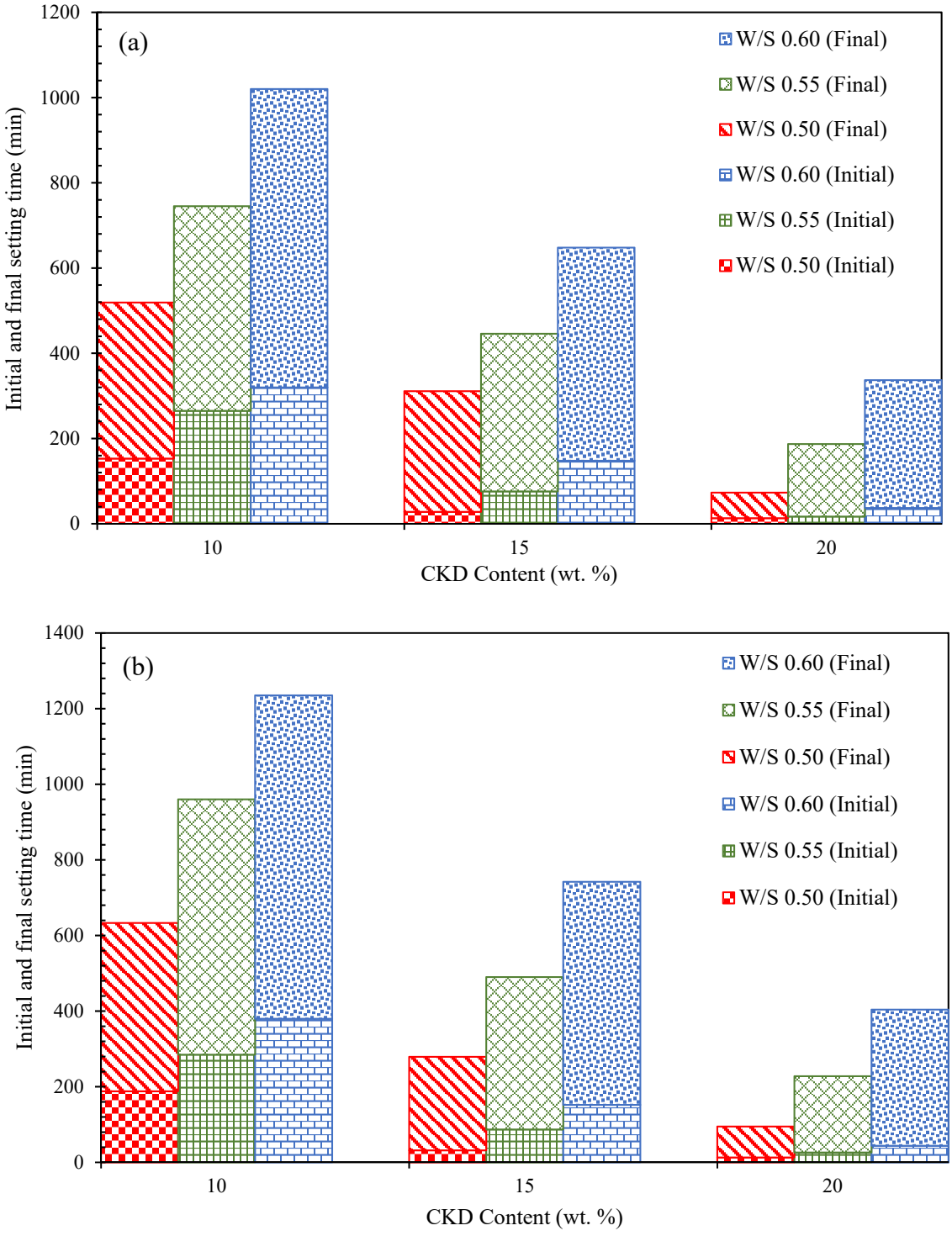

Fig. 11: Initial and final setting time at different CKD contents, W/S ratios, 35 °C curing temperature, and (a) 1 wt.% SP; and (b) 2 wt.% SP.

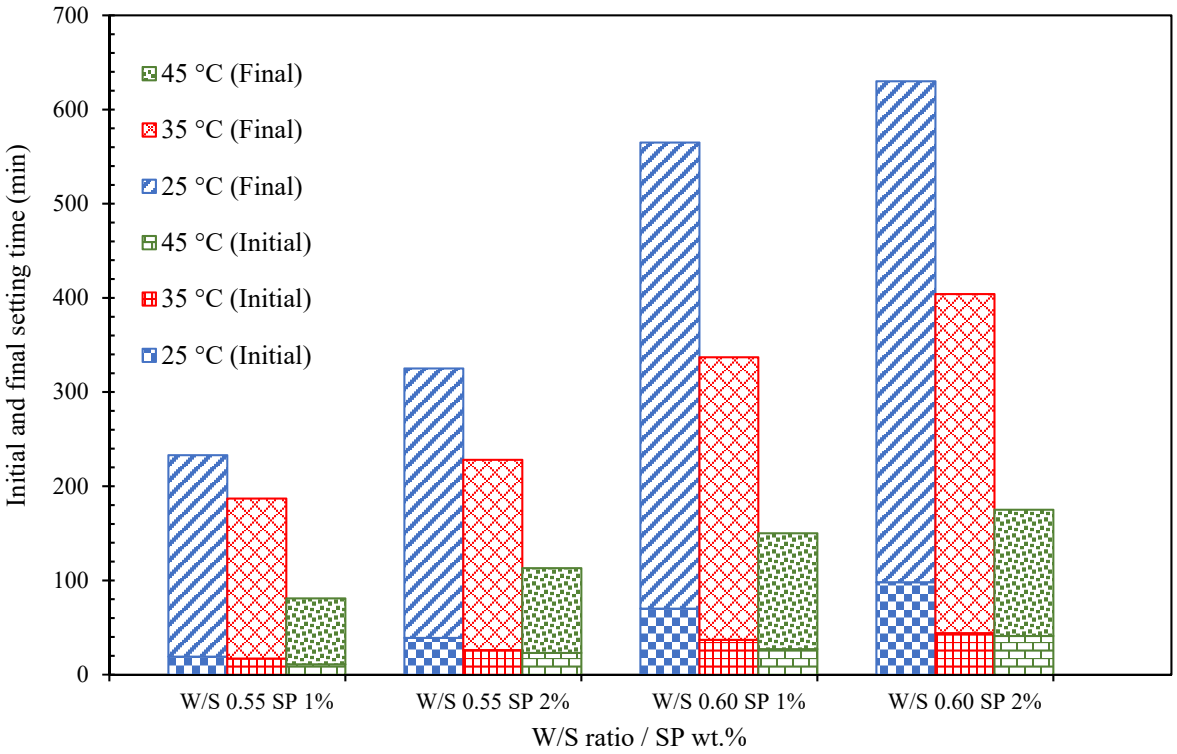

Fig. 12: Effect of curing temperature on initial and final setting times of cementitious material with W/S = 0.55 and 0.60, 1 and 2 wt.% SP, and 20 wt.% CKD.

5.3.3 Mechanical properties

This section presents the results of mechanical tests on the hybrid cementitious material at different conditions, including peak unconfined compressive strength (UCS), residual UCS, Young's modulus and tensile strength, and discusses the effect of various factors on these mechanical properties. Based on the study of pumpability and setting time in the previous subsections, 20 wt.% CKD, W/S = 0.55 or 0.60, 1 or 2 wt.% SP were recommended to meet the pumpability and setting time requirements. Therefore, the mechanical tests were conducted on hybrid cementitious materials with 20 wt.% CKD, W/S = 0.55 and 0.60, 1 and 2 wt.% SP, different BP contents, and different curing temperatures and curing times.

Fig. 13 presents a typical stress-strain curve from unconfined compression test and how the peak UCS, residual UCS and Young's modulus are determined from it. Since the residual UCS changes with strain, the residual UCS at 5% strain is selected in the discussion below. The complete stress-strain curves from all unconfined compression tests are presented in Section 7.0. The tensile strength is simply determined using the peak load from the split tensile test.

Peak UCS

To enhance the mechanical performance of the cementitious material, BP (CAR, GEL, or CNF), at 0, 0.1, 0.2, 0.3, 0.4, or 0.5 wt.% of FA+CKD, was incorporated. Fig. 14 shows the effect of included BP on the 7-day peak UCS of the hybrid cementitious material with 20 wt.% CKD, W/S = 0.55 and 0.60, 1 and 2 wt.% SP, and cured at 35 °C. As can be seen, overall, the incorporation of BP has essentially no effect on (for CAR and CNF) or leads to very slight decrease (for GEL)

of the 7-day peak UCS of the hybrid cementitious material. This is good because the main purpose of including BP is to increase the residual strength of the hybrid cementitious material (see later discussion).

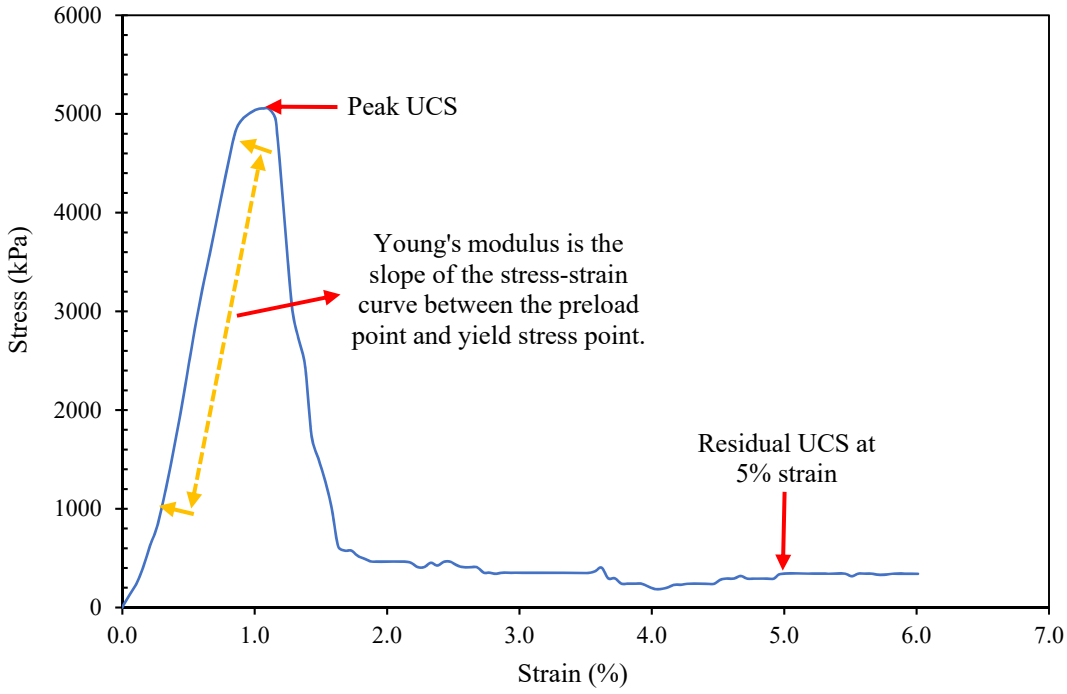

Fig. 13: A typical stress-strain curve from unconfined compression test and how peak UCS, residual UCS and Yong's modulus are determined (after ASTM E111-17 (2017)).

It can also be seen from Fig. 14 about the effect of water content and SP dosage on the 7-day peak UCS of the hybrid cementitious material. Overall, as expected, the increase of W/S ratio and SP dosage leads to a decrease of the 7-days peak UCS.

The effect of curing temperature on the mechanical properties of the hybrid cementitious material with 20 wt.% CKD, W/S = 0.55 and 0.60, 1 and 2 wt.% SP, and 0.3 wt.% CAR, 0.3 wt.% GEL or 0.5 wt.% CNF was studied by decreasing and increasing the curing temperature from 35 °C to 25 °C and 45 °C, respectively. The single BP content (0.3 wt.% CAR, 0.3 wt.% GEL and 0.5 wt.% CNF) was selected by considering the highest residual UCS at 35 °C curing temperature (see next subsection). Fig. 15 shows the variation of the 7-day peak UCS with curing temperature at different conditions. As expected, the 7-day peak UCS increases when the curing temperature increases from 25 °C to 45 °C. This is in a good agreement with the findings of Hardjito et al. (2004) and Rangan (2008) who showed that increasing curing temperature resulted in an increase in the UCS of geopolymer concrete.

The effect of curing time on the mechanical properties of the hybrid cementitious material at different compositions and 35 °C curing temperature was also studied. Fig. 16 shows the variation of peak UCS with curing time. As expected, the peak UCS increases with longer curing time. It is also noted that the peak UCS tends to increase at a higher speed at the beginning from 3 to 7 days than that at a later time. This is beneficial to field applications of the hybrid cementitious material because the strength will be gained quickly at the beginning.

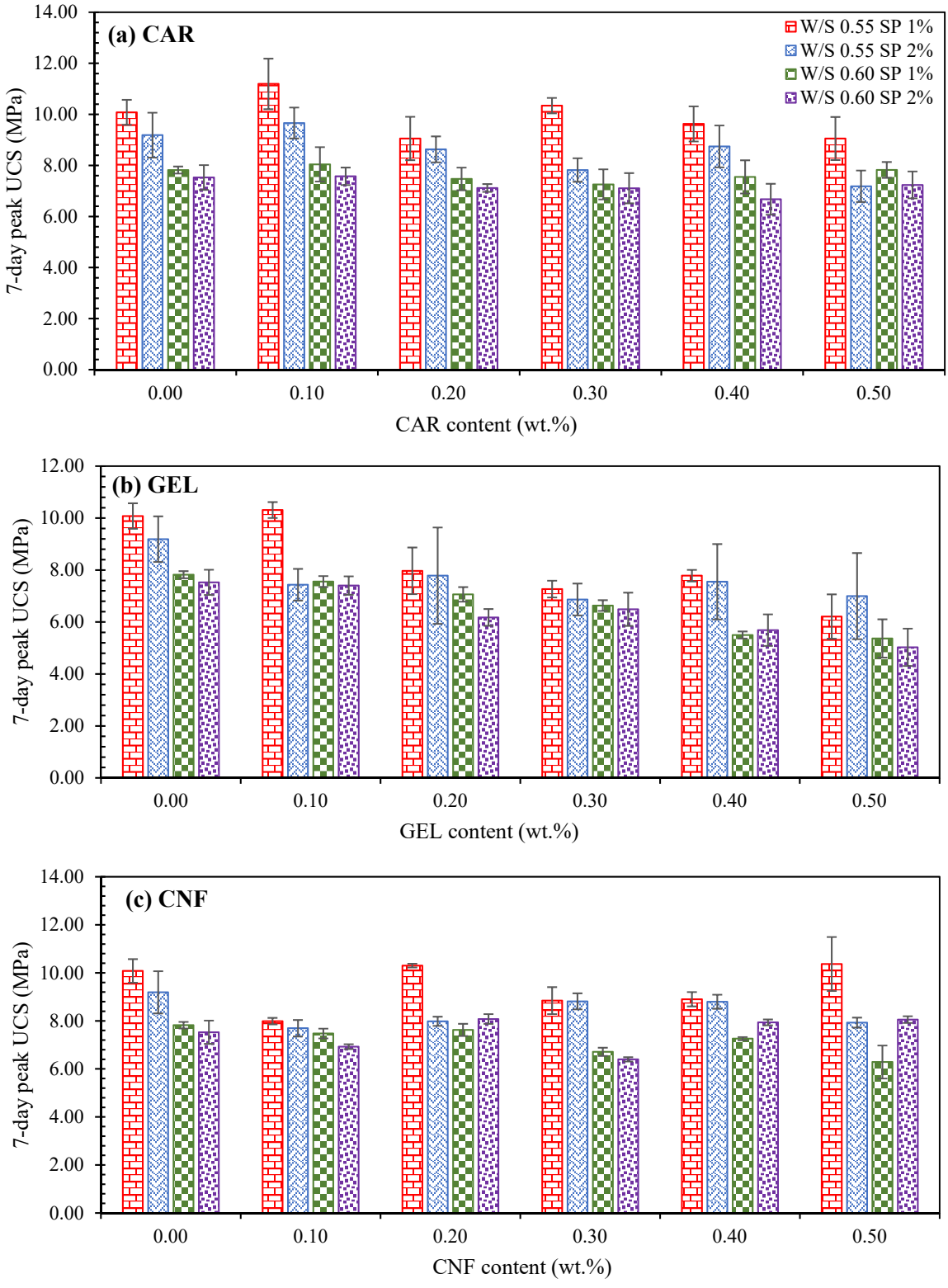

Fig. 14: Effect of BP content on 7-day peak UCS of hybrid cementitious material with 20 wt.% CKD, W/S = 0.55 and 0.60, 1 and 2 wt.% SP, cured at 35 °C, and containing: (a) Carrageenan (CAR); (b) Gellun gum (GEL); and (c) Cellulose nanofibers (CNF).

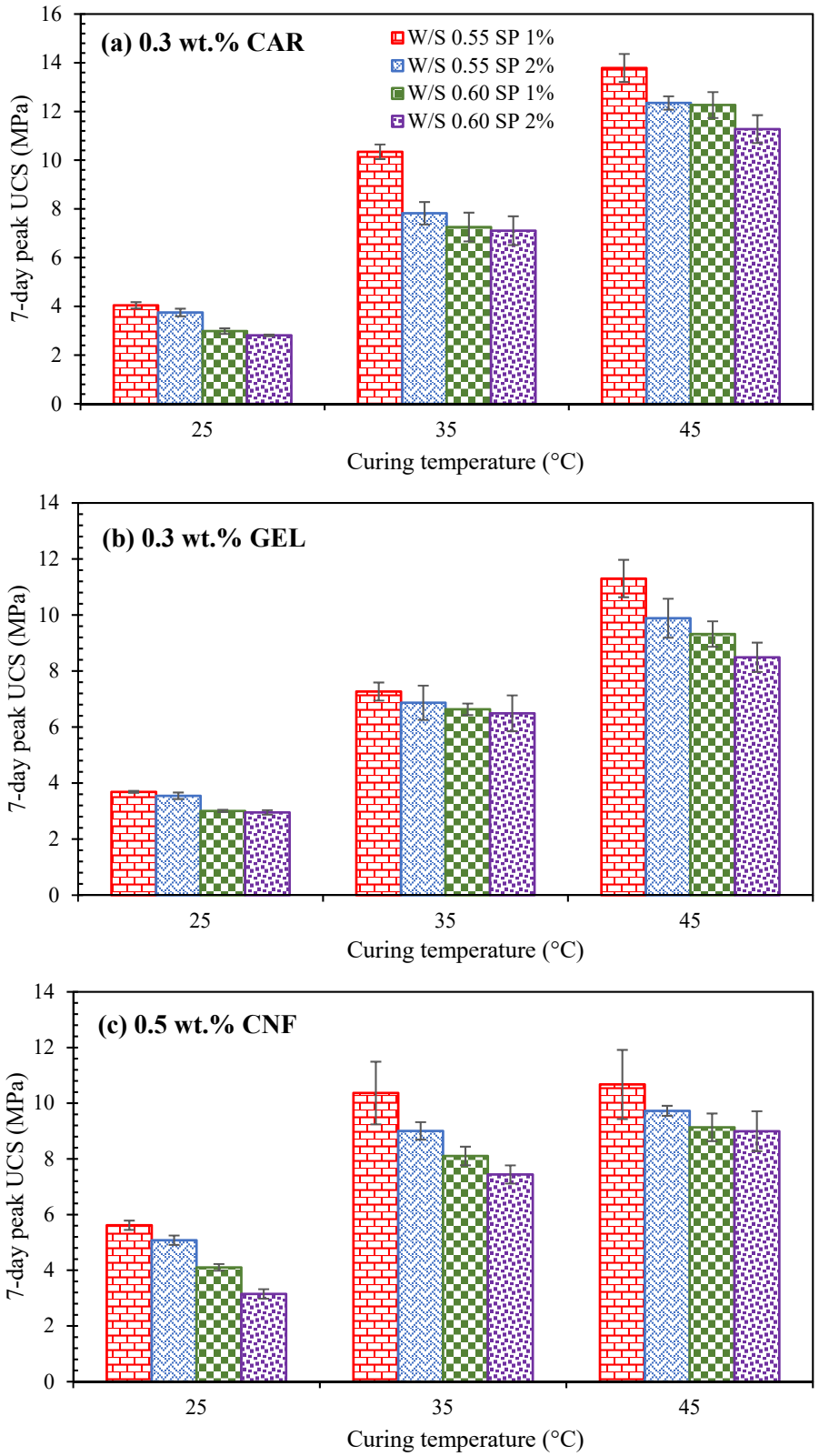

Fig. 15: Effect of curing temperature on 7-day peak UCS of hybrid cementitious material with 20 wt.% CKD, W/S = 0.55 and 0.60, 1 and 2 wt.% SP, and containing: (a) 0.3 wt.% carrageenan (CAR); (b) 0.3 wt.% gellun gum (GEL); and (c) 0.5 wt.% cellulose nanofibers (CNF).

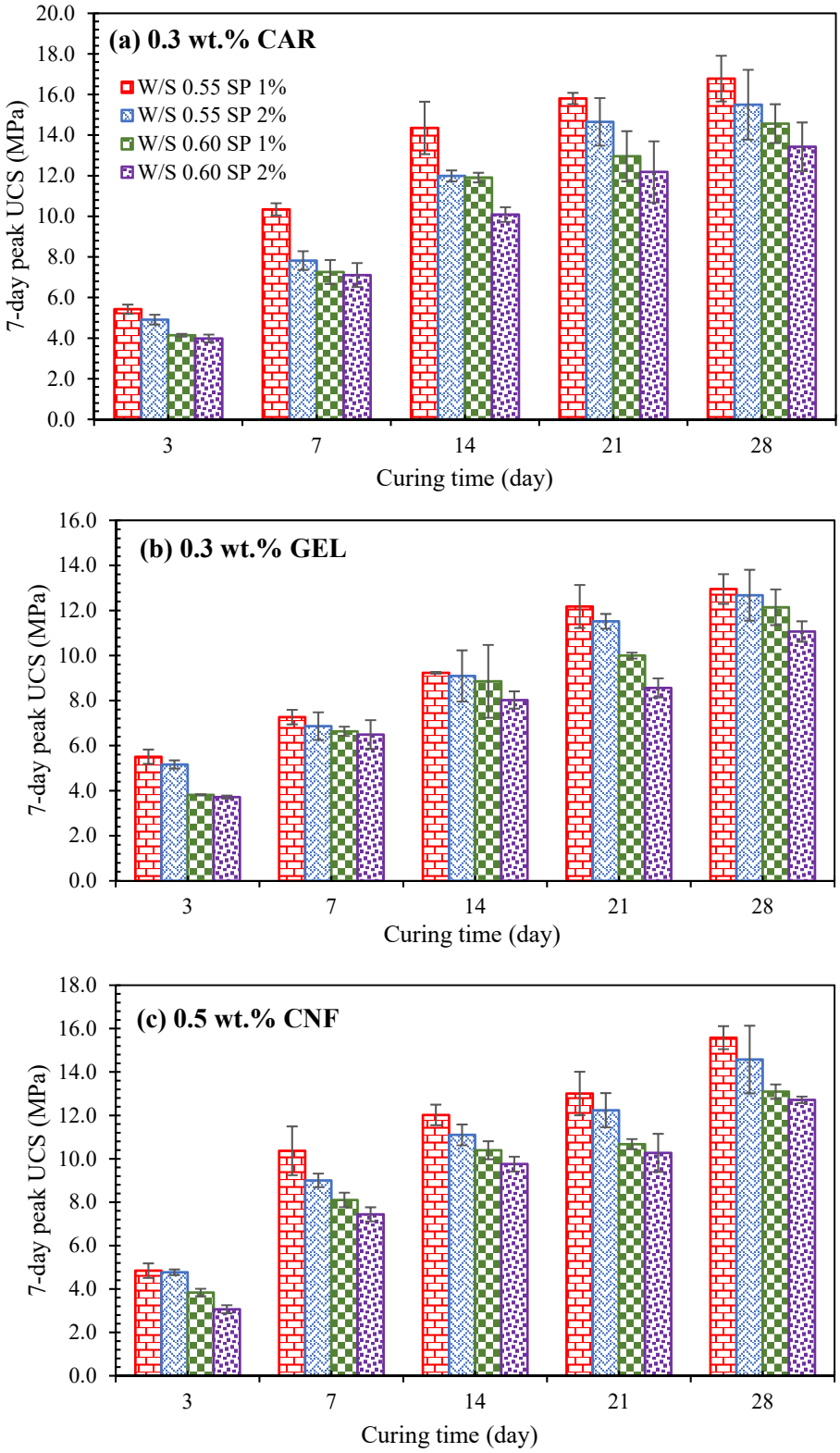

Fig. 16: Effect of curing time on peak UCS of hybrid cementitious material with 20 wt.% CKD, W/S = 0.55 and 0.60, 1 and 2 wt.% SP, cured at 35 °C, and containing: (a) 0.3 wt.% carrageenan (CAR); (b) 0.3 wt.% gellun gum (GEL); and (c) 0.5 wt.% cellulose nanofibers (CNF).

Residual UCS

Fig. 17 shows the effect of included BP on the 7-day residual UCS of the hybrid cementitious material with 20 wt.% CKD, W/S = 0.55 and 0.60, 1 and 2 wt.% SP, and cured at 35 °C. Again, because the residual strength changes with strain randomly (see Section 7.0 about the complete stress-strain curves), only the residual UCS at 5% strain is shown in the figure for easy discussion. It can be seen that the inclusion of BP may lead to increase or decrease of the residual UCS, depending on the W/S ratio, SP amount and BP content. However, the results clearly show that at 0.3 wt.% carrageenan (CAR), 0.3 wt.% gellun gum (GEL), and 0.5 wt.% cellulose nanofibers (CNF), the 7-day residual UCS reaches the highest or second highest value at nearly all W/S ratios and SP amounts and the values are much higher than the corresponding values at 0 wt.% BP. So, by including an appropriate amount of BP, the residual UCS of the hybrid cementitious material can be significantly increased. This is in agreement with the studies which showed the improvement of ductility and toughness of geopolymer after inclusion of BP by several researchers including Li et al. (2013), Li and Zhang (2016), and Abdollahnejad et al. (2017).

It can also be seen from Fig. 17 that the increase of W/S ratio or SP dosage may lead to increase, decrease or essentially no change of the 7-day residual UCS, depending on the W/S ratio, the SP amount, and the BP type and content. This is possibly due to the different interactions at various W/S ratios, SP amounts and BP types and contents. It may also be because the residual UCS varies randomly with strain (see the complete stress-strain curves in Section 7.0) and Fig. 17 only shows the residual UCS values at 5% strain

Based on the results in Fig. 17 about the 7-day residual UCS at different BP types and contents, 0.3 wt.% carrageenan (CAR), 0.3 wt.% gellun gum (GEL), and 0.5 wt.% cellulose nanofibers (CNF) were selected as the respective BP dosage for the hybrid cementitious material so that the highest residual strength can be obtained.

Fig. 18 shows the effect of curing temperature on the 7-day residual UCS of the hybrid cementitious material with 20 wt.% CKD, W/S = 0.55 and 0.60, 1 and 2 wt.% SP, and containing 0.3 wt.% CAR, 0.3 wt.% GEL, and 0.5 wt.% CNF, respectively. Higher curing temperature may lead to increase, decrease or essentially no change of the 7-day residual UCS, depending on the W/S ratio, SP amount, BP type, and curing temperature. This may be due to the fact that the residual UCS varies randomly with strain (see the complete stress-strain curves in Section 7.0) and Fig. 18 only shows the residual UCS values at 5% strain.

Fig. 19 shows the effect of curing time on the residual UCS of the hybrid cementitious material with 20 wt.% CKD, W/S = 0.55 and 0.60, 1 and 2 wt.% SP, cured at 35 °C, and containing 0.3 wt.% CAR, 0.3 wt.% GEL, and 0.5 wt.% CNF, respectively. The residual UCS can either increase, decrease or be about the same as time increases. Again, this may be due to the fact that the residual UCS varies randomly with strain (see the complete stress-strain curves in Section 7.0) and Fig. 19 only shows the residual UCS values at 5% strain.

The effect of water content and SP dosage on the residual strength of the hybrid cementitious material, as described above, can also be further seen from Figs. 18 and 19.

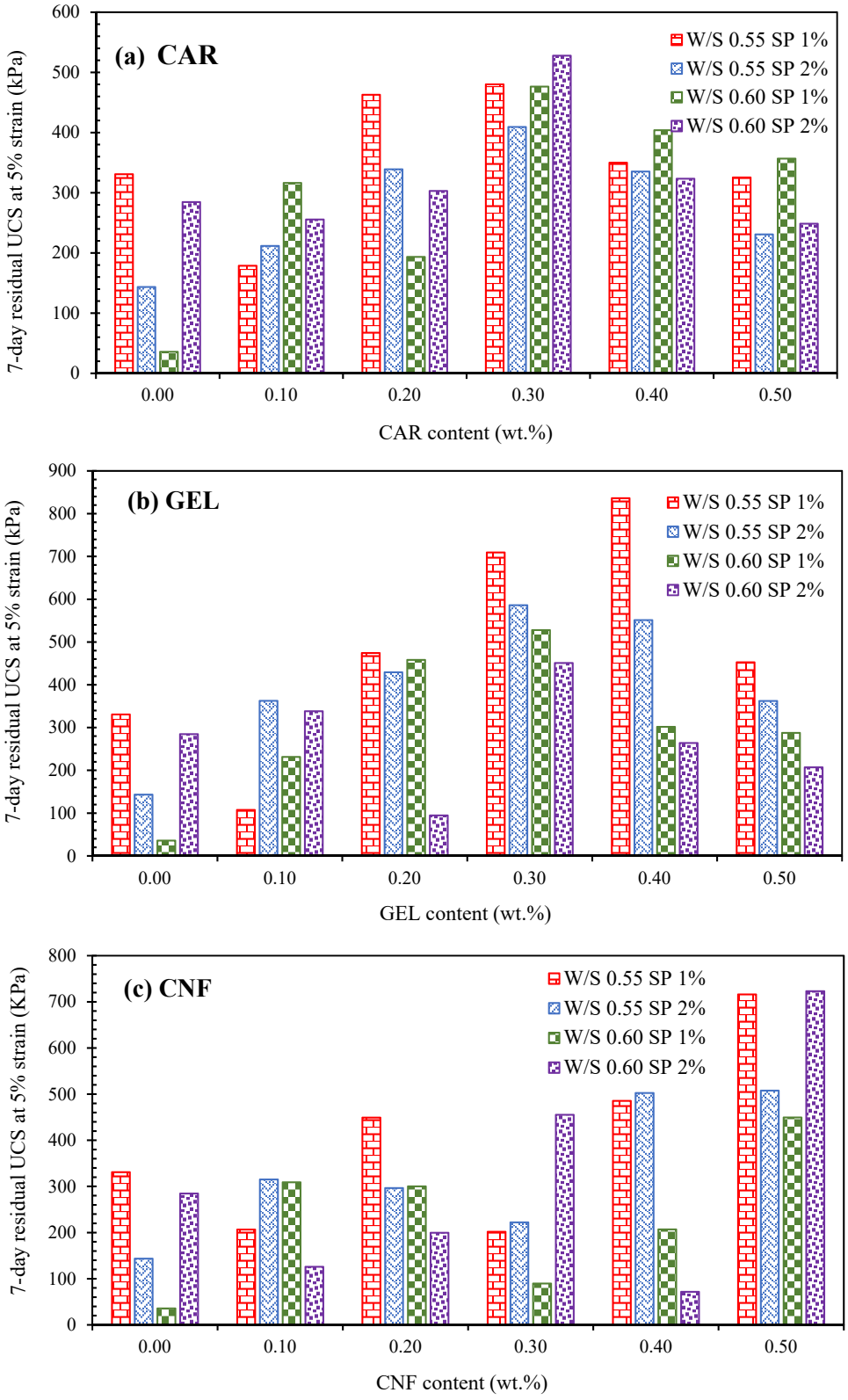

Fig. 17: Effect of BP content on 7-day residual UCS of hybrid cementitious material at 5% strain with 20 wt.% CKD, W/S = 0.55 and 0.60, 1 and 2 wt.% SP, and cured at 35 °C: (a) Carrageenan (CAR); (b) Gellun gum (GEL); and (c) Cellulose nanofibers (CNF).

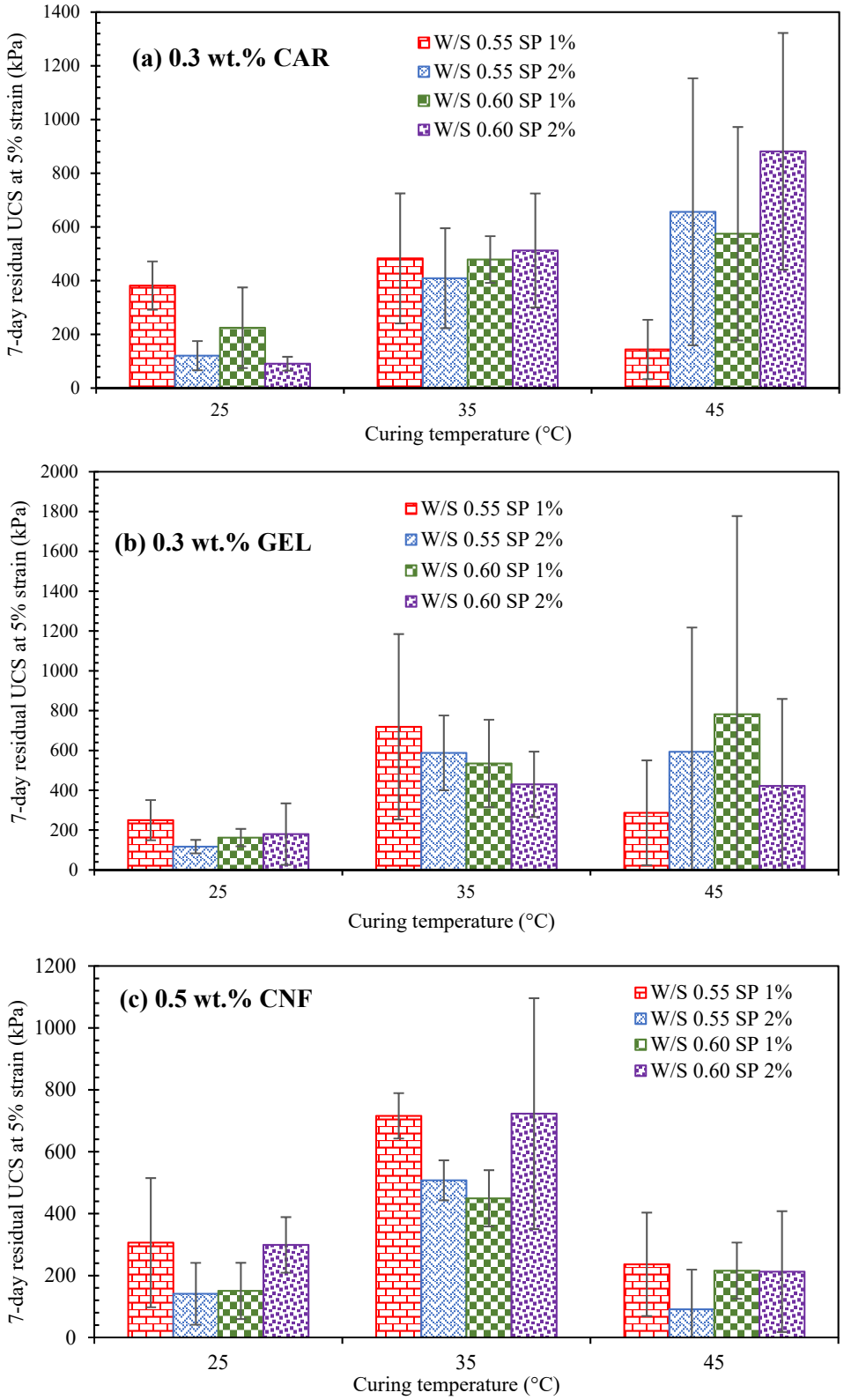

Fig. 18: Effect of curing temperature on 7-day residual strength of hybrid cementitious material at 5% strain with 20 wt.% CKD, W/S = 0.55 and 0.60, 1 and 2 wt.% SP, and containing: (a) 0.3 wt.% carrageenan (CAR); (b) 0.3 wt.% gellun gum (GEL); and (c) 0.5 wt.% cellulose nanofibers (CNF).

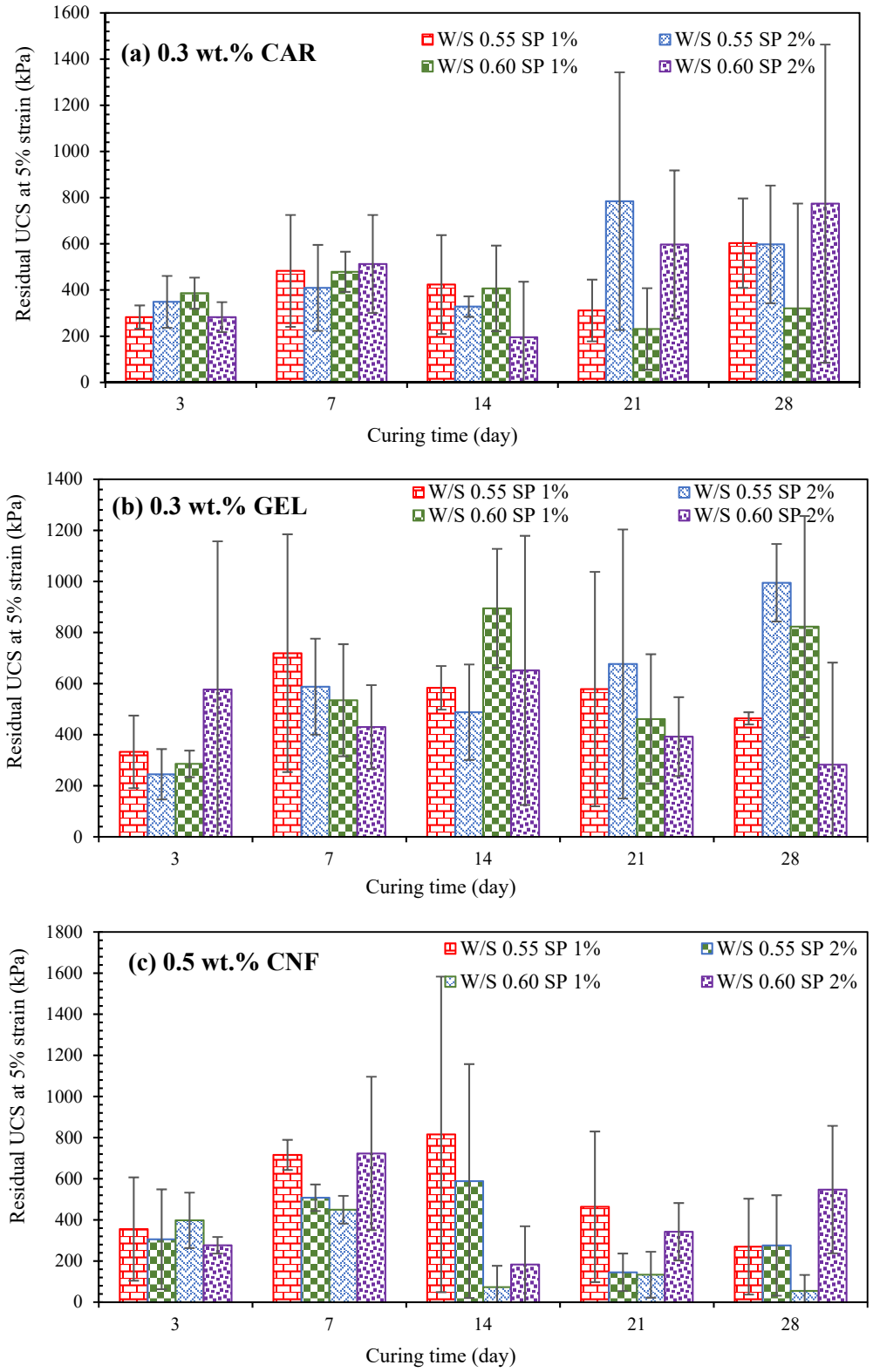

Fig. 19: Effect of curing time on residual UCS of hybrid cementitious material at 5% strain with 20 wt.% CKD, W/S = 0.55 and 0.60, 1 and 2 wt.% SP, cured at 35 °C, and containing: (a) 0.3 wt.% carrageenan (CAR); (b) 0.3 wt.% gellun gum (GEL); and (c) 0.5 wt.% cellulose nanofibers (CNF).

Young's modulus

Fig. 20 shows the effect of included BP on the 7-day Young's modulus of the hybrid cementitious material with 20 wt.% CKD, W/S = 0.55 and 0.60, 1 and 2 wt.% SP, and cured at 35 °C. As can be seen, overall, the incorporation of BP has essentially no effect on the 7-day Young's modulus of the hybrid cementitious material. Again, this is good because the main purpose of including BP is to increase the residual strength of the hybrid cementitious material.

It can also be seen from Fig. 20 about the effect of increasing water content and SP dosage on the 7-day Young's modulus of the hybrid cementitious material. Overall, the increase of W/S ratio leads to a decrease of the 7-day Young's modulus. However, the increase of SP content can lead to slight increase or decrease of the 7-day Young's modulus depending the W/S ratio and the BP type and content.

Fig. 21 shows the effect of curing temperature on the 7-day Young's modulus of the hybrid cementitious material with 20 wt.% CKD, W/S = 0.55 and 0.60, 1 and 2 wt.% SP, and containing 0.3 wt.% carrageenan (CAR), 0.3 wt.% gellun gum (GEL), and 0.5 wt.% cellulose nanofibers (CNF), respectively. As expected, the 7-day Young's modulus increases when the curing temperature increases from 25 °C to 45 °C.

Fig. 22 shows the effect of curing time on the Young's modulus of the hybrid cementitious material with 20 wt.% CKD, W/S = 0.55 and 0.60, 1 and 2 wt.% SP, cured at 35 °C, and containing 0.3 wt.% CAR, 0.3 wt.% GEL and 0.5 wt.% CNF, respectively. The Young's modulus increases significantly from 3 to 14 days and stays about the same. So, the stiffness of the hybrid cementitious material reaches its maximum value within about 14 days.

The effect of water content and SP dosage on the Young's modulus of the hybrid cementitious material, as described above, can also be further seen from Figs. 21 and 22.

Tensile strength

Based on the unconfined compression test results presented above, tensile strength tests were conducted only on the hybrid cementitious material with 0.3 wt.% CAR, 0.3 wt.% GEL and 0.5 wt.% CNF, respectively. Fig. 23 shows the effect of curing temperature on the 28-day tensile strength of the hybrid cementitious material with 20 wt.% CKD, W/S = 0.55 and 0.60, 1 and 2 wt.% SP, and containing 0.3 wt.% CAR, 0.3 wt.% GEL and 0.5 wt.% CNF, respectively. As can be seen, the tensile strength increases with higher curing temperature from 25 °C to 45 °C.

The effect of curing time on the tensile strength of the hybrid cementitious material was also studied. Fig. 24 shows the 7- and 28-day tensile strength of the hybrid cementitious material with 20 wt.% CKD, W/S = 0.55 and 0.60, 1 and 2 wt.% SP, cured at 35 °C, and containing 0.3 wt.% CAR, 0.3 wt.% GEL and 0.5 wt.% CNF, respectively. Clearly, the 28-day tensile strength is higher than the 7-day tensile strength.

The effect of water content and SP dosage on the tensile strength of the hybrid cementitious material can also be seen from Figs. 23 and 24. Overall, the increase of W/S ratio and SP amount leads to a decrease of the tensile strength.

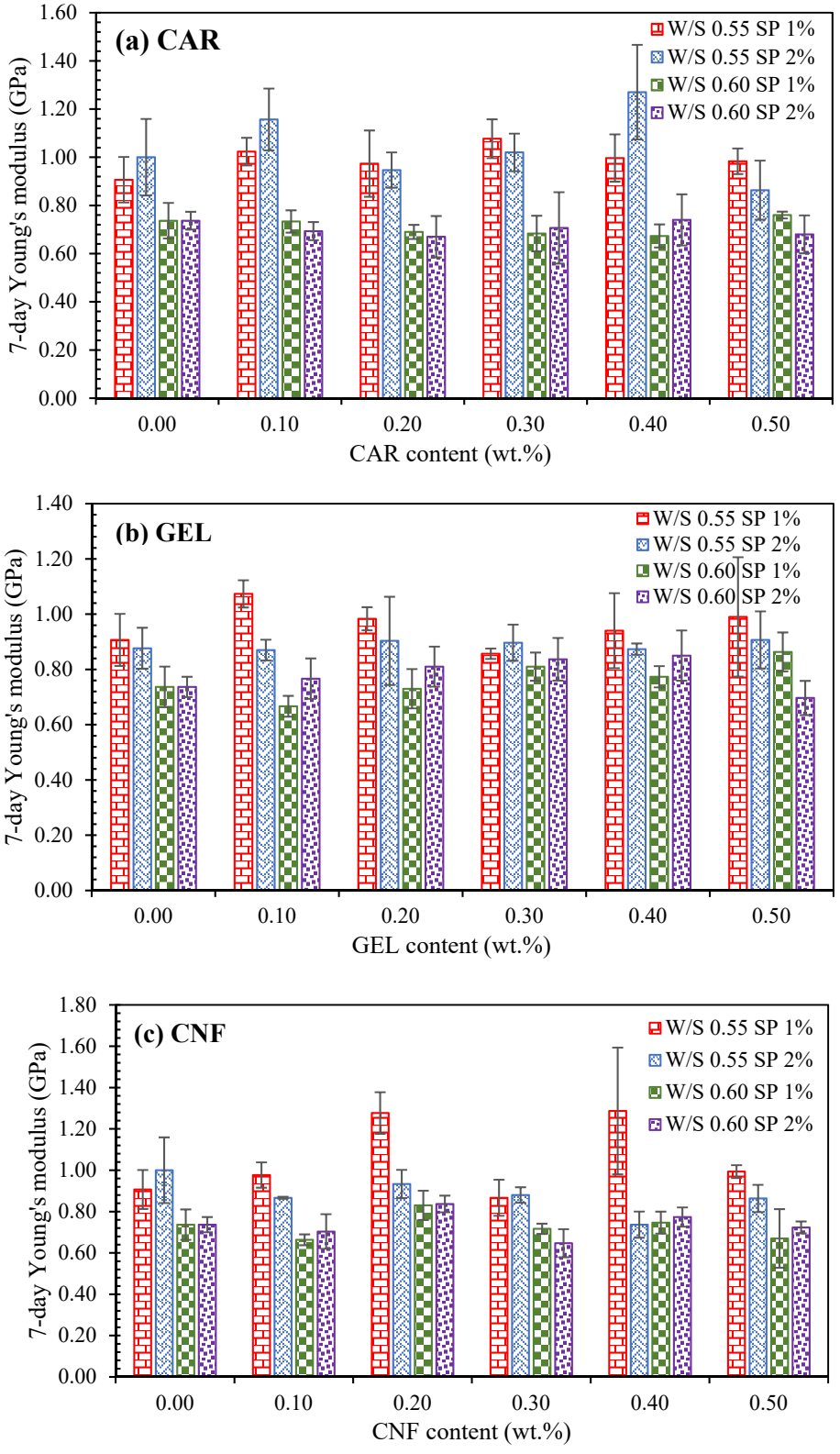

Fig. 20: Effect of BP content 7-day Young's modulus of hybrid cementitious material with 20 wt.% CKD, W/S = 0.55 and 0.60, 1 and 2 wt.% SP, and cured at 35 °C: (a) Carrageenan (CAR); (b) Gellun gum (GEL); and (c) Cellulose nanofibers (CNF).

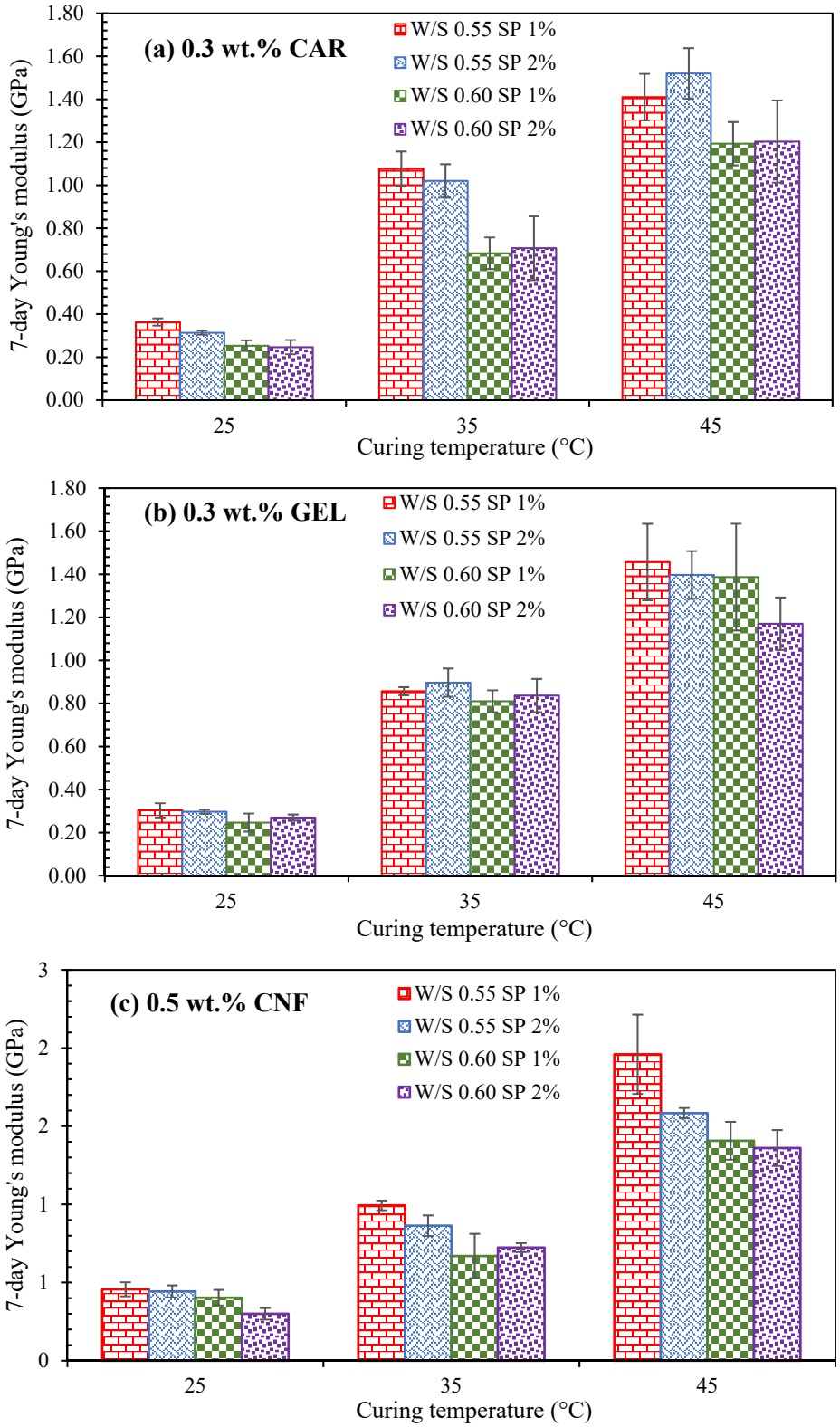

Fig. 21: Effect of curing temperature on 7-day Young's modulus of hybrid cementitious material with 20 wt.% CKD, W/S = 0.55 and 0.60, 1 and 2 wt.% SP, and containing: (a) 0.3 wt.% carrageenan (CAR); (b) 0.3 wt.% gellun gum (GEL); and (c) 0.5 wt.% cellulose nanofibers (CNF).

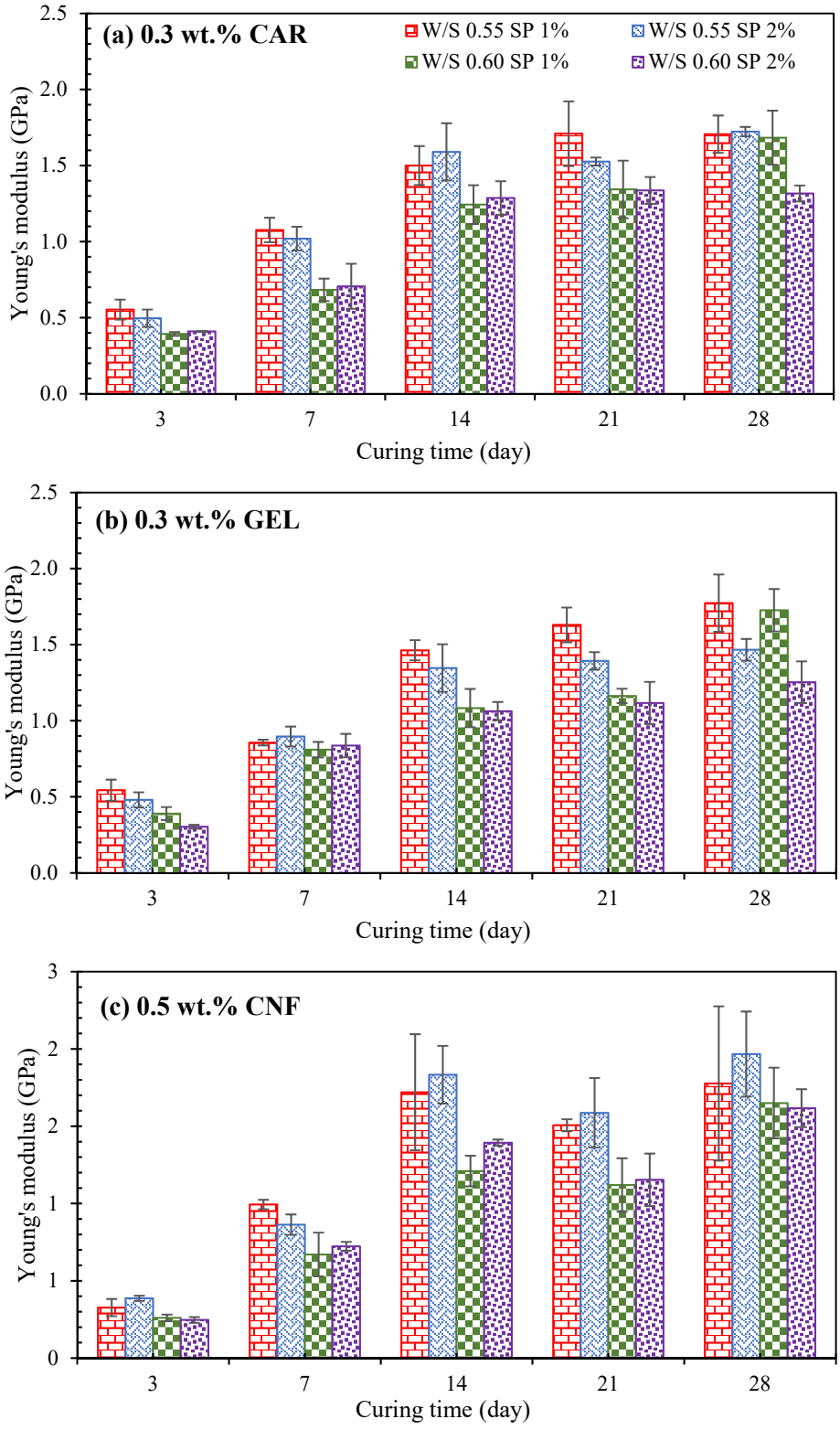

Fig. 22: Effect of curing time on Young's modulus of hybrid cementitious material with 20 wt.% CKD, W/S = 0.55 and 0.60, 1 and 2 wt.% SP, cured at 35 °C, and containing: (a) 0.3 wt.% carrageenan (CAR); (b) 0.3 wt.% gellun gum (GEL); and (c) 0.5 wt.% cellulose nano-fibers (CNF).

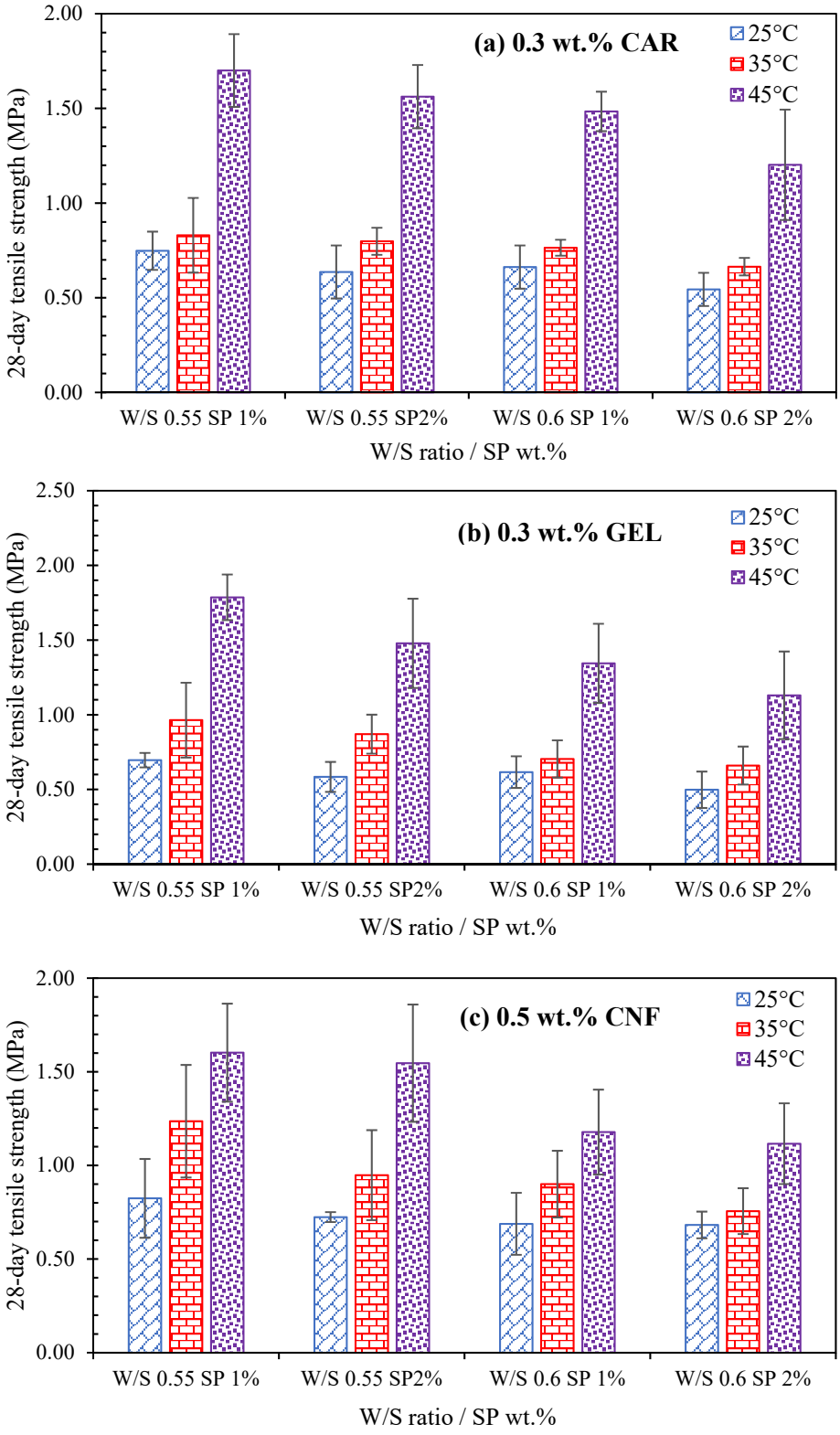

Fig. 23: Effect of curing temperature on 28-day tensile strength of hybrid cementitious material with 20 wt.% CKD, W/S = 0.55 and 0.60, 1 and 2 wt.% SP, and containing: (a) 0.3 wt.% carrageenan (CAR); (b) 0.3 wt.% gellun gum (GEL); and (c) 0.5 wt.% cellulose nanofibers (CNF).

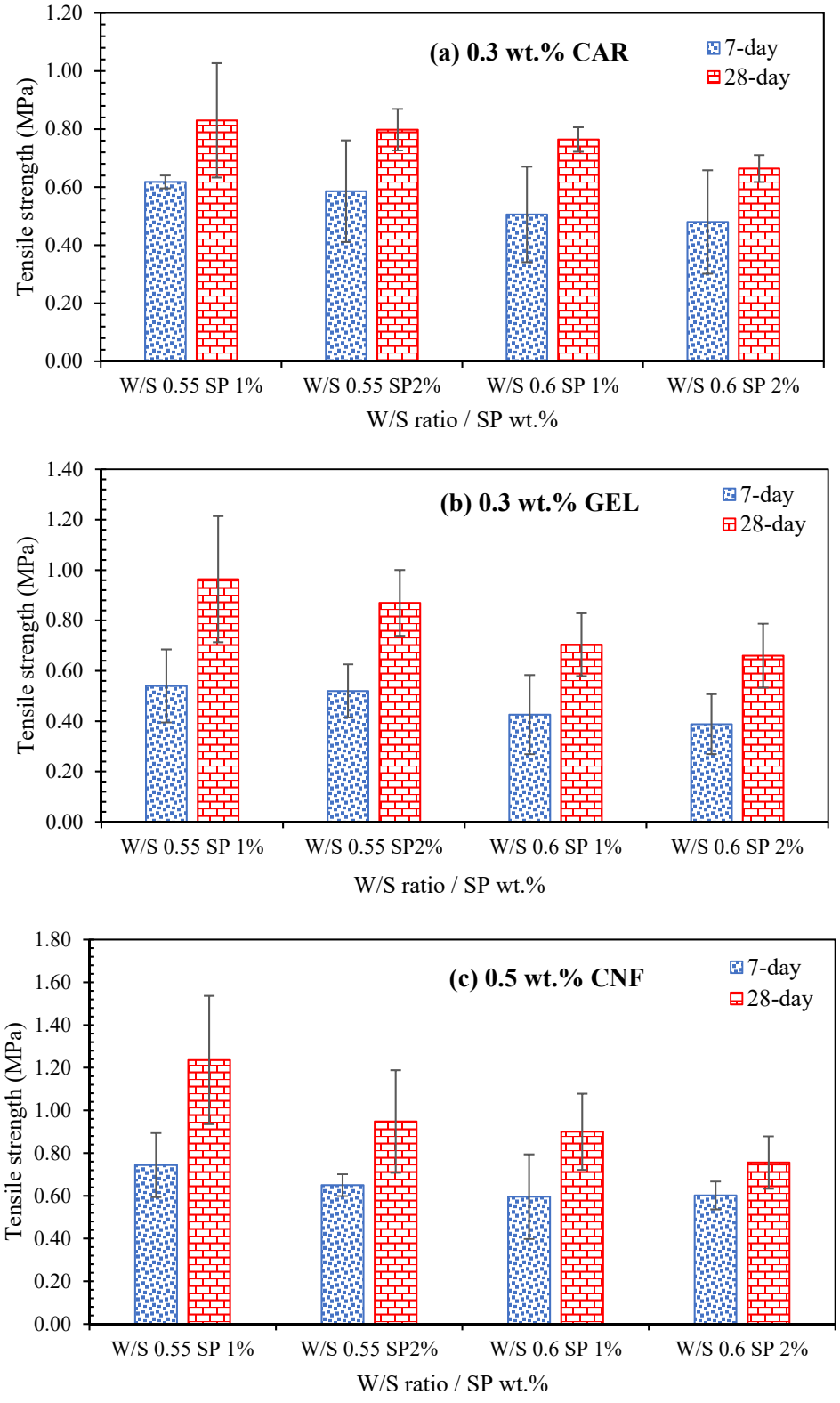

Fig. 24: Effect of curing time on tensile strength of hybrid cementitious material with W/S = 0.55 and 0.60, 1 and 2 wt.% SP, cured at 35 °C, and containing: (a) 0.3 wt.% carrageenan (CAR); (b) 0.3 wt.% gellun gum (GEL); and (c) 0.5 wt.% cellulose nanofibers (CNF).

5.4 Microstructure and chemical composition study

5.4.1 SEM imaging and EDX analysis

SEM imaging and EDX analysis were conducted to investigate the effect of CKD content, W/S ratio and BP dosage on the microstructure and elemental composition of the hybrid cementitious material. Fig. 25 shows the SEM micrographs of the cementitious material at different CKD contents and with the same W/S = 0.50, 1 wt.% SP, 0 wt.% BP, and cured at 35 °C for 7 days. At 0 wt.% CKD, the sponge-like geopolymer gels which act as the binder can be clearly seen. When 10, 15 or 20 wt.% is included, the sponge-like geopolymer gels can be hardly seen and the material looks more compact and denser. This is due to the formation of calcium silicate hydrate (CSH) gels when calcium is available from the added CKD and the coexistence of the geopolymer and CSH gels (Ahmari and Zhang 2013). Some cracks can also be observed when CKD is included, which is due to the fast setting and curing at the presence of CKD (Mehta et al. 2017). Some unreacted or partially reacted FA particles can be clearly seen at all CKD contents. This may be due to the low alkalinity (5 M NaOH) used in preparing the cementitious material.

Fig. 26 shows the SEM micrographs of the cementitious material at different W/S ratios and with the same 20 wt.% CKD, 1 wt.% SP, 0 wt.% BP, and cured at 35 °C for 7 days. With the W/S ratio increased from 0.55 to 0.55 and 0.60, there are no more cracks and the microstructure looks more porous. This is because increased water content decreases the setting and curing speed and evaporation of more water generates more voids.

The chemical composition of the cementitious material at different CKD contents and W/S ratios from the EDX analysis, shown as Si/Al, Na/Al, and Ca/Si ratios, are summarized in Table 3. The Si/Al ratio increases with higher CKD content. This is because the added CKD elevates alkalinity and dissolution of more Si (Ahmari and Zhang 2013). The Ca/Si ratio increases with higher CKD content simply due to the availability of more Ca. When W/S increases, the Si/Al increases but the Ca/Si decreases. This is because at the same NaOH concentration, a higher W/S ratio means more NaOH is available and thus more Si is dissolved.

Fig. 27 shows the SEM micrographs of the cementitious material at 0 and 0.3 wt.% CAR and with the same 20 wt.% CKD, W/S = 0.55, 1 wt.% SP, and cured at 35 °C for 7 days. Due to the very low dosage of BP included, the microstructure looks similar and the Si/Al, Na/Al, and Ca/Si ratios are also very close at the two different BP contents.

5.4.2 XRD analysis

XRD analyses were also performed on the cementitious material at different CKD contents and W/S ratios, the same 1 wt.% SP, 0 wt.% BP, and cured at 35 ˚C for 7 days. Fig. 28 shows the XRD patterns. For comparison, the XRD patterns of pure fly ash and pure CKD are also shown in the figure. The XRD patterns of the cementitious material at 0 wt.% CKD maintain the same crystalline peaks as the pure fly ash with no emergence of new peaks, indicating that the partially reacted particles are the main constituent of the geopolymer matrix. In addition, the amorphous phase with a broad hump extending from approximately 15–40° can be clearly seen in the 0 wt.% CKD cementitious material. When CKD is included, a new peak corresponding to CSH can be seen. The CSH peak is higher when more CKD is included at the same W/S ratio of 0.50. Also, the CSH peak at 20 wt.% CKD is lower when the W/S ratio increases from 0.50 to 0.60.

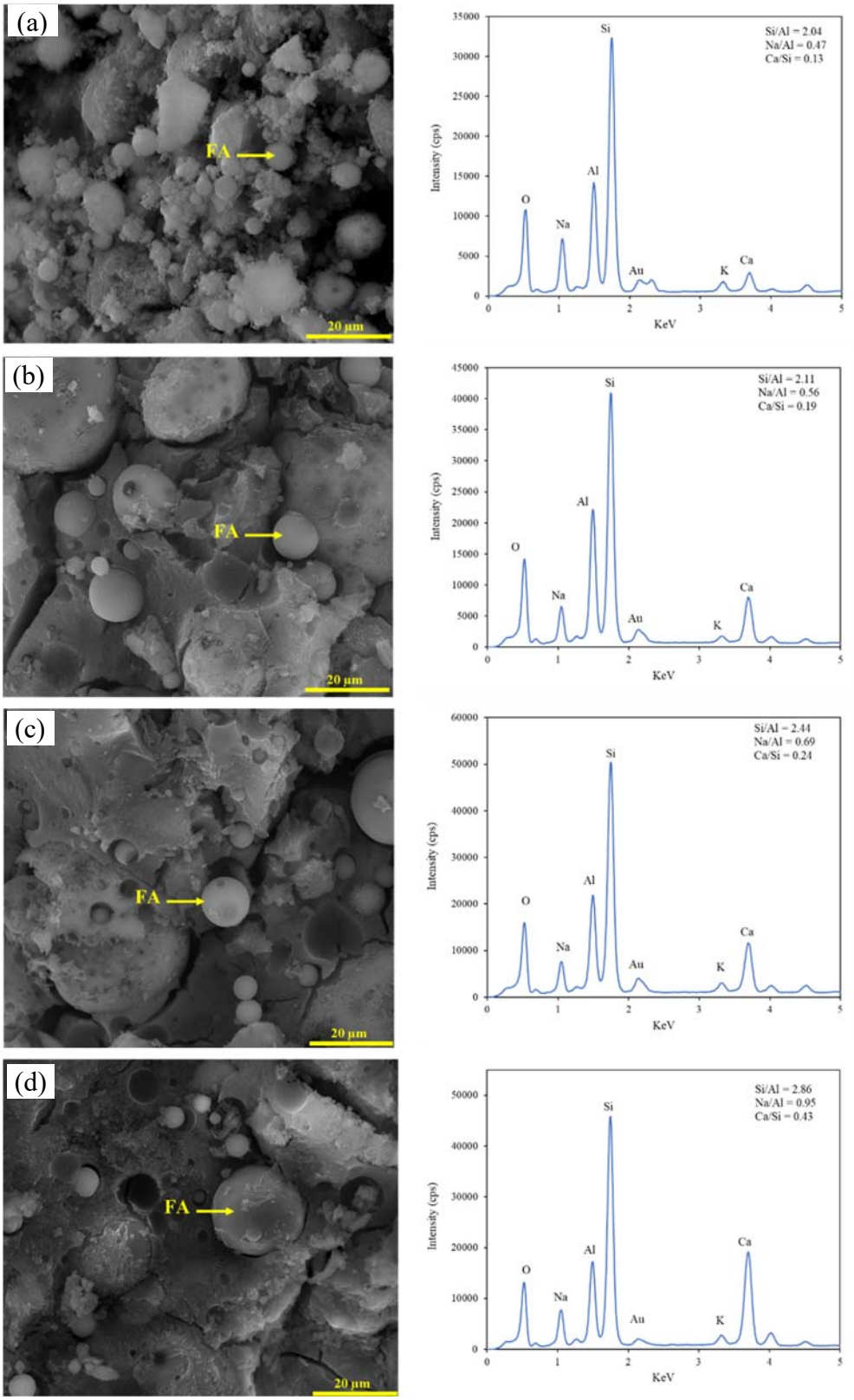

Fig. 25: SEM micrographs of cementitious material at different CKD contents and with the same W/S = 0.50, 1 wt.% SP, 0 wt.% BP, and cured at 35 °C for 7 days: (a) 0 wt.% CKD; (b) 10 wt.% CKD; (c) 15 wt.% CKD; and (d) 20 wt.% CKD.

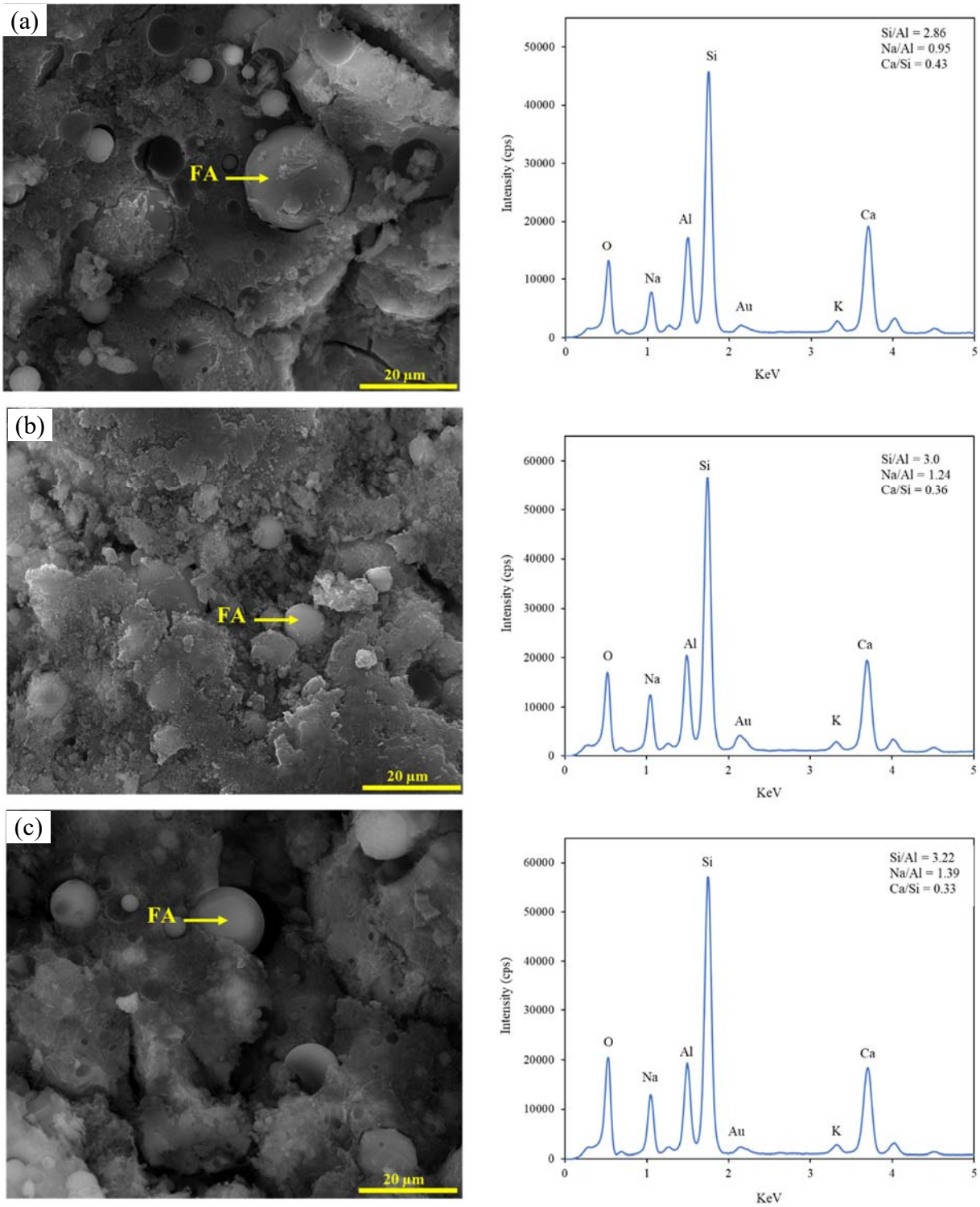

Fig. 26: SEM micrographs of cementitious material at different W/S ratios and with the same 20 wt.% CKD, 1 wt.% SP, 0 wt.% BP, and cured at 35 °C for 7 days: (a) W/S = 0.50; (b) W/S = 0.55; and (c) W/S = 0.60.

Table 3: Si/Al, Na/Al and Ca/Si ratios of cementitious material at different CKD contents and W/S ratios, the same 1 wt.% SP, 0 wt.% BP, and cured at 35 °C for 7 days.

	CKD (wt.%) / W/S ratio					
	0 / 0.50	10 / 0.50	15 / 0.50	20 / 0.50	20 / 0.55	20 / 0.60
Si/Al	2.04	2.11	2.44	2.86	3.00	3.22
Na/Al	0.47	0.56	0.69	0.95	1.24	1.39
Ca/Si	0.13	0.19	0.24	0.43	0.36	0.33

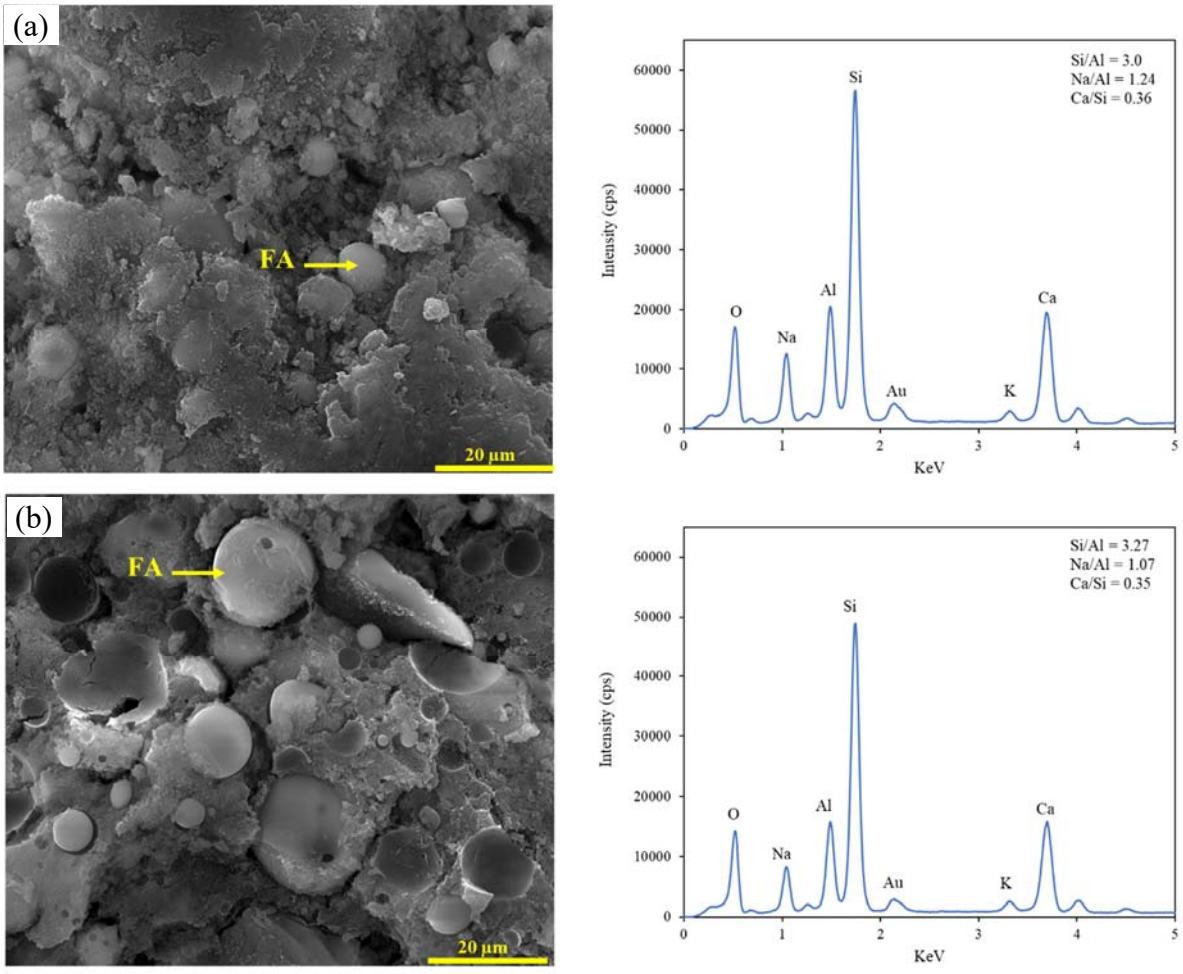

Fig. 27: SEM micrographs of cementitious material at 0 and 0.3 wt.% CAR and with the same 20 wt.% CKD, W/S = 0.55, 1 wt.% SP, and cured at 35 °C for 7 days: (a) 0 wt.% CAR; and (b) 0.3 wt.% CAR.

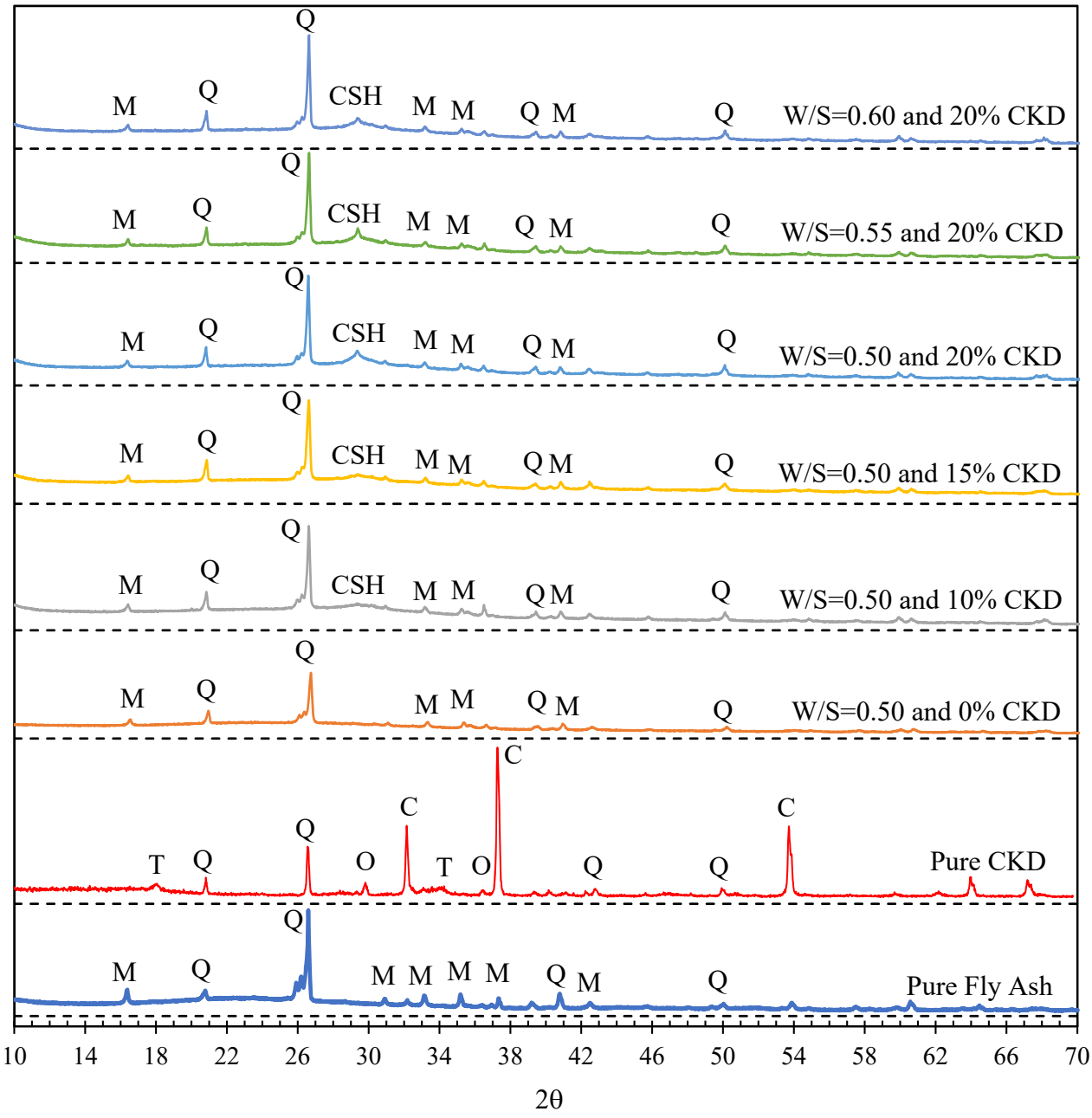

Fig. 28: XRD patterns of unreacted fly ash, pure CKD, and cementitious material at different CKD contents and W/S ratios, the same 1 wt.% SP, 0 wt.% BP, and cured at 35 ˚C for 7 days (M: $Al_{2.272}O_{4.864}Si_{0.728}$, Q: SiO_2, C: CaO, O: $CaCO_3$, T: $Ca(OH)_2$, CSH: calcium silicate hydrate).

6.0 Technology Readiness Assessment

This section describes the protocol for advancing the developed technology to a working prototype level. To this end, the results of the systematic proof-of-concept experimental study of the novel hybrid geopolymer-biopolymer cementitious material are first summarized. Then, a preliminary demonstration and validation based on testing of small size bagged cylinder specimens prepared with the developed hybrid cementitious material is presented. Finally, a prototype development plan for advancing the proof-of-concept to a fully functional working prototype is oulined.

6.1 Summary of proof-of-concept experimental study results

To evaluate the proof-of-concept technology, systematic pumpability, setting time, unconfined compression tests were conducted on the hybrid cementitious material specimens at different conditions. SEM imaging and EDX and XRD analyses were also performed to study the microstructure and chemical composition of the hybrid cementitious material. The pumpability of the two streams were evaluated through viscosity tests. SP was used to adjust and control the pumpability of stream 1. The results show that increasing water content or SP dosage improves the pumpability of stream 1. At 20 wt.% CKD, stream 1 with W/S = 0.55 or 0.6 and 1 or 2 wt.% SP is pumpable even 2 hours after mixing. To be conservative for the pumpability of stream 1, W/S = 0.60 with 2 wt.% SP is suggested. Stream 2 is an alkaline solution prepared with 5 M NaOH and SS/SH = 1 containing a very low dosage (≤ 0.5 wt.%) of BP and thus can be easily pumped. CKD as a high calcium content material was used to adjust and control the setting time of the low-calcium FA based geopolymer. The results show that inclusion of 20 wt.% CKD can provide the required short initial and final setting time. The added BP essentially does not affect the setting time due to the very low dosage used.

BP (carrageenan, gellun gum, or cellulose nanofibers) was used to enhance the mechanical properties of the cementitious material. It is found that by incorporating BP, the peak strength is slightly decreased but the residual strength is significantly increased. The maximum residual strength is obtained at 0.3 wt.% carrageenan, 0.3 wt.% gellun gum, and 0.5 wt.% cellulose nanofibers, respectively. The results also show that the peak UCS of the hybrid GP-BP cementitious material at proposed dosages is much higher than that of the cementitious material currently used in practice.

6.2 Preliminary small-scale demonstration and validation

As a preliminary demonstration and validation, small size (152.4 mm diameter and 304.8 mm height) cylinder specimens with no bag, with bag, and with bag and plastic cable ties outside the bag were produced and tested (Fig. 29). The bags were manufactured using polyester fabric and the plastic cable ties were used to partially represent the reinforcement wires of crib bags used in practice. Considering the scope of work, only the hybrid cementitious material with 20 wt.% CKD, W/S = 0.60, 2 wt.% SP, and 0 or 0.3 wt.% CAR was prepared for producing the cylinder specimens. Unconfined compression tests were conducted on the cylinder specimens following ASTM C39/C39M. (2016) with the Test Mark CM-3000 machine (Fig. 30) at a loading rate of 0.25 MPa/sec.

Fig. 31 shows the axial stress-strain curves of the 0 wt.% CAR specimen with no bag, the 0.3 wt.% CAR specimen with no bag, the 0.3 wt.% CAR specimen with bag, and the 0.3 wt.% CAR specimen with bag and plastic cable ties. For the two specimens with no bag, the incorporation of

biopolymer resulted in a slight decrease in the peak UCS but an increase in the residual UCS. With inclusion of 0.3 wt.% CAR, the peak UCS slightly deceased from 9.66 MPa to 9.11 MPa but the residual UCS at 13% strain increased from 0.09 MPa to 0.19 MPa. With the utilization of bag and plastic cable ties, both the peak UCS and residual UCS increased significantly. Specifically, the peak UCS increased from 9.66 MPa to 14.1 MPa (with only bag) and 12.5 MPa (with bag and plastic cable ties) and the residual UCS at 13% strain increased from 0.19 MPa to 3.87 MPa (with only bag) and 4.0 MPa (with bag and plastic cable ties), respectively. The effect of the external reinforcement from the plastic cable ties on the peak and residual strength was not significant possibly because the plastic cable ties were not so stiff as the metal wires used in real crib bags and failed during the test (see Fig. 32b). However, the plastic cable ties decreased the sudden drop of stress right after the peak as clearly shown in the figure. It is also noted that the bag failed along the sewing line, indicating that the string used for sewing the fabric was not strong enough.

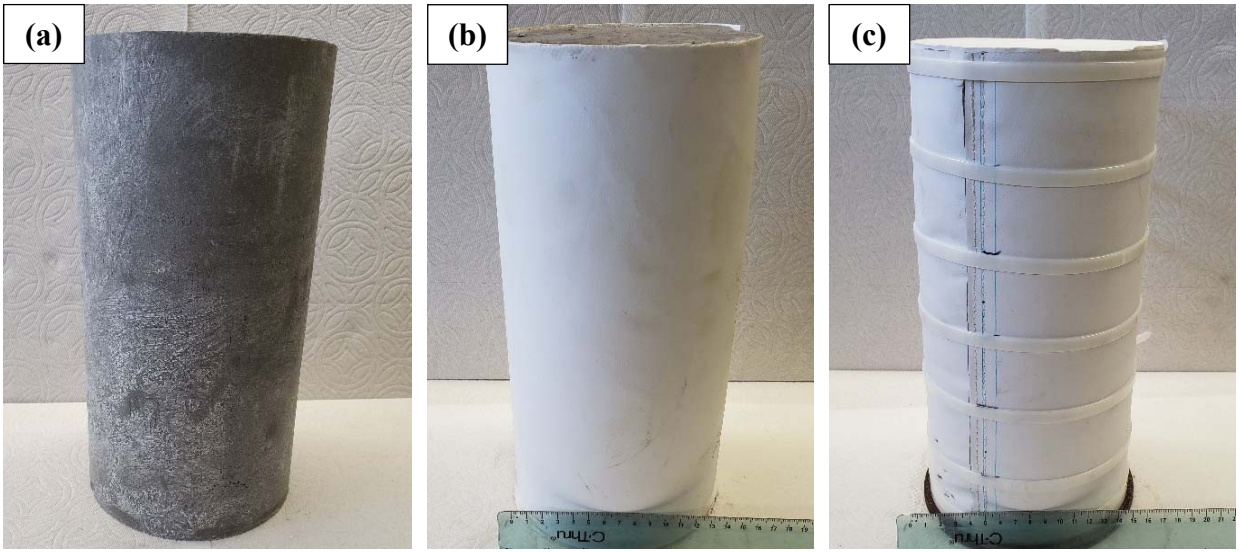

Fig. 29: Small size hybrid cementitious material cylinder specimens with 5 M NaOH, SS/SH = 1, 20 wt.% CKD, 2 wt.% SP, 0.3 wt.% CAR, and cured at 35 °C: (a) with no bag; (b) with bag; and (c) with bag and plastic cable ties.

As a comparison, Fig. 33 shows the stress-strain curve of the small size 0.3 wt.% CAR specimen with bag and plastic cable ties and those of full size crib bag specimens currently used in practice from Barczak and Tadolini (2008), and Heitzman (2001) and Jennmar (2013). As can be clearly seen, the 0.3 wt.% CAR specimen with bag and plastic cable ties and containing the hybrid GP-BP cementitious material has significantly higher peak strength than the full size crib bag specimens currently used in practice. The residual strength of the former is also much higher than the later. It needs to be noted that the plastic cable ties are much more flexible than the metal wire reinforcement used in crib bag. Also, the 0.3 wt.% CAR specimen with bag and plastic cable ties is much smaller than the full size crib bag specimens. Therefore, it is important to produce smecimens using full size crib bags and the hybrid GP-BP cementitious material and test them so that the superior behavior of the new hybrid cementitious material is fully demonstrated and validated at prototype scale. This is further detailed in Section 6.3.

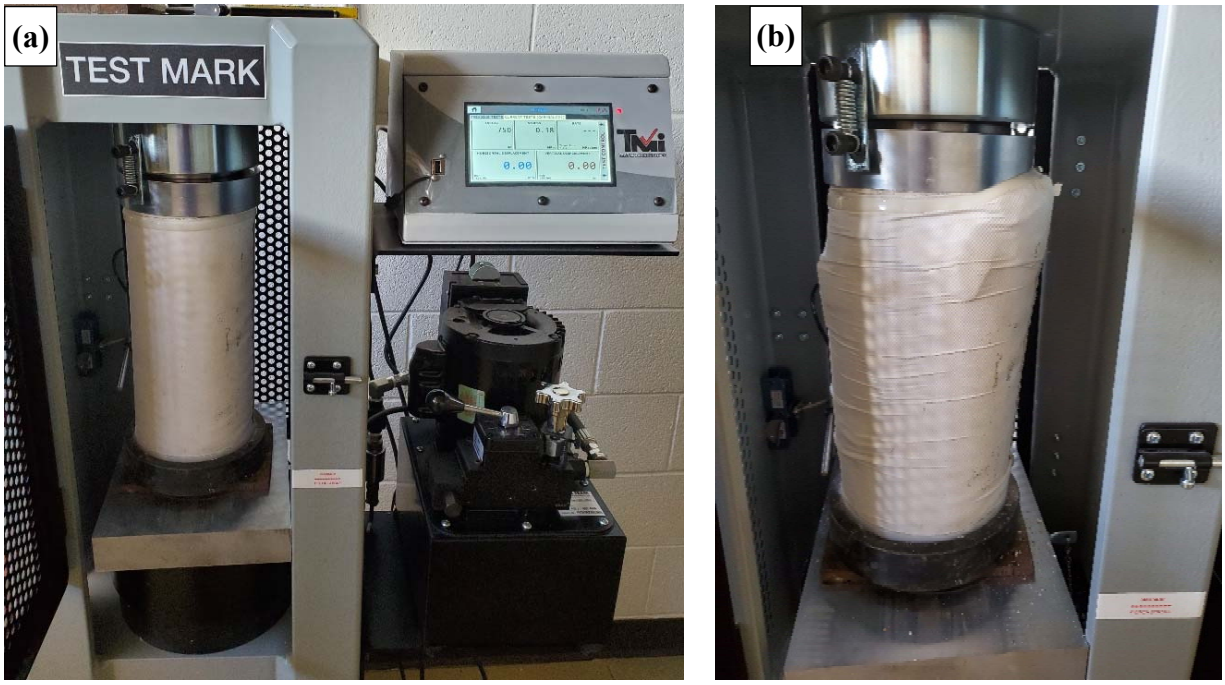

Fig. 30: (a) Test Mark CM-3000 machine for unconfined compression test; and (b) Bagged specimen right after test.

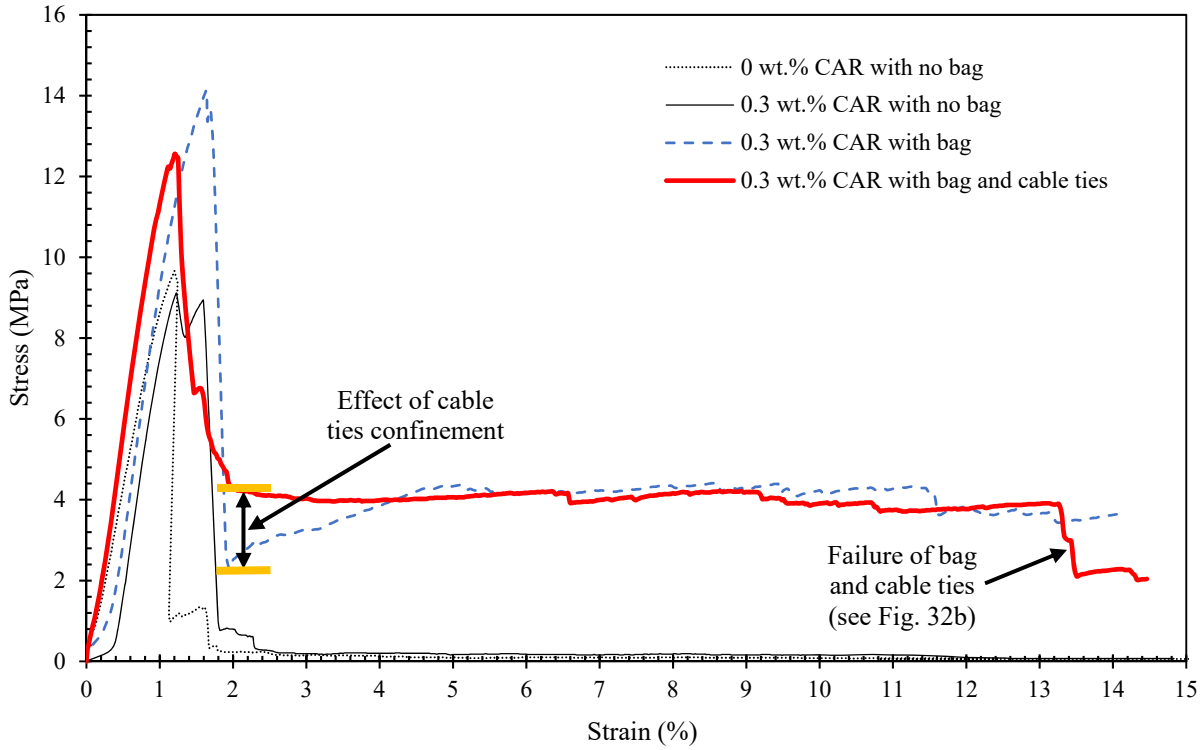

Fig. 31: Stress-strain curves of small hybrid cementitious material cylinder specimens.

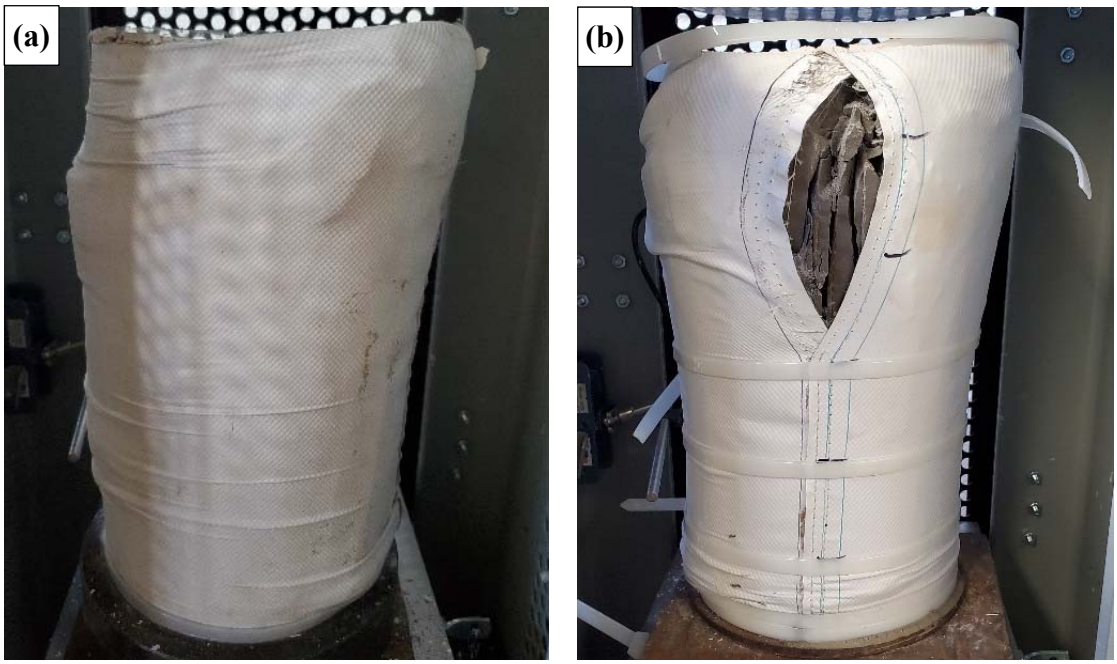

Fig. 32: Small size bagged hybrid cementitious material cylinder specimens with 5 M NaOH, SS/SH = 1, 20 wt.% CKD, 2 wt.% SP, 0.3 wt.% CAR, and cured at 35 °C after failure: (a) with polyester bag; and (b) with polyester bag and plastic cable ties.

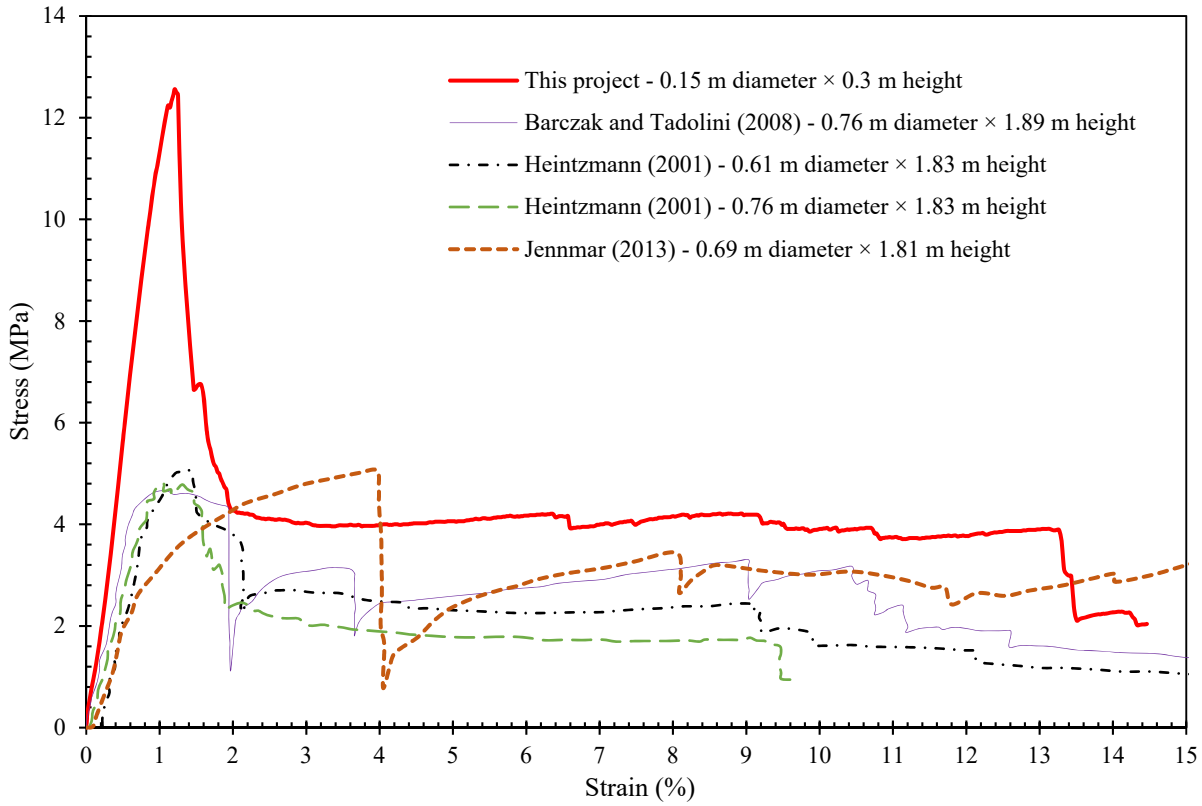

Fig. 33: Comparison of stress-strain curves of the small size 0.3 wt.% CAR specimen with polyester bag and plastic cable ties in this project with those of full size crib bag specimens used in practice.

6.3 Prototype development plan

The systematic proof-of-concept laboratory investigations and the small-scale demonstration and validation together clearly show the superior behavior of the new hybrid cementitious material for enhancing pumpable roof support. But how the new hybrid cementitious material will behave at prototype still needs to be evaluated. With the new technology completely ready for prototype development, a prototype development plan has been prepared to advance the technology to a fully functional working prototype, including large-scale demonstration and validation tests at the University of Arizona (UA) and the NIOSH Mine Roof Simulator (MRS) Laboratory, collaborations with Jennmar Corporation and mine companies, and working closely with the technology transfer department at UA, as detailed below.

- First, full size crib bag specimens will be produced using the new hybrid geopolymer-biopolymer cementitious material and tested with the MTS 810 materials testing setup at the University of Arizona (Fig. 34). This will provide a first step full scale demonstration and validation. We have already discussed potential full-scale tests with Jennmar Corporation, and they are very interested and will be willing to provide crib bags for producing the full-size crib bag specimens.

Fig. 34: MTS 810 materials testing setup.

- Second, the new hybrid geopolymer-biopolymer cementitious material will be tested and demonstrated in a simulated and controllable operational environment using the NIOSH Mine Roof Simulator (MRS). NIOSH investigators have used the MRS to test a large number of pumpable roof supports constructed with the current CSA cement and Portland cement. The

results show that both types of cements tend to be too brittle. Accordingly, the NIOSH investigators plan to study supports using less brittle cementitious materials than the two commonly used cements. We have already discussed with the MRS Laboratory about testing the new hybrid geopolymer-biopolymer cementitious material and they are very interested and willing to collaborate.

- Third, we will continue our successful collaborations with mining companies. They will provide suggestions, help and support related to the transfer of the new hybrid geopolymer-biopolymer cementitious material to mining practice.
- Fourth, we will work closely with Tech Launch Arizona, the technology transfer department at the University of Arizona, to commercialize the new hybrid geopolymer-biopolymer cementitious material and transfer it to real applications in mining practice. The PI has already established a close collaboration with Tech Launch Arizona and has been working with them to commercialize the mine tailings-based geopolymer cementitious material he developed and to file patents for his other inventions.

7.0 Appendices

This section presents the stress-strain curves from unconfined compression tests on hybrid cementitious material specimens at different conditions, including

- Figs. A1 – A3 about the effect of BP content,
- Figs. A4 – A6 about the effect of curing temperature, and
- Figs. A7 – A9 about the effect of curing time.

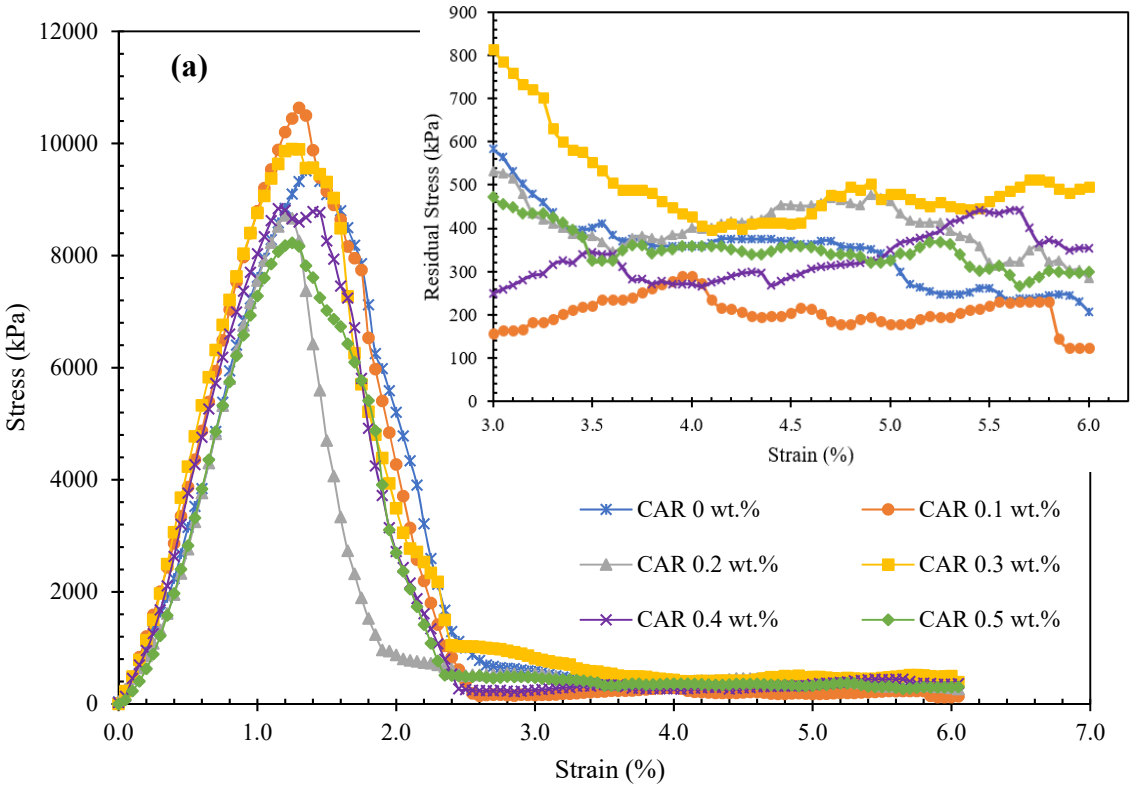
(a)
Stress (kPa)
Strain (%)
Residual Stress (kPa)
Strain (%)
CAR 0 wt.%
CAR 0.1 wt.%
CAR 0.2 wt.%
CAR 0.3 wt.%
CAR 0.4 wt.%
CAR 0.5 wt.%

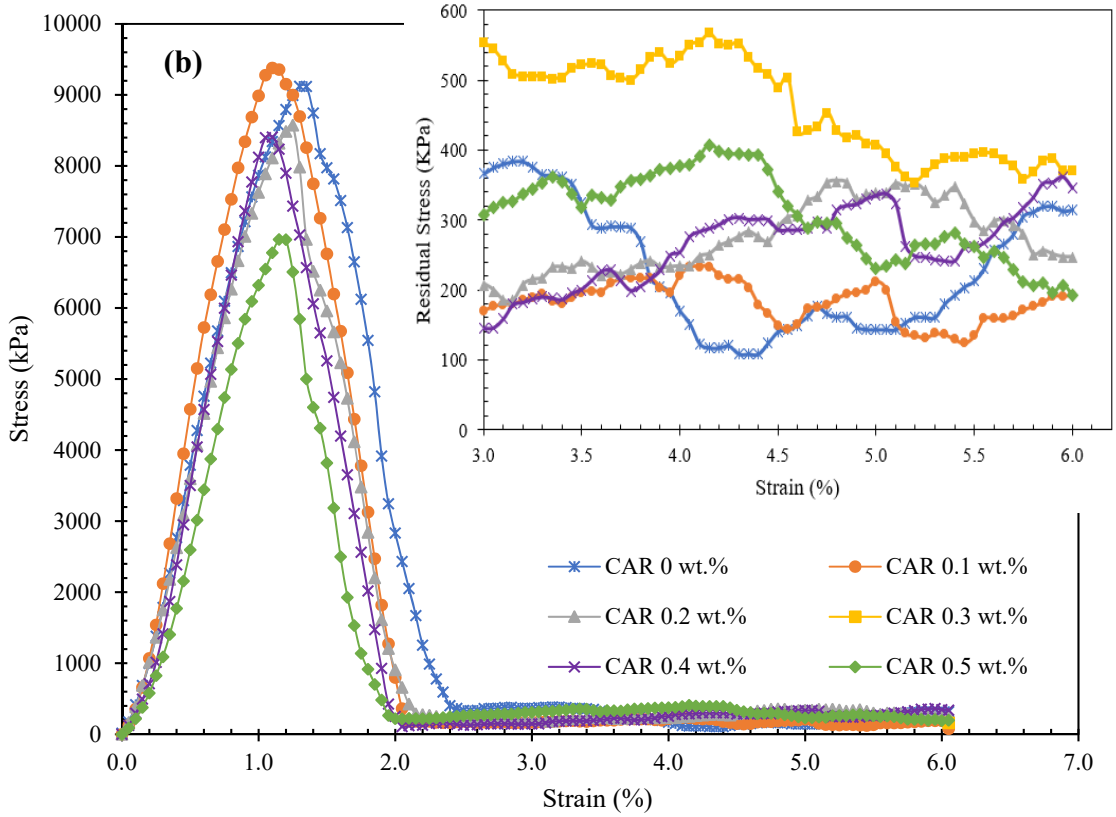
(b)
Stress (kPa)
Strain (%)
Residual Stress (KPa)
Strain (%)
CAR 0 wt.%
CAR 0.1 wt.%
CAR 0.2 wt.%
CAR 0.3 wt.%
CAR 0.4 wt.%
CAR 0.5 wt.%

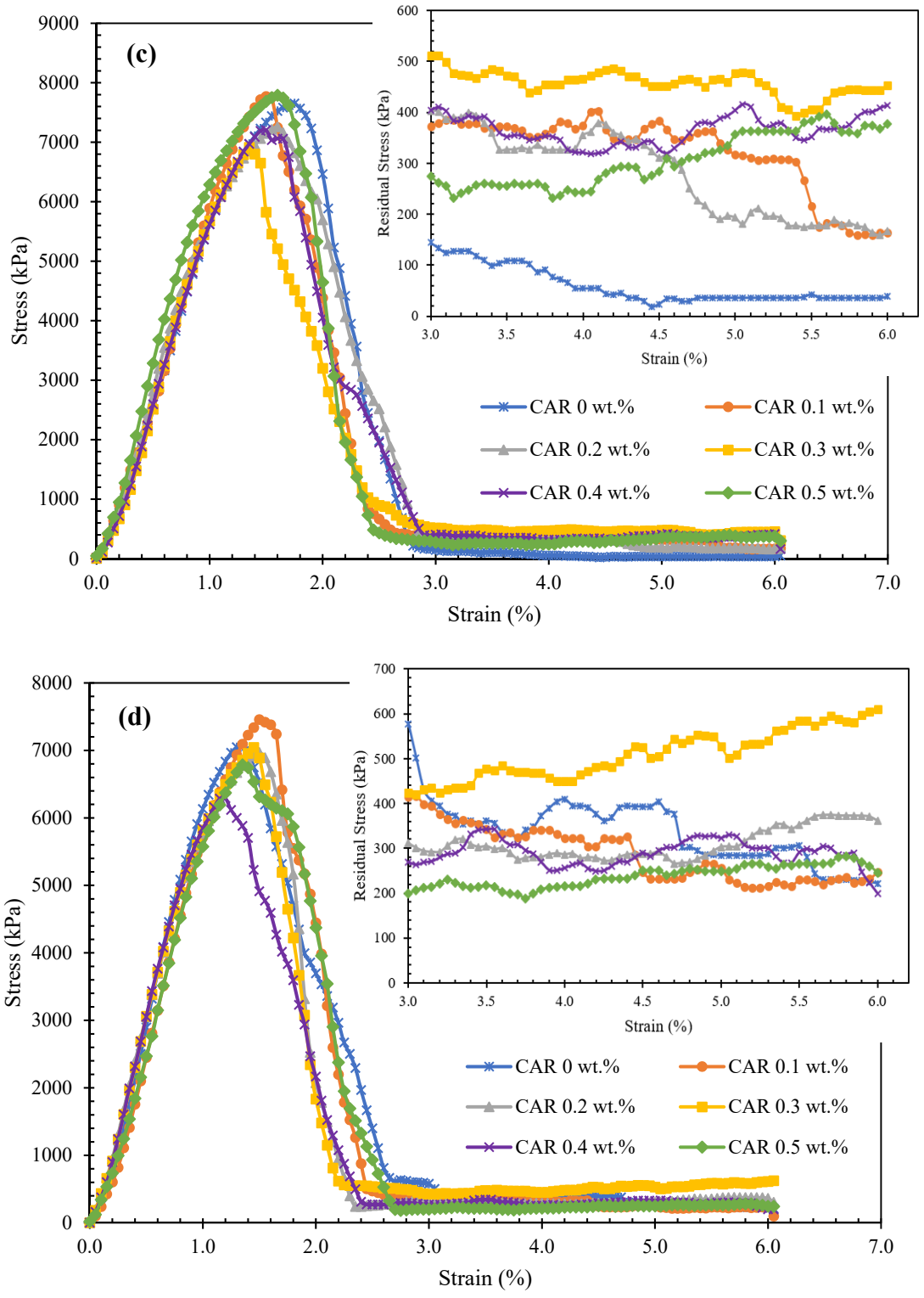

Fig. A1: Unconfined compression stress-strain curves of hybrid cementitious material specimens containing different amount of CAR and after 7 days' curing at 35 °C: (a) W/S = 0.55, SP = 1 wt.%; (b) W/S = 0.55, SP = 2 wt.%; (c) W/S = 0.60, SP = 1 wt.%; and (d) W/S = 0.60, SP = 2 wt.%.

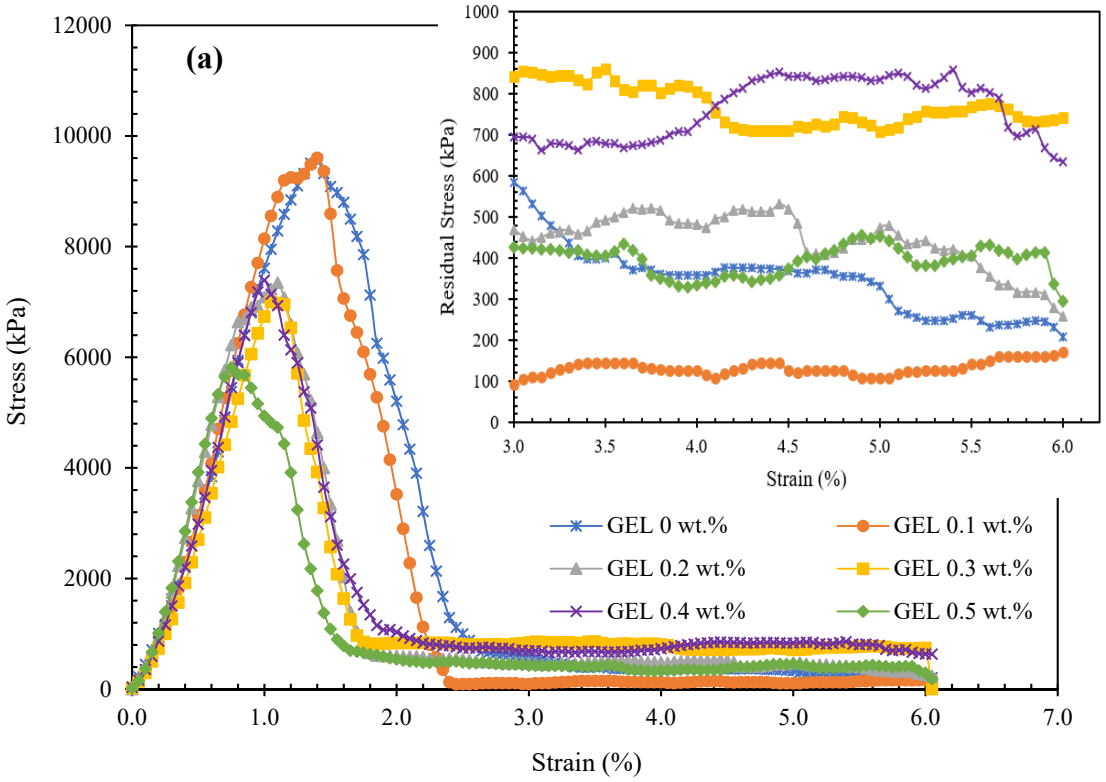
(a)
Stress (kPa)
Strain (%)
Residual Stress (kPa)
Strain (%)
GEL 0 wt.%
GEL 0.1 wt.%
GEL 0.2 wt.%
GEL 0.3 wt.%
GEL 0.4 wt.%
GEL 0.5 wt.%

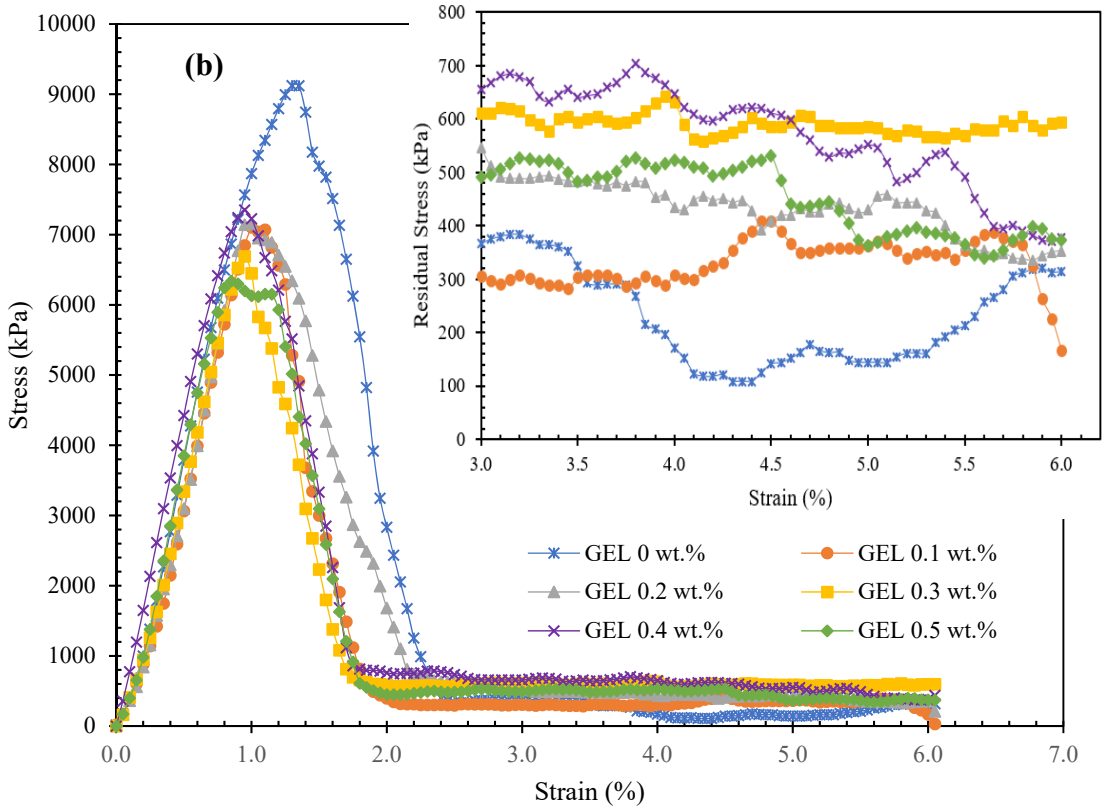
(b)
Stress (kPa)
Strain (%)
Residual Stress (kPa)
Strain (%)
GEL 0 wt.%
GEL 0.1 wt.%
GEL 0.2 wt.%
GEL 0.3 wt.%
GEL 0.4 wt.%
GEL 0.5 wt.%

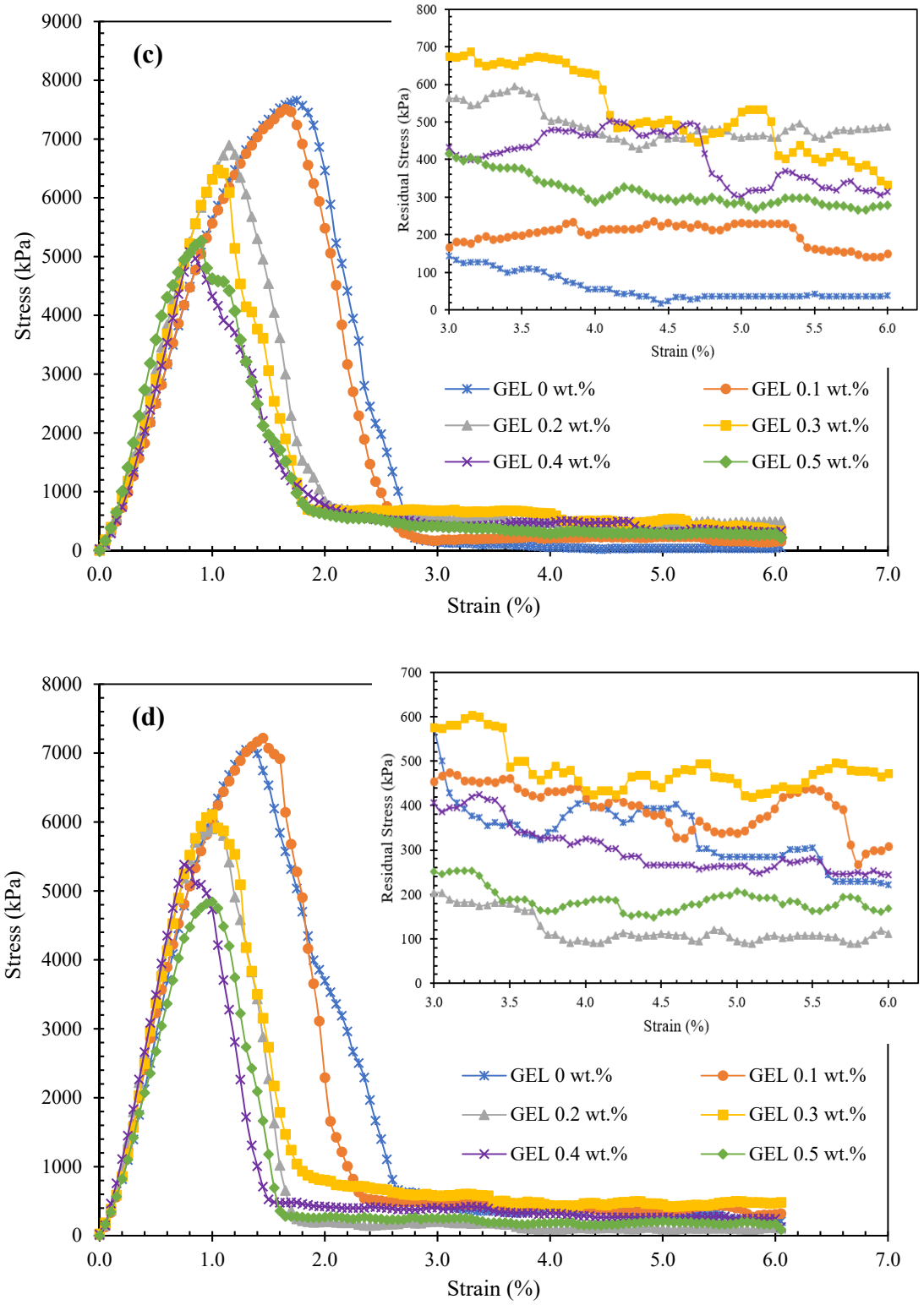

Fig. A2: Unconfined compression stress-strain curves of hybrid cementitious material specimens containing different amount of GEL and after 7 days' curing at 35 °C: (a) W/S = 0.55, SP = 1 wt.%; (b) W/S = 0.55, SP = 2 wt.%; (c) W/S = 0.60, SP = 1 wt.%; and (d) W/S = 0.60, SP = 2 wt.%.

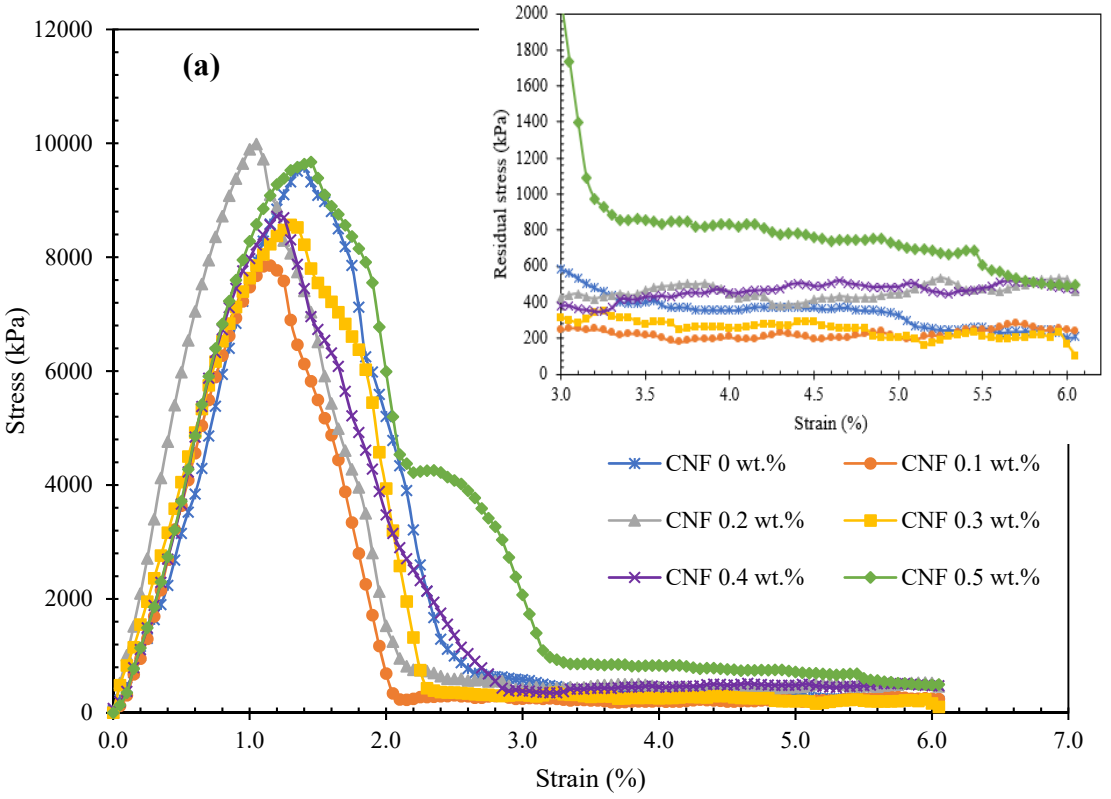
(a)
Stress (kPa)
Strain (%)
Residual stress (kPa)
CNF 0 wt.%
CNF 0.1 wt.%
CNF 0.2 wt.%
CNF 0.3 wt.%
CNF 0.4 wt.%
CNF 0.5 wt.%

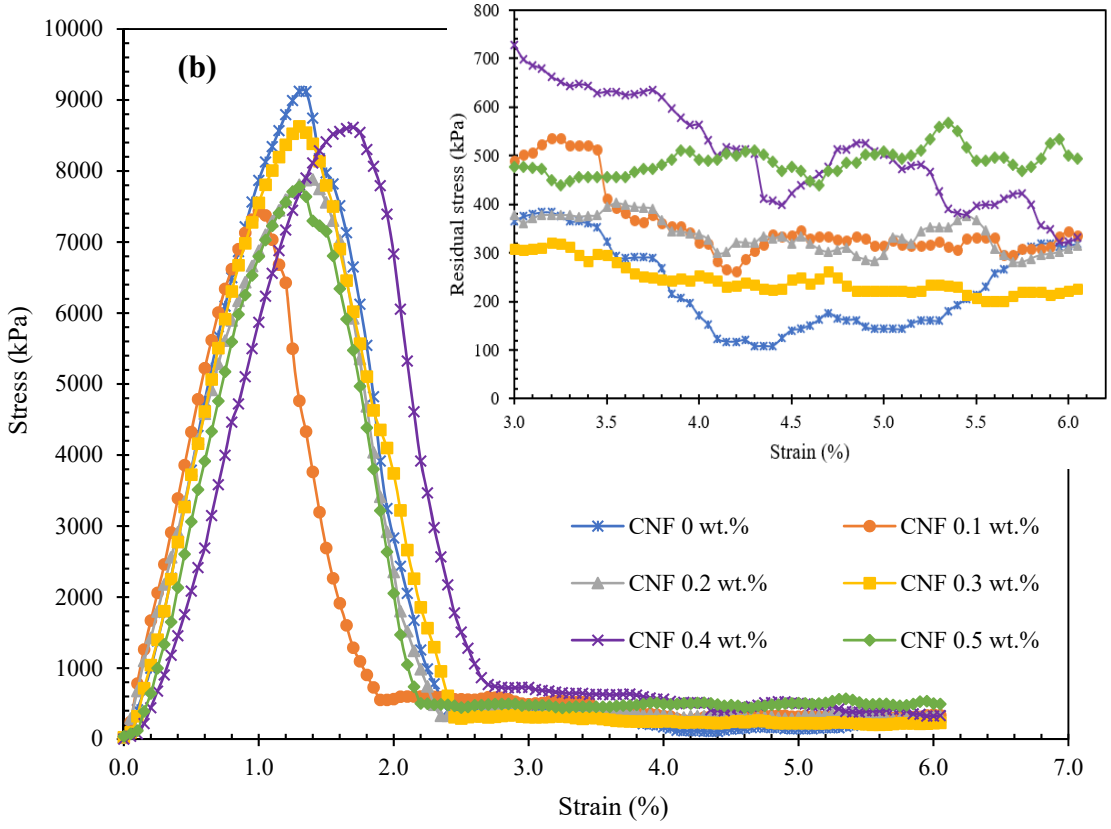
(b)
Stress (kPa)
Strain (%)
Residual stress (kPa)
CNF 0 wt.%
CNF 0.1 wt.%
CNF 0.2 wt.%
CNF 0.3 wt.%
CNF 0.4 wt.%
CNF 0.5 wt.%

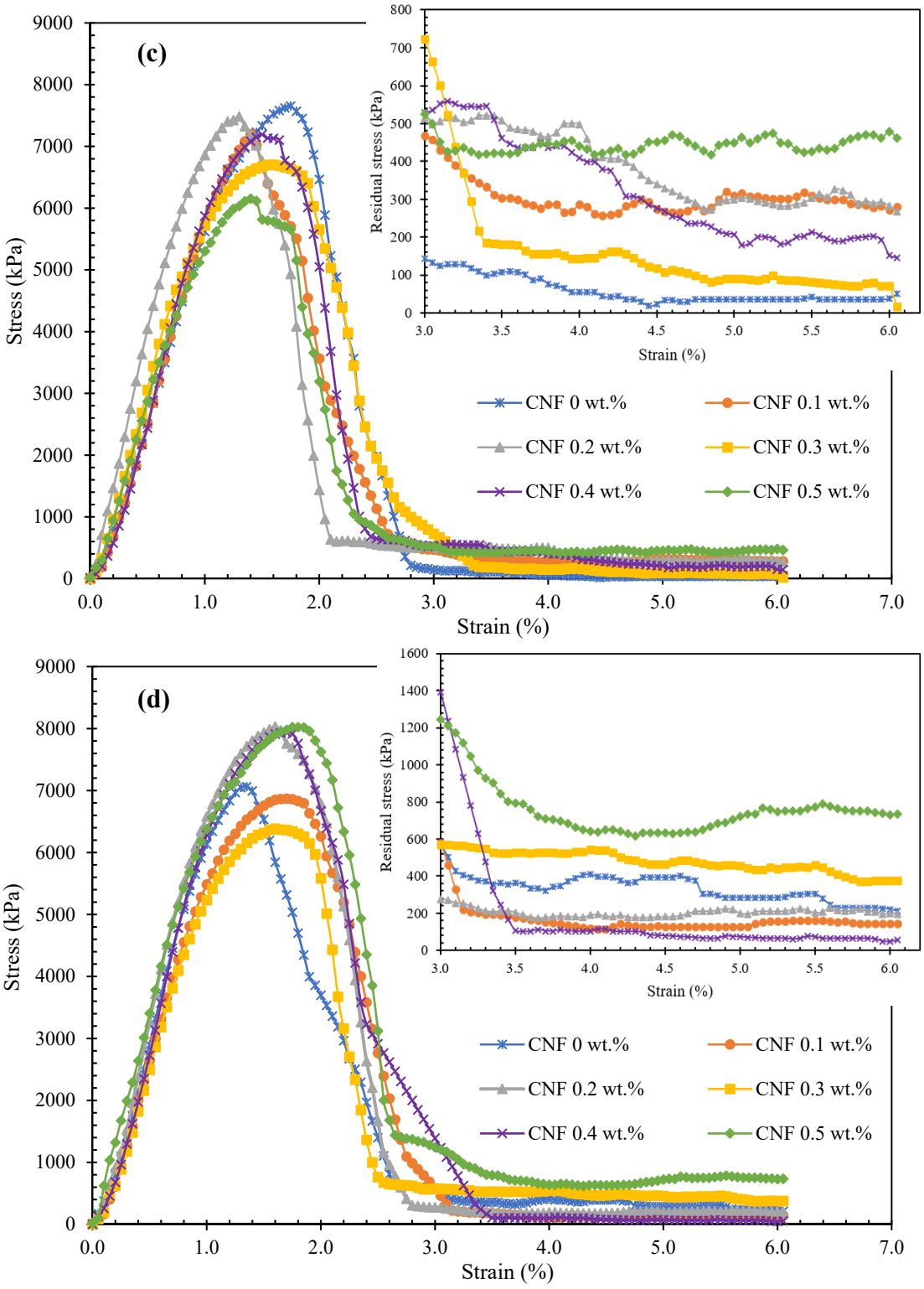

Fig. A3: Unconfined compression stress-strain curves of hybrid cementitious material specimens containing different amount of CNF and after 7 days' curing at 35 °C: (a) W/S = 0.55, SP = 1 wt.%; (b) W/S = 0.55, SP = 2 wt.%; (c) W/S = 0.60, SP = 1 wt.%; and (d) W/S = 0.60, SP = 2 wt.%.

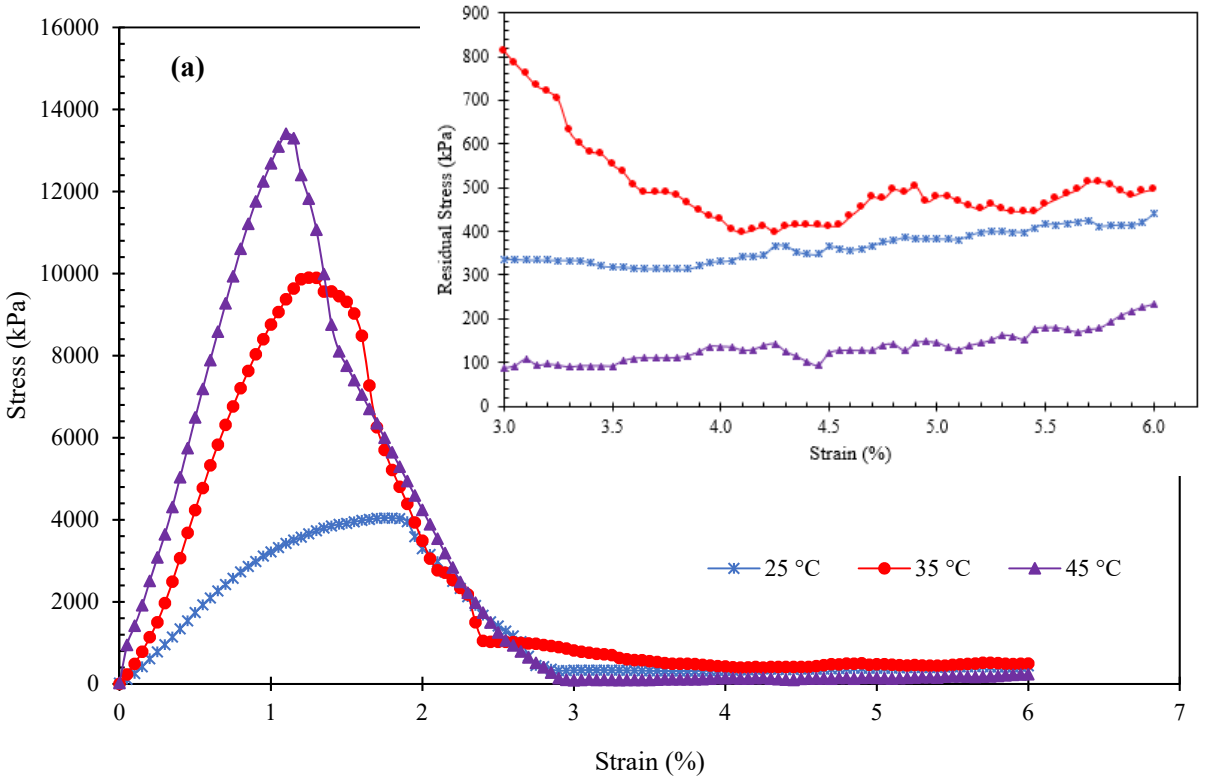
(a)
Stress (kPa)
Strain (%)
Residual Stress (kPa)
Strain (%)
25 °C
35 °C
45 °C

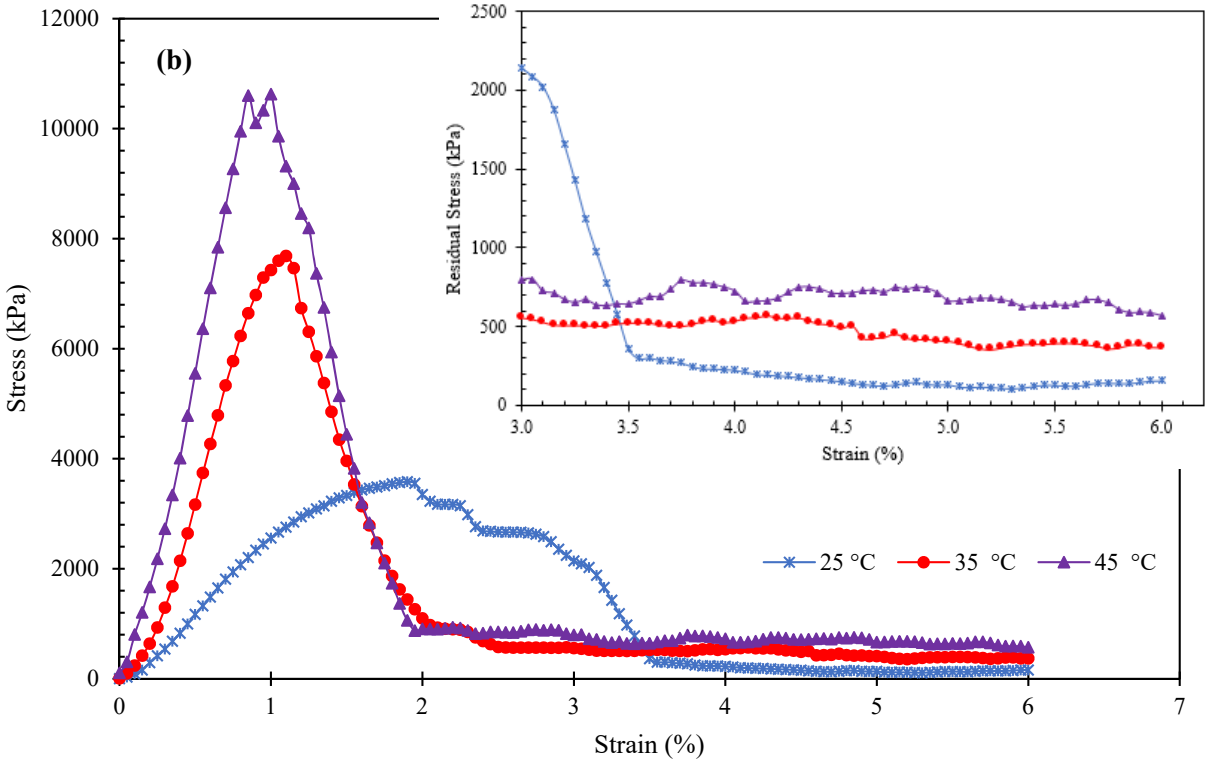
(b)
Stress (kPa)
Strain (%)
Residual Stress (kPa)
Strain (%)
25 °C
35 °C
45 °C

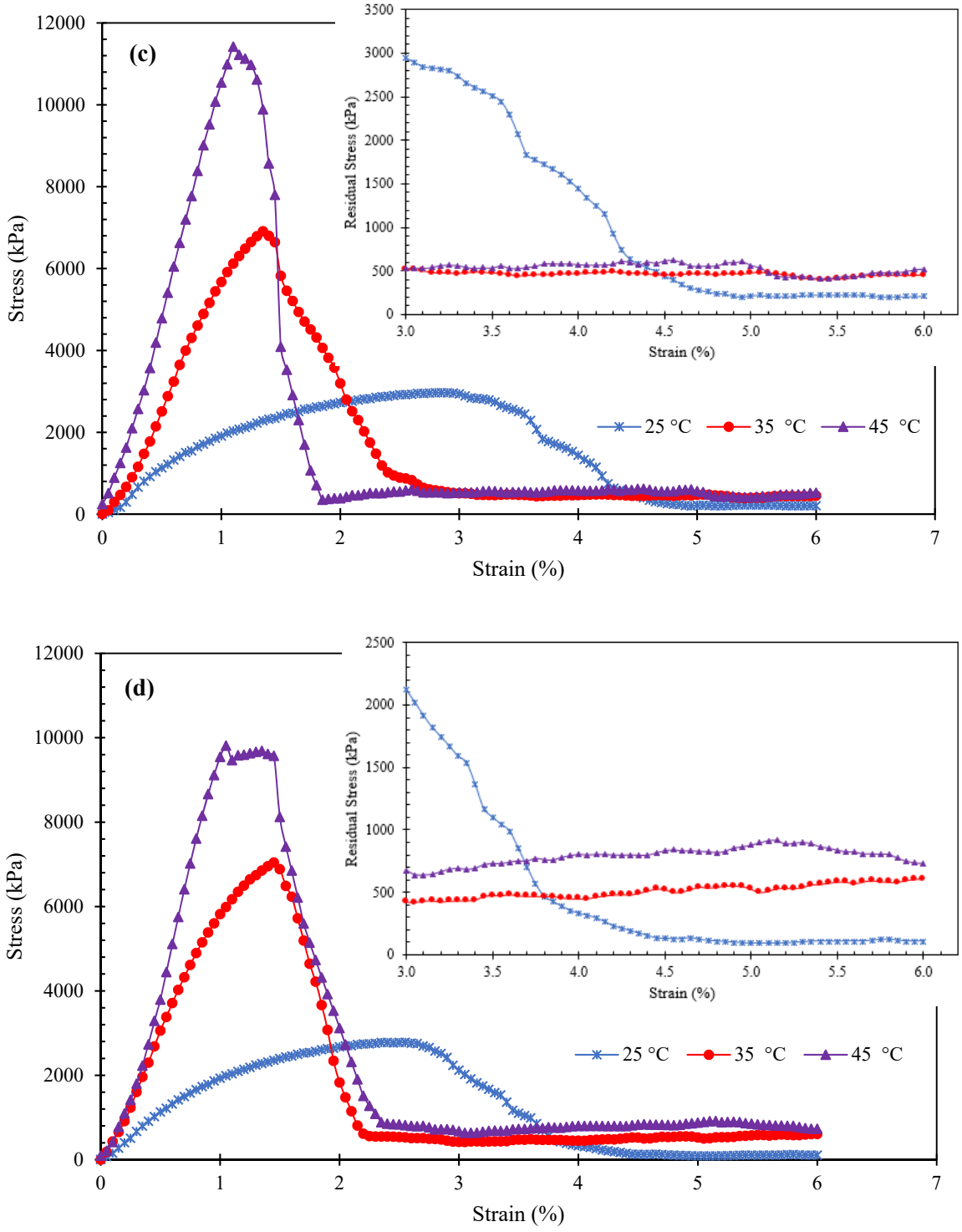

Fig. A4: Unconfined compression stress-strain curves of hybrid cementitious material specimens containing 20 wt.% CKD, 0.3 wt.% CAR and after 7 days' curing at different temperatures: (a) W/S = 0.55, SP = 1 wt.%; (b) W/S = 0.55, SP = 2 wt.%; (c) W/S = 0.60, SP = 1 wt.%; and (d) W/S = 0.60, SP = 2 wt.%.

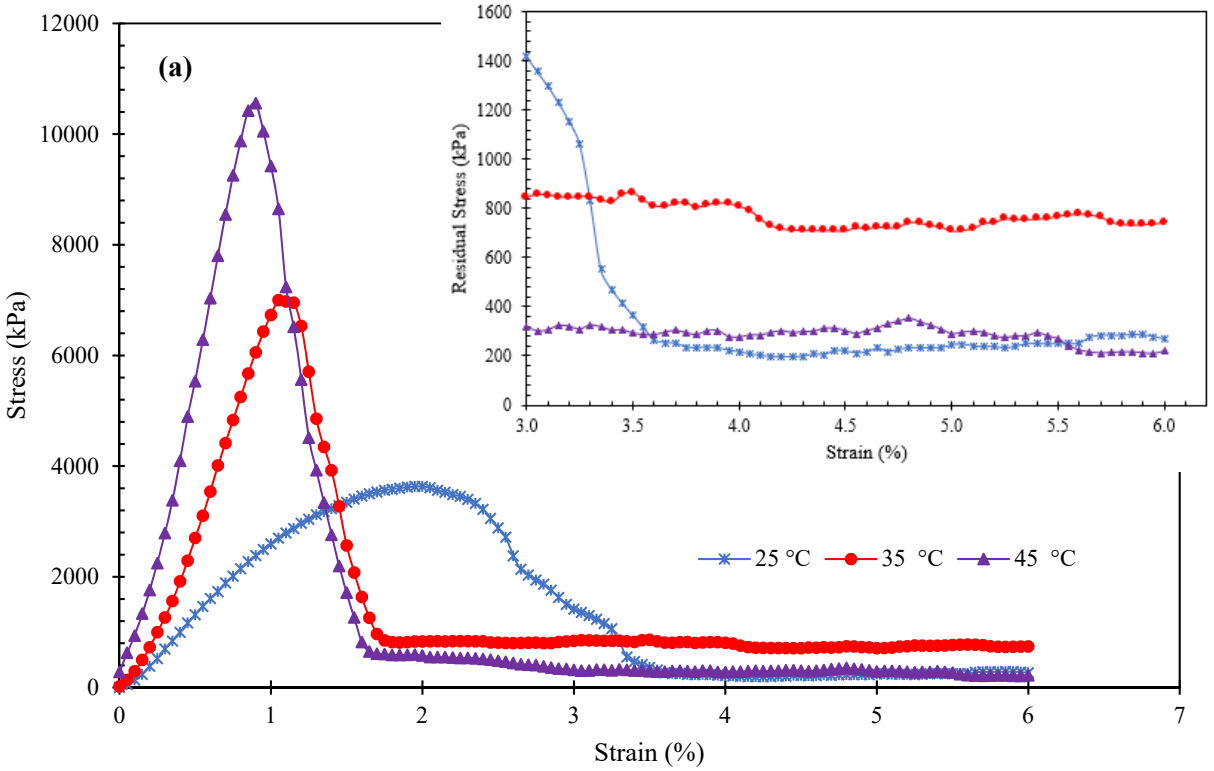
(a)
Stress (kPa)
Strain (%)
Residual Stress (kPa)
25 °C
35 °C
45 °C

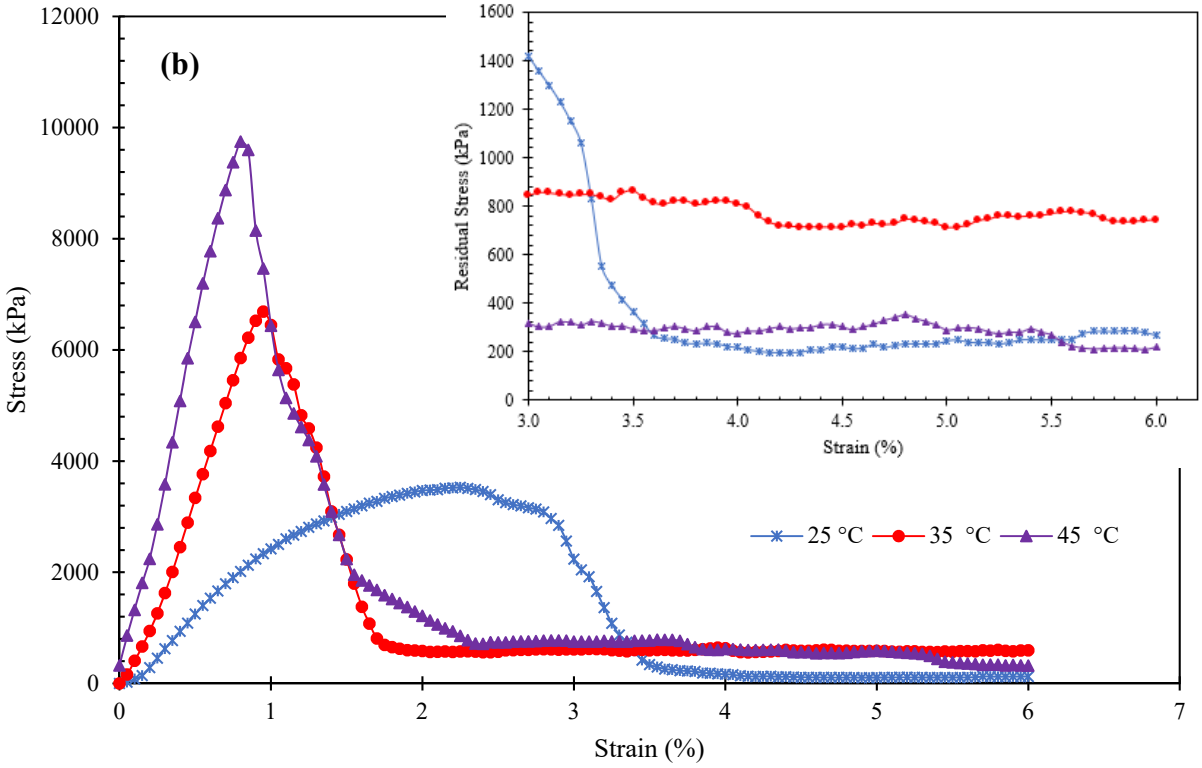
(b)
Stress (kPa)
Strain (%)
Residual Stress (kPa)
25 °C
35 °C
45 °C

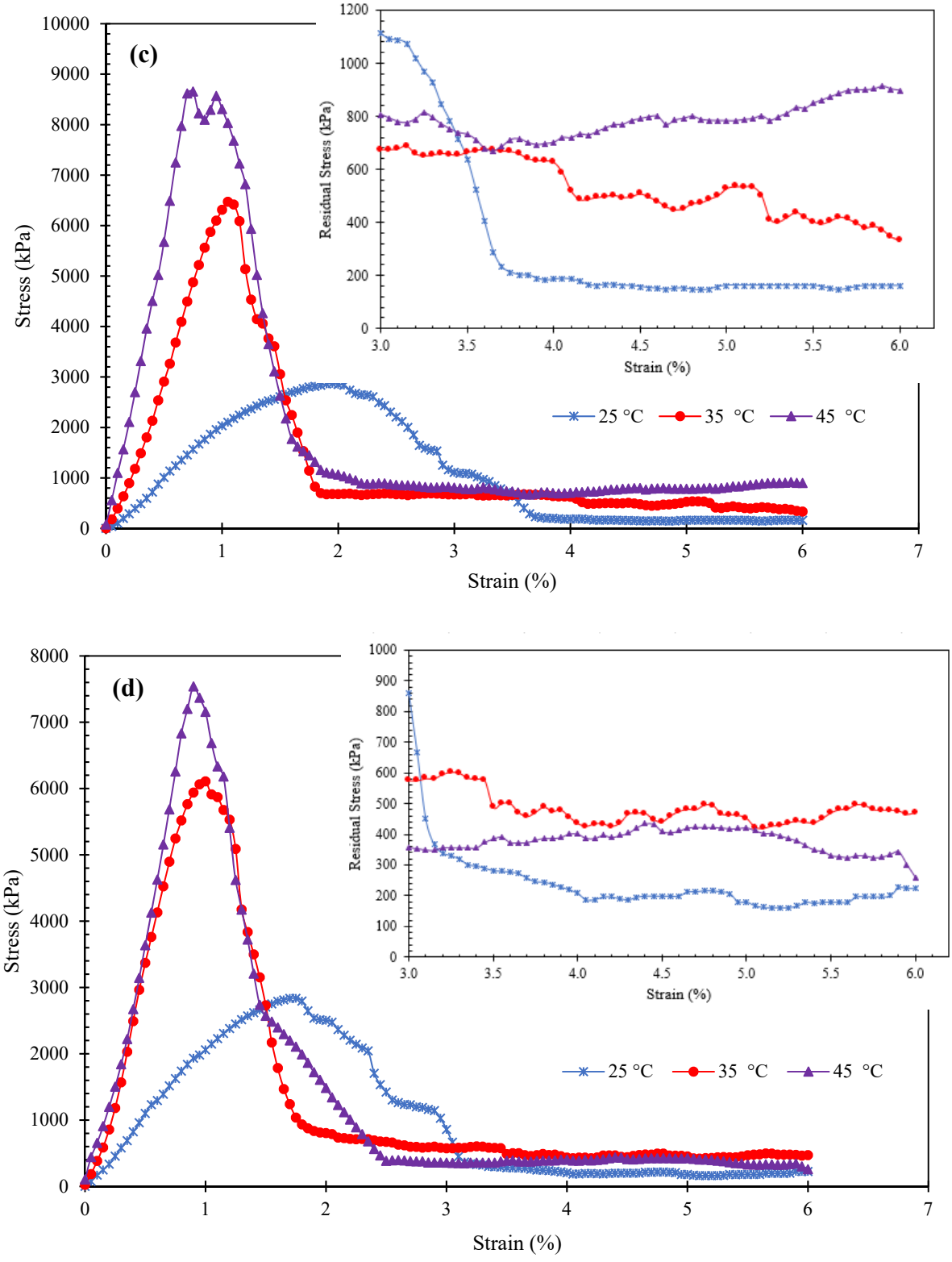

Fig. A5: Unconfined compression stress-strain curves of hybrid cementitious material specimens containing 20 wt.% CKD, 0.3 wt.% GEL and after 7 days' curing at different temperatures: (a) W/S = 0.55, SP = 1 wt.%; (b) W/S = 0.55, SP = 2 wt.%; (c) W/S = 0.60, SP = 1 wt.%; and (d) W/S = 0.60, SP = 2 wt.%.

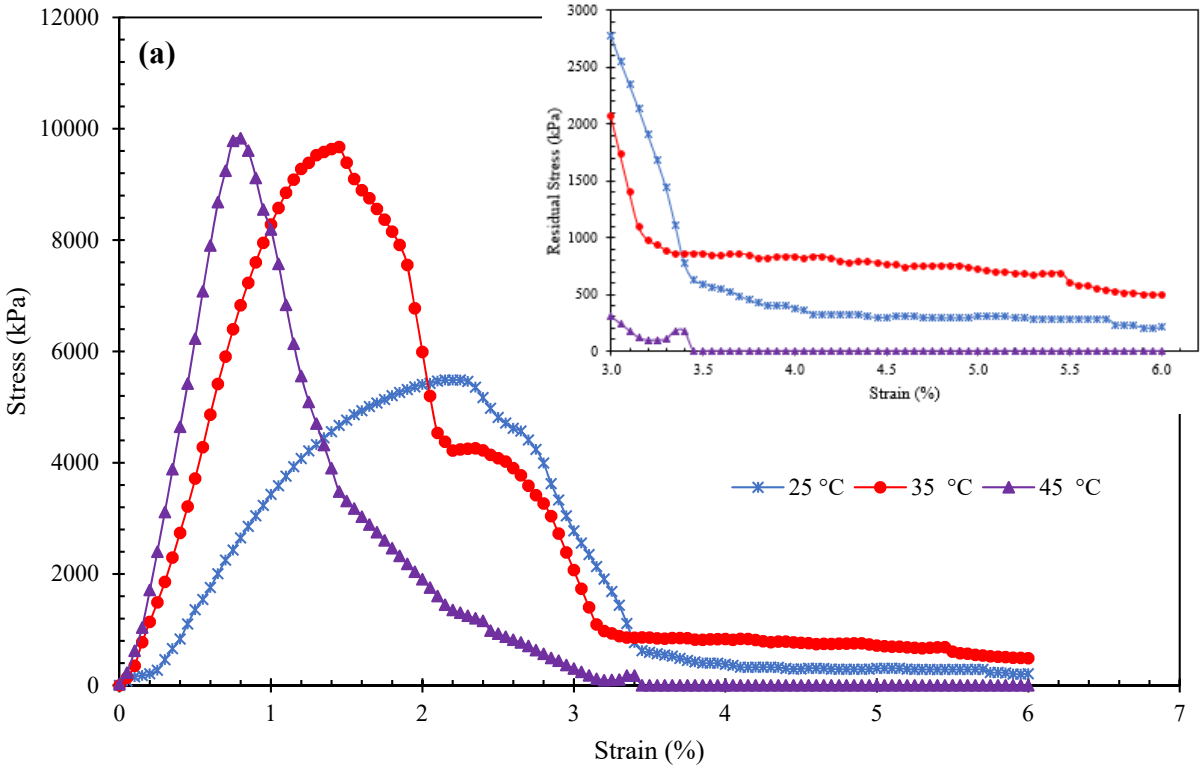
(a)
Stress (kPa)
Strain (%)
Residual Stress (kPa)
Strain (%)
25 °C
35 °C
45 °C

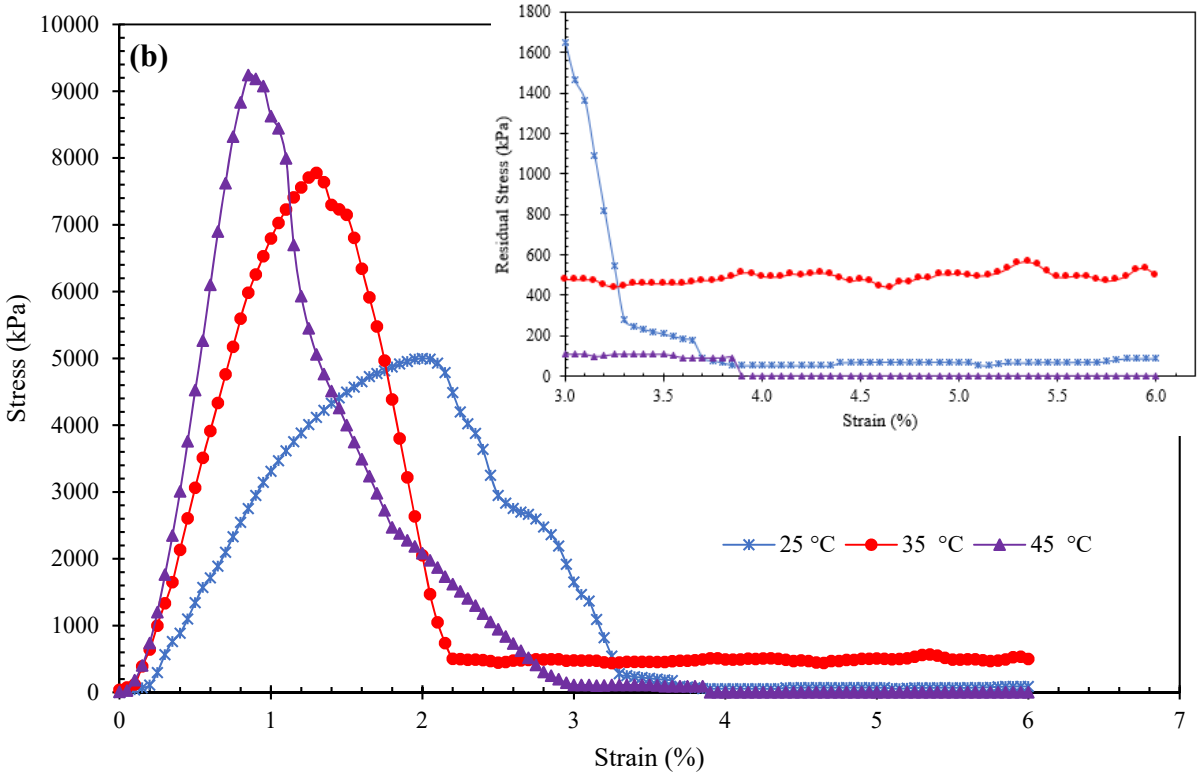
(b)
Stress (kPa)
Strain (%)
Residual Stress (kPa)
Strain (%)
25 °C
35 °C
45 °C

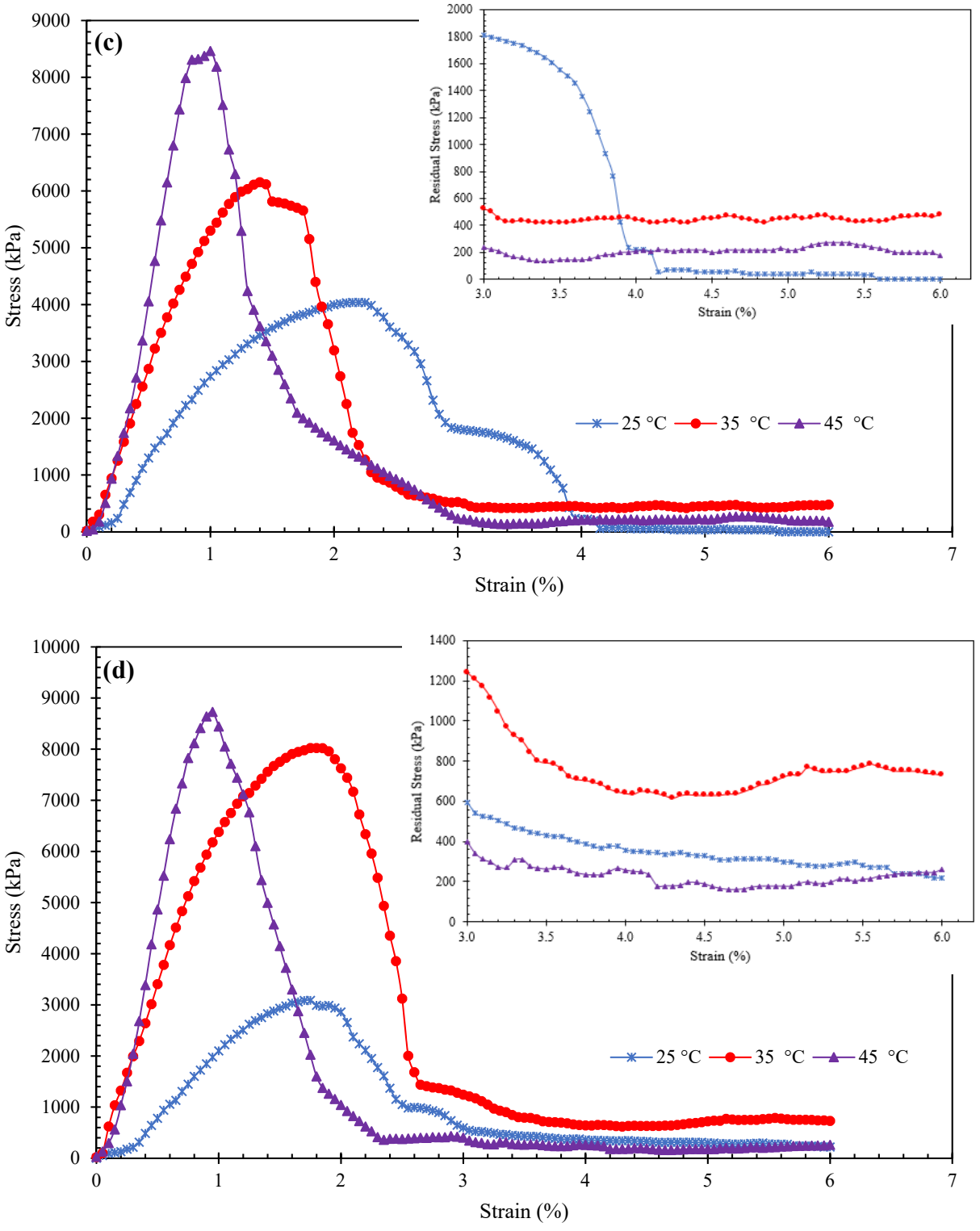

Fig. A6: Unconfined compression stress-strain curves of hybrid cementitious material specimens containing 20 wt.% CKD, 0.5 wt.% CNF and after 7 days' curing at different temperatures: (a) W/S = 0.55, SP = 1 wt.%; (b) W/S = 0.55, SP = 2 wt.%; (c) W/S = 0.60, SP = 1 wt.%; and (d) W/S = 0.60, SP = 2 wt.%.

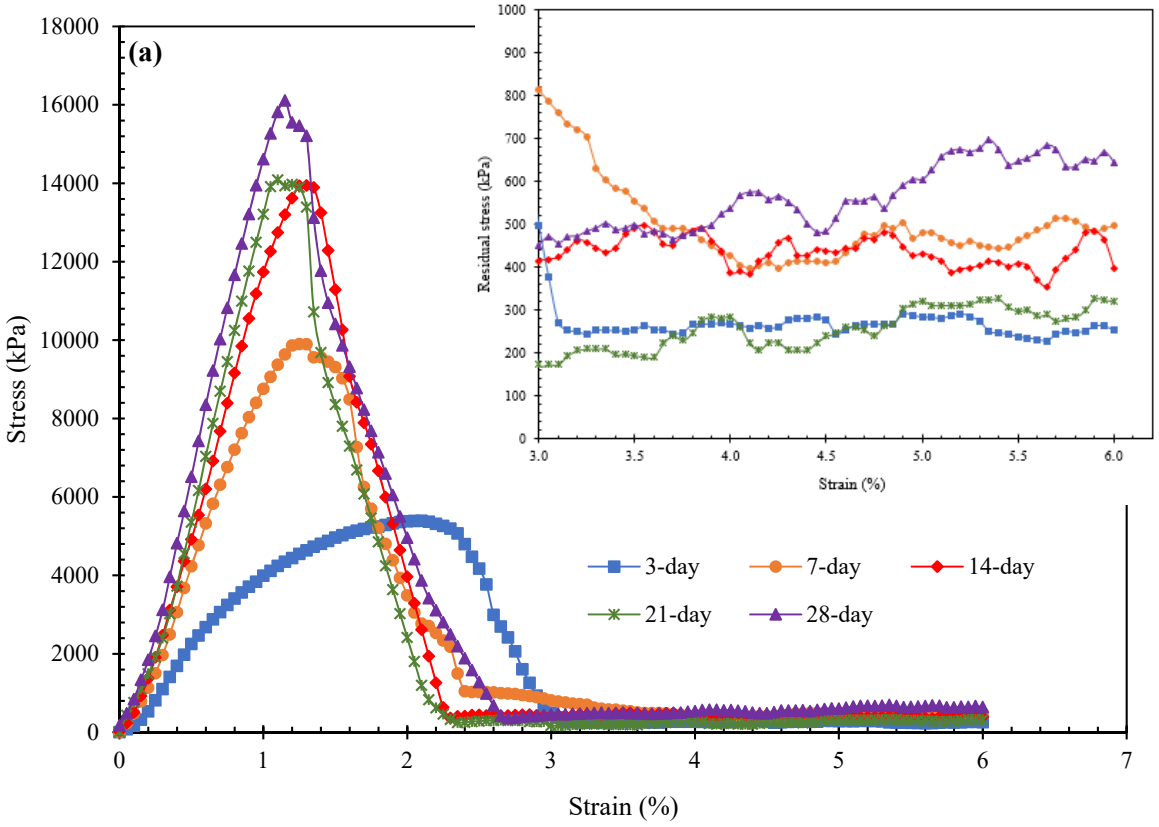
(a)
Stress (kPa)
Strain (%)
Residual stress (kPa)
Strain (%)
3-day
7-day
14-day
21-day
28-day

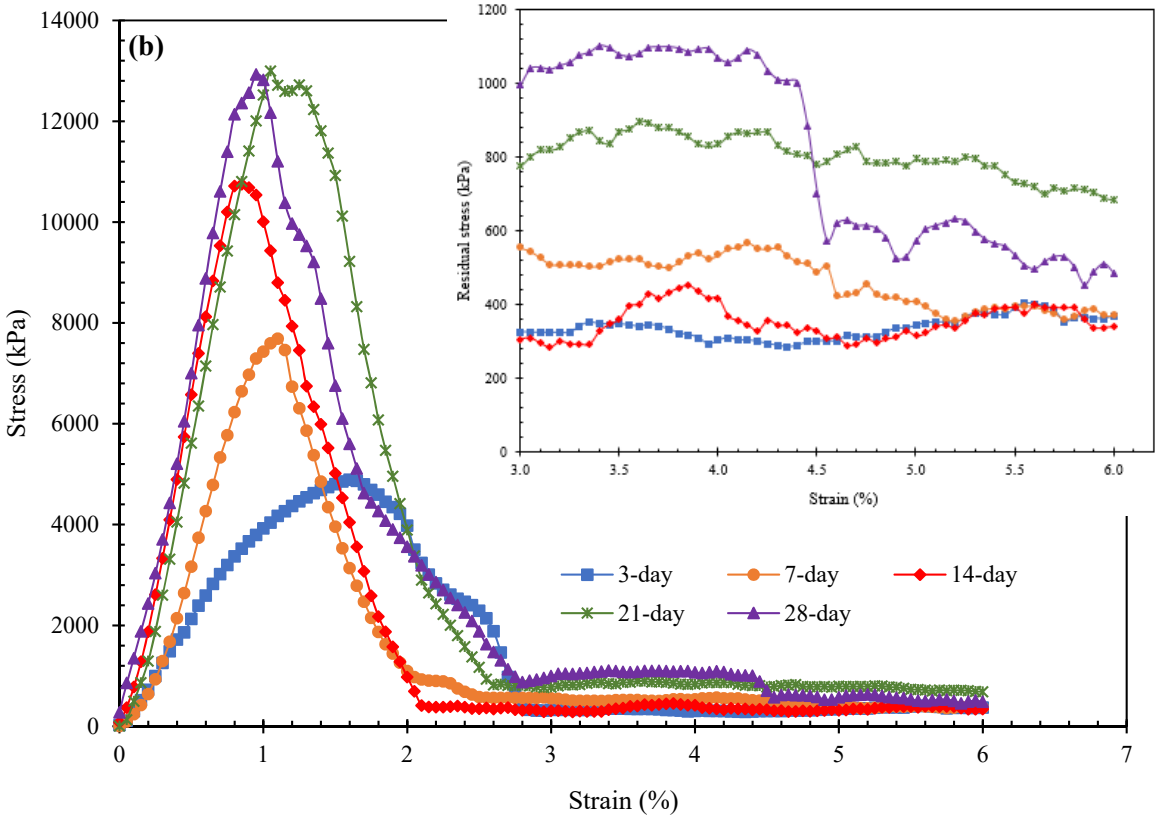
(b)
Stress (kPa)
Strain (%)
Residual stress (kPa)
Strain (%)
3-day
7-day
14-day
21-day
28-day

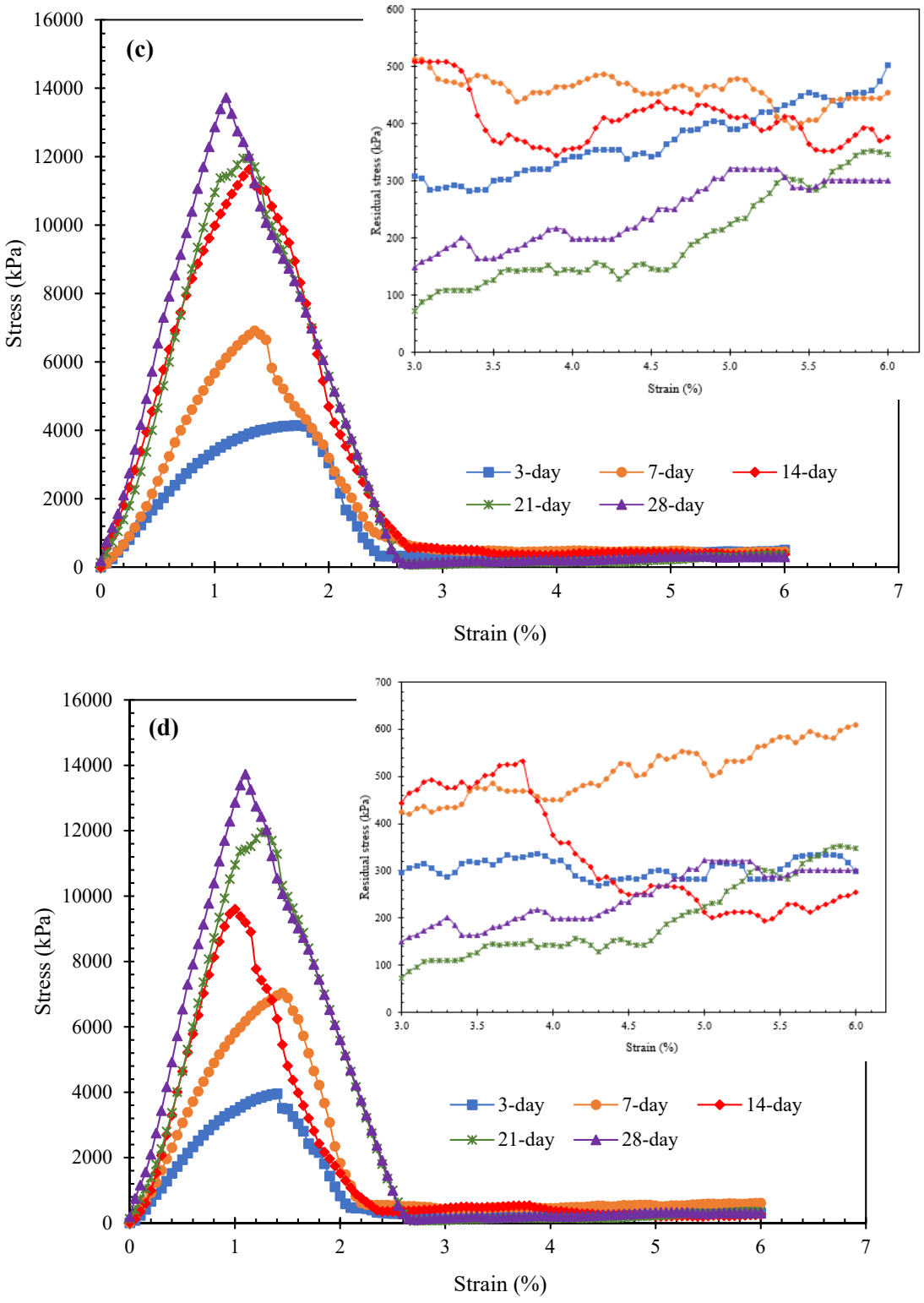

Fig. A7: Unconfined compression stress-strain curves of hybrid cementitious material specimens containing 20 wt.% CKD, 0.3 wt.% CAR and after different time of curing at 35 °C: (a) W/S = 0.55, SP = 1 wt.%; (b) W/S = 0.55, SP = 2 wt.%; (c) W/S = 0.60, SP = 1 wt.%; and (d) W/S = 0.60, SP = 2 wt.%.

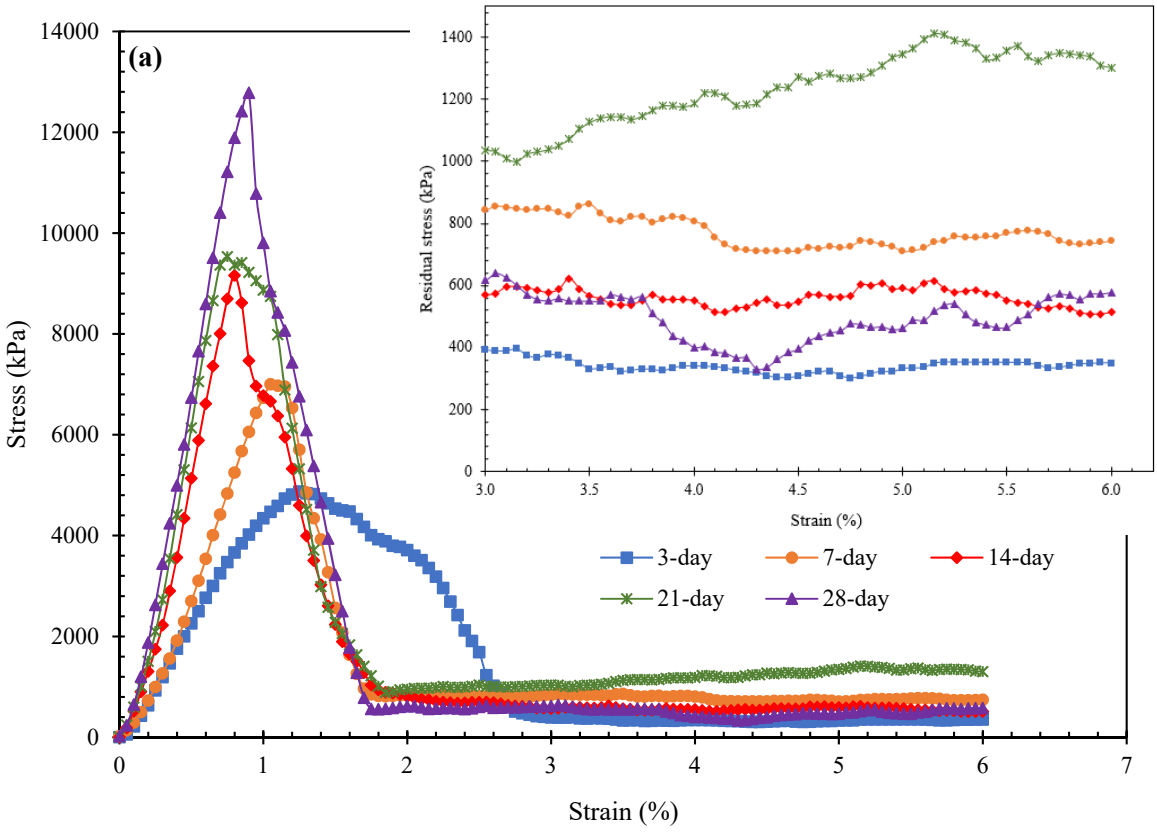
(a)
Stress (kPa)
Strain (%)
Residual stress (kPa)
Strain (%)
3-day
7-day
14-day
21-day
28-day

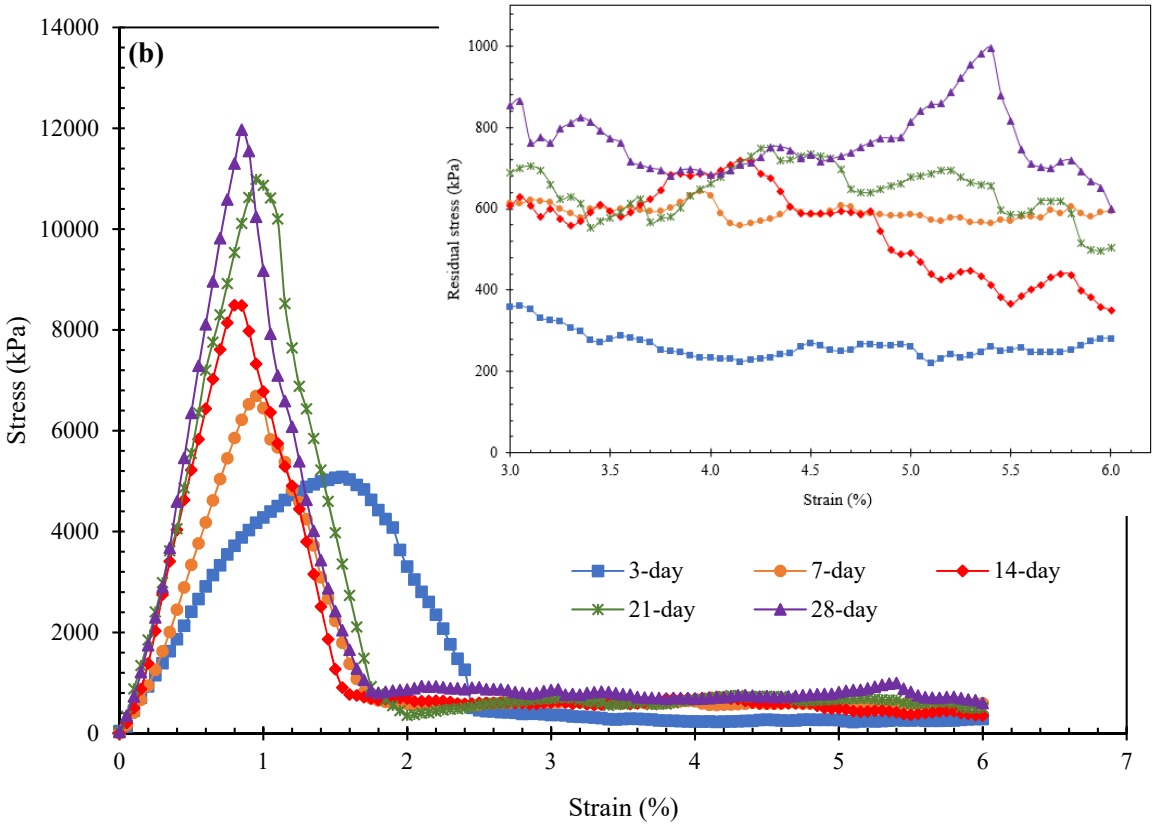
(b)
Stress (kPa)
Strain (%)
Residual stress (kPa)
Strain (%)
3-day
7-day
14-day
21-day
28-day

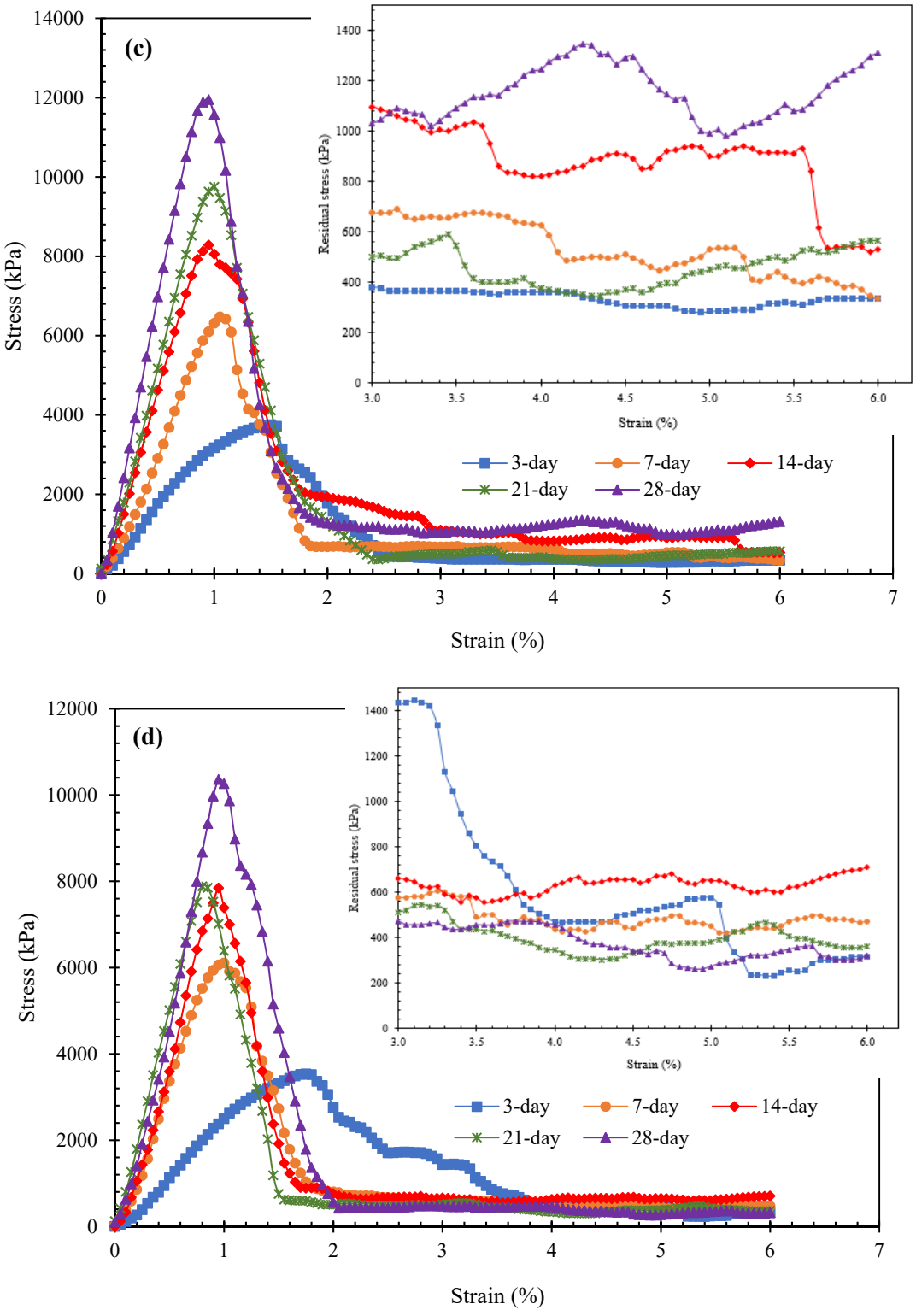

Fig. A8: Unconfined compression stress-strain curves of hybrid cementitious material specimens containing 20 wt.% CKD, 0.3 wt.% GEL and after different time of curing at 35 °C: (a) W/S = 0.55, SP = 1 wt.%; (b) W/S = 0.55, SP = 2 wt.%; (c) W/S = 0.60, SP = 1 wt.%; and (d) W/S = 0.60, SP = 2 wt.%.

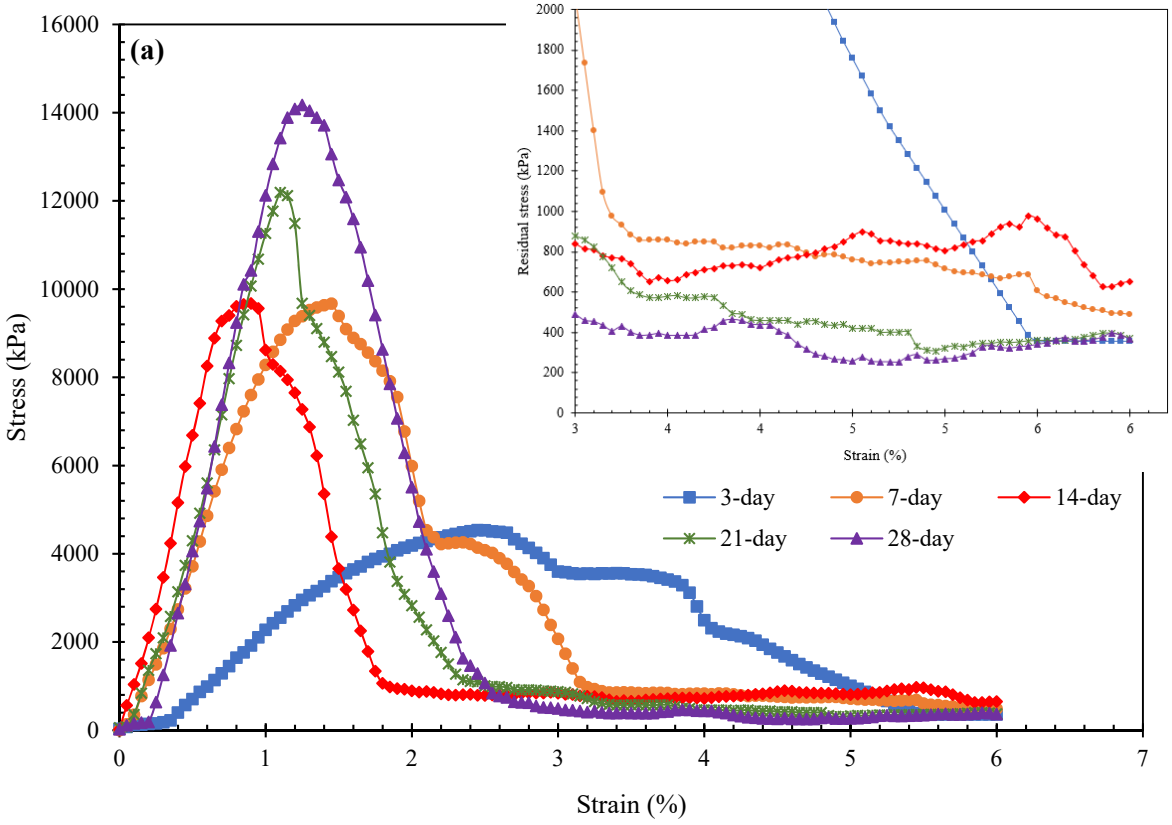
(a)
Stress (kPa)
Strain (%)
Residual stress (kPa)
Strain (%)
3-day
7-day
14-day
21-day
28-day

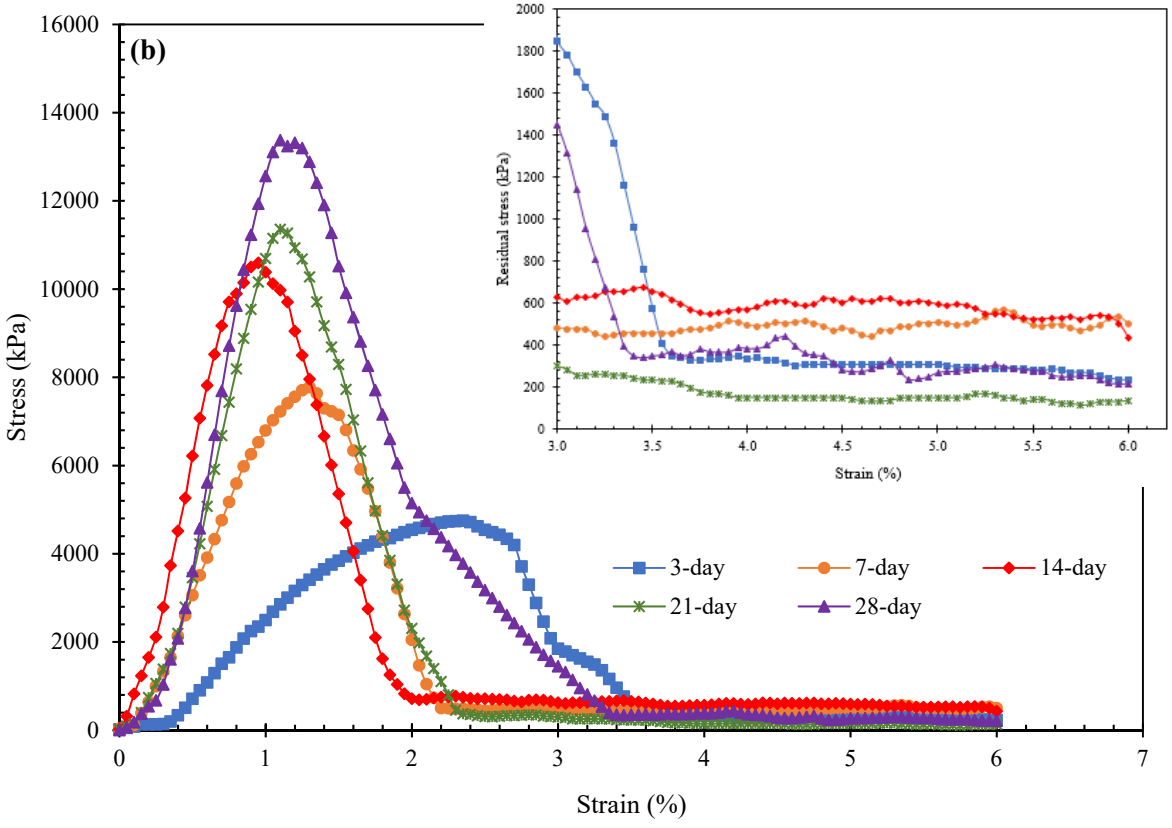
(b)
Stress (kPa)
Strain (%)
Residual stress (kPa)
Strain (%)
3-day
7-day
14-day
21-day
28-day

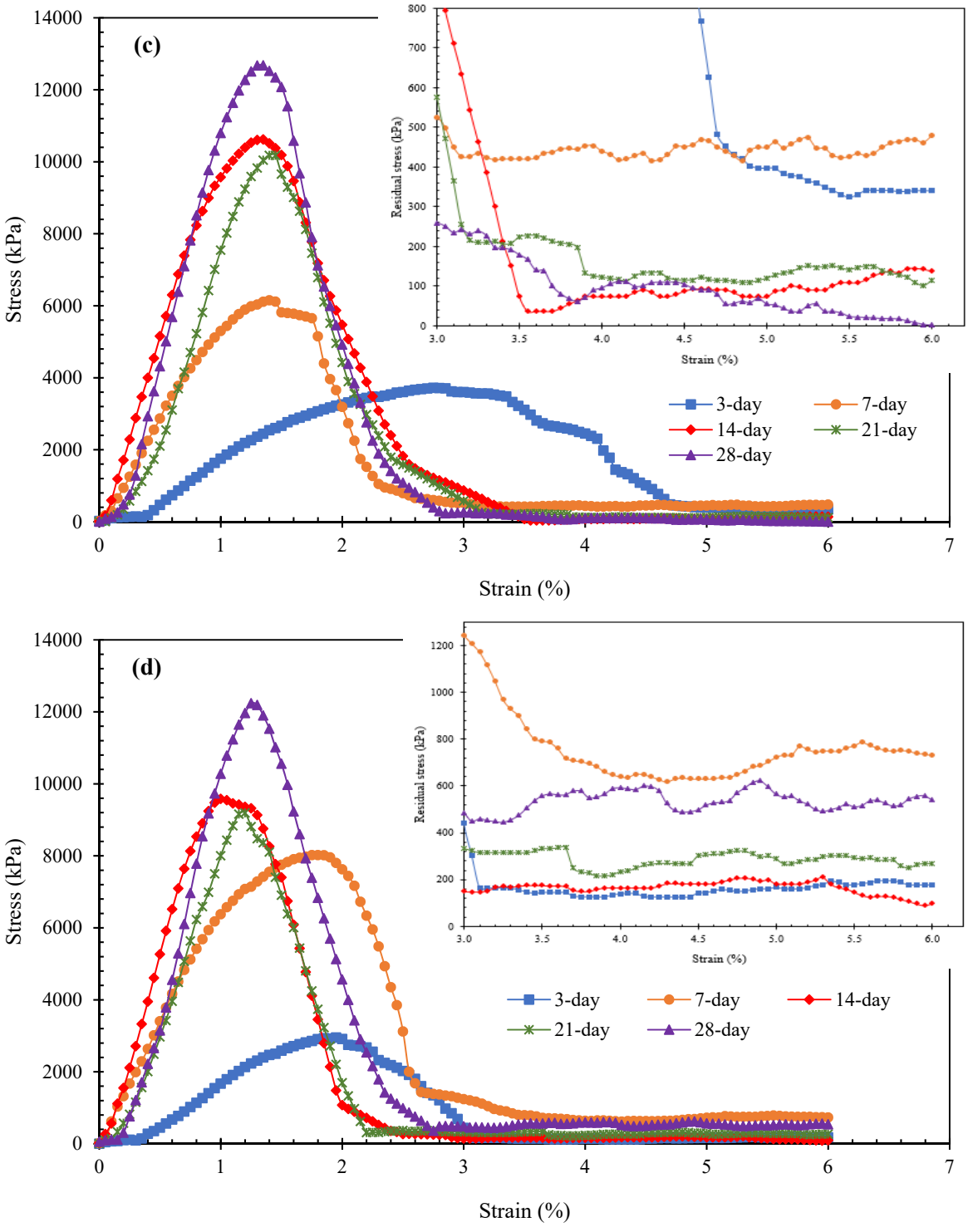

Fig. A9: Unconfined compression stress-strain curves of hybrid cementitious material specimens containing 20 wt.% CKD, 0.5 wt.% CNF and after different time of curing at 35 °C: (a) W/S = 0.55, SP = 1 wt.%; (b) W/S = 0.55, SP = 2 wt.%; (c) W/S = 0.60, SP = 1 wt.%; and (d) W/S = 0.60, SP = 2 wt.%.

8.0 Acknowledgement/Disclaimer

This study was sponsored by the Alpha Foundation for the Improvement of Mine Safety and Health, Inc. (ALPHA FOUNDATION). The views, opinions and recommendations expressed herein are solely those of the authors and do not imply any endorsement by the ALPHA FOUNDATION, its Directors and staff.

9.0 References

Abdollahnejad, Z., Kheradmand, M., & Pacheco-Torgal, F. (2017). Short-term compressive strength of fly ash and waste glass alkali-activated cement-based binder mortars with two biopolymers. *Journal of Materials in Civil Engineering*, *29*(7), 1–18. https://doi.org/10.1061/(ASCE)MT.1943-5533.0001920

Ahmari, S., & Zhang, L. (2013). Utilization of cement kiln dust (CKD) to enhance mine tailings-based geopolymer bricks. *Construction and Building Materials*, 40, 1002-1011.

API (American Petroleum Institute) (1990). API SPEC 10: Specifications for materials and testing for well cements. *American Petroleum Institute*.

Ashton, H. C. (2009). The Incorporation of Nanomaterials into Polymer Media. *In Polymer Nanocomposites Handbook*, 35–58.

ASTM C191. (2013). Standard Test Method for Time of Setting of Hydraulic Cement by Vicat Needle. *ASTM International, West Conshohocken, PA,* 1–8. https://doi.org/10.1520/C0191-13.2

ASTM C39/C39M. (2016). Standard Test Method for Compressive Strength of Cylindrical Concrete Specimens. *ASTM International, West Conshohocken, PA,* 1–7. https://doi.org/ 10.1520/ C0039

ASTM D3967 (2008). Standard Test Method for Splitting Tensile Strength of Intact Rock Core Specimens. *ASTM International, West Conshohocken, PA,* 20–23. https://doi.org/10.1520/ D3967-08.2

ASTM E111-17 (2017). Standard Test Method for Young's Modulus, Tangent Modulus, and Chord Modulus, *ASTM International, West Conshohocken, PA,* 1–7. https://doi.org/10.1520/ E0111-17.

Barczak, T. M., & Tadolini, S. C. (2008). Pumpable roof supports : an evolution in longwall roof support technology. *Transactions of the Society for Mining, Metallurgy, and Exploration*, *324*, 19–31.

Batchler, T. (2017). Analysis of the design and performance characteristics of pumpable roof supports. *International Journal of Mining Science and Technology*, *27*(1), 91–99. https://doi.org/10.1016/j.ijmst.2016.10.003

Bernal, S., De Gutierrez, R., Delvasto, S., & Rodriguez, E. (2010). Performance of an alkali-activated slag concrete reinforced with steel fibers. *Construction and Building Materials*, *24*(2), 208–214. https://doi.org/10.1016/j.conbuildmat.2007.10.027

Bhalerao, N., Wayal, A. S., Patil, P. G., & Bharimalla, A. K. (2015). A Review on Effect of Nano Cellulose on Concrete. *International Journal of Civil and Structural Engineering Research*, *3*(1), 251–254.

Cai, X., Tong, H., Shen, X., Chen, W., Yan, J., & Hu, J. (2009). Preparation and characterization of homogeneous chitosan-polylactic acid/hydroxyapatite nanocomposite for bone tissue engineering and evaluation of its mechanical properties. *Acta Biomaterialia*, *5*(7), 2693–2703. https://doi.org/10.1016/j.actbio.2009.03.005

Chang, I., Im, J., Lee, S. W., & Cho, G. C. (2017). Strength durability of gellan gum biopolymer-

treated Korean sand with cyclic wetting and drying. *Construction and Building Materials*, *143*, 210–221. https://doi.org/10.1016/j.conbuildmat.2017.02.061

Cheng, J., Li, W., & Zhang, P. (2015). A novel backfill material for roof supports in the cut-through entries of longwall mining. *Tehnicki Vjesnik - Technical Gazette*, *22*(1), 201–208. https://doi.org/10.17559/TV-20141130115523

Comrie, D. C., & Kriven, W. M. (2004). Composite cold ceramic geopolymer in a refractory application. *Advances in Ceramics Matrix Composites IX, Proceedings*, *153*, 211–225.

Davidovits, J. (1988). Soft mineralogy and geopolymers. In *1st international conference on Geopolymers* (pp. 19–24). Compiegne, France.

Davidovits, J. (1991). Geopolymers: inorganic polymeric new materials. *Journal of Thermal Analysis*, *37*(8), 1633–1656.

Davidovits, J. (1994). High-Alkali Cements for 21st Century Concretes. *Special Publication*, *144*. https://doi.org/10.14359/4523

Davidovits, J. (2008). *Geopolymer chemistry & application*. F-02100 Saint-Quentin, France: Institute Géopolymèr.

Davidovits, J., Stone, A. M., Chemical, A., News, S., & Re, P. (1989). Waste solidification and disposal method, (19), 12–15.

Deb, P. S., Sarker, P. K., & Barbhuiya, S. (2015). Effects of nano-silica on the strength development of geopolymer cured at room temperature. *Construction and Building Materials*, *101*, 675–683. https://doi.org/10.1016/j.conbuildmat.2015.10.044

Dias, D. P., & Thaumaturgo, C. (2005). Fracture toughness of geopolymeric concretes reinforced with basalt fibers. *Cement and Concrete Composites*, *27*(1), 49–54. https://doi.org/10.1016/j.cemconcomp.2004.02.044

Dimas, D. D., Giannopoulou, I. P., & Panias, D. (2009). Utilization of alumina red mud for synthesis of inorganic polymeric materials. *Mineral Processing and Extractive Metallurgy Review*, *30*(3), 211–239. https://doi.org/10.1080/08827500802498199

Dunlop, J. W. C., & Fratzl, P. (2010). Biological Composites. *Annual Review of Materials Research*, *40*, 1–24. https://doi.org/10.1146/annurev-matsci-070909-104421

Duxson, P., Fernández-Jiménez, A., Provis, J. L., Lukey, G. C., Palomo, A., & Van Deventer, J. S. J. (2007). Geopolymer technology: The current state of the art. *Journal of Materials Science*, *42*(9), 2917–2933. https://doi.org/10.1007/s10853-006-0637-z

E111-17, A. (2017). Standard Test Method for Young's Modulus, Tangent Modulus, and Chord Modulus. *ASTM International*, 1–7. https://doi.org/10.1520/E0111-17

Espinosa, H. D., Rim, J. E., Barthelat, F., & Buehler, M. J. (2009). Merger of structure and material in nacre and bone - Perspectives on de novo biomimetic materials. *Progress in Materials Science*, *54*(8), 1059–1100. https://doi.org/10.1016/j.pmatsci.2009.05.001

Esterhuizen, G., & Berk, I. (2016). Application of the strength reduction method in coal mine roof support design. In *ISMS symposium* (pp. 659–665).

Garcia-lodeiro, I., Palomo, A., Fernández-jiménez, A., & Macphee, D. E. (2011). Cement and Concrete Research Compatibility studies between N-A-S-H and C-A-S-H gels . Study in the

ternary, *41*, 923–931. https://doi.org/10.1016/j.cemconres.2011.05.006

Giancaspro, J., Balaguru, P. N., & Lyon, R. E. (2003). Recent advances in inorganic polymer composites. *The Thirteenth International Offshore and Polar Engineering Conference. International Society of Offshore and Polar Engineers.*

Gong, W., Xu, H., Lutze, W., & Pegg, Ii. L. (2019). Patent Application Publication (10) Pub. No. US 2019 / 0059733 A1 (43). United States.

Granizo, M. L., Blanco-Varela, M. T., & Martínez-Ramírez, S. (2007). Alkali activation of metakaolins: Parameters affecting mechanical, structural and microstructural properties. *Journal of Materials Science*, *42*(9), 2934–2943. https://doi.org/10.1007/s10853-006-0565-y

Grobert, N. (2007). Carbon nanotubes - becoming clean. *Materials Today*, *10*(1–2), 28–35. https://doi.org/10.1016/S1369-7021(06)71789-8

Hammell, J., Balaguru, P., Lyon, R. E., & Davidovits, J. (1999). Influence of reinforcement types on the flexural properties of geopolymer composites. *Geopolymere 99*.

Hardjito, D., & Wallah, S. (2004). On the development of fly ash-based geopolymer concrete. *ACI Materials Jounal*, *101*(6), 467–472. Retrieved from http://www.concrete.org/Publications/InternationalConcreteAbstractsPortal.aspx?m=details&i=13485

Hird, D. (2011). Pumpable cementitious grout system for use in the production of underground roof support systems and other load bearing structures. Retrieved from https://patents.google.com/patent/US20110174194A1/en

Huseien, G. F., Mirza, J., Ismail, M., & Hussin, M. W. (2016). Influence of different curing temperatures and alkali activators on properties of GBFS geopolymer mortars containing fly ash and palm-oil fuel ash. *Construction and Building Materials*, *125*, 1229–1240. https://doi.org/10.1016/j.conbuildmat.2016.08.153

Jackson, A. P., Vincent, J. F. V., Briggs, D., Crick, R. A., Davies, S. F., Hearn, M. J., & Turner, R. M. (1986). Application of surface analytical techniques to the study of fracture surfaces of mother-of-pearl. *Journal of Materials Science Letters*, *5*(10), 975–978. https://doi.org/10.1007/BF01730253

Jackson, A. P., Vincent, J. F. V., & Turner, R. M. (1990). Comparison of nacre with other ceramic composites. *Journal of Materials Science*, *25*(7), 3173–3178. https://doi.org/10.1007/BF00587670

Jennmar. (2013). J-CRIB Pumpable Crib. *Jennmar Co.* Retrieved from https://www.jennmar.com/

Jiao, L., Su, M., Chen, L., Wang, Y., Zhu, H., & Dai, H. (2016). Natural cellulose nanofibers as sustainable enhancers in construction cement. *PLoS ONE*, *11*(12), 1–13. https://doi.org/10.1371/journal.pone.0168422

Kumar, S., Kumar, R., & Mehrotra, S. P. (2010). Influence of granulated blast furnace slag on the reaction, structure and properties of fly ash based geopolymer. *Journal of Materials Science*, *45*(3), 607–615. https://doi.org/10.1007/s10853-009-3934-5

Kusbiantoro, A., Ibrahim, M. S., Muthusamy, K., & Alias, A. (2013). Development of Sucrose and Citric Acid as the Natural based Admixture for Fly Ash based Geopolymer. *Procedia Environmental Sciences*. https://doi.org/10.1016/j.proenv.2013.02.075

Lee, N. K., & Lee, H. K. (2013). Setting and mechanical properties of alkali-activated fly ash/slag concrete manufactured at room temperature. *Construction and Building Materials*, *47*, 1201–1209. https://doi.org/10.1016/j.conbuildmat.2013.05.107

Li, W., & Xu, J. (2009). Mechanical properties of basalt fiber reinforced geopolymeric concrete under impact loading. *Materials Science and Engineering A*, *505*(1–2), 178–186. https://doi.org/10.1016/j.msea.2008.11.063

Li, Z., Chen, R., & Zhang, L. (2013). Utilization of chitosan biopolymer to enhance fly ash-based geopolymer. *Journal of Materials Science*, *48*(22), 7986–7993. https://doi.org/10.1007/s10853-013-7610-4

Li, Z., & Zhang, L. (2016). Fly ash-based geopolymer with kappa-carrageenan biopolymer. *Biopolymers and Biotech Admixtures for Eco-Efficient Construction Materials*, 173–192. https://doi.org/10.1016/B978-0-08-100214-8.00009-9

Lin, T., Jia, D., He, P., Wang, M., & Liang, D. (2008). Effects of fiber length on mechanical properties and fracture behavior of short carbon fiber reinforced geopolymer matrix composites. *Materials Science and Engineering A*, *497*(1–2), 181–185. https://doi.org/10.1016/j.msea.2008.06.040

Lin, T., Jia, D., Wang, M., He, P., & Liang, D. (2009). Effects of fibre content on mechanical properties and fracture behaviour of short carbon fibre reinforced geopolymer matrix composites. *Bulletin of Materials Science*, *32*(1), 77–81. https://doi.org/10.1007/s12034-009-0011-2

Loong, C. K., Rey, C., Kuhn, L. T., Combes, C., Wu, Y., Chen, S. H., & Glimcher, M. J. (2000). Evidence of hydroxyl-ion deficiency in bone apatites: An inelastic neutron-scattering study. *Bone*, *26*(6), 599–602. https://doi.org/10.1016/S8756-3282(00)00273-8

MacKenzie, K. J. D., & Bolton, M. J. (2009). Electrical and mechanical properties of aluminosilicate inorganic polymer composites with carbon nanotubes. *Journal of Materials Science*, *44*(11), 2851–2857. https://doi.org/10.1007/s10853-009-3377-z

Majidi, B. (2009). Geopolymer technology, from fundamentals to advanced applications: a review. *Materials Technology*. https://doi.org/10.1179/175355509X449355

Mann, S. (2001). *Biomineralization: Principles and Concepts in Bioinorganic Materials Chemistry*. Oxford University Press.

Mark, C., & Barczak, T. M. (2000). Proceedings: New Technology For Coal Mine Roof Support. In *New Technology for Coal Mine Roof Support* (pp. 23–42). Cincinnati, OH: U.S. Department of Health and Human Services, Public Health Service, Centers for Disease Control and Prevention, National Institute for Occupational Safety and Health, DHHS (NIOSH).

Mehta, A., & Siddique, R. (2017). Properties of low-calcium fly ash based geopolymer concrete incorporating OPC as partial replacement of fly ash. *Construction and Building Materials*, *150*, 792–807. https://doi.org/10.1016/j.conbuildmat.2017.06.067

Metaxa, Z. S., Konsta-Gdoutos, M. S., & Shah, S. P. (2010). Carbon Nanofiber-Reinforced cement-based materials. *Transportation Research Record*, (2142), 114–118. https://doi.org/10.3141/2142-17

Meyers, M. A., Lin, A. Y. M., Chen, P. Y., & Muyco, J. (2008). Mechanical strength of abalone

nacre: Role of the soft organic layer. *Journal of the Mechanical Behavior of Biomedical Materials*, *1*(1), 76–85. https://doi.org/10.1016/j.jmbbm.2007.03.001

Milligan, A. J., & Morel, F. M. M. (2002). A proton buffering role for silica in diatoms. *Science*, *297*(5588), 1848–1850. https://doi.org/10.1126/science.1074958

Moniruzzaman, M., & Winey, K. I. (2006). Polymer nanocomposites containing carbon nanotubes. *Macromolecules*, *39*(16), 5194–5205. https://doi.org/10.1021/ma060733p

Murugan, R., & Ramakrishna, S. (2004). Bioresorbable composite bone paste using polysaccharide based nano hydroxyapatite. *Biomaterials*, *25*(17), 3829–3835. https://doi.org/10.1016/j.biomaterials.2003.10.016

Nath, P., & Sarker, P. K. (2014). Effect of GGBFS on setting, workability and early strength properties of fly ash geopolymer concrete cured in ambient condition. *Construction and Building Materials*, *66*, 163–171. https://doi.org/10.1016/j.conbuildmat.2014.05.080

Nath, P., & Sarker, P. K. (2015). Use of OPC to improve setting and early strength properties of low calcium fly ash geopolymer concrete cured at room temperature. *Cement and Concrete Composites*, *55*, 205–214. https://doi.org/10.1016/j.cemconcomp.2014.08.008

Nath, P., & Sarker, P. K. (2017). Flexural strength and elastic modulus of ambient-cured blended low-calcium fly ash geopolymer concrete. *Construction and Building Materials*, *130*, 22–31. https://doi.org/10.1016/j.conbuildmat.2016.11.034

Nath, P., Sarker, P. K., & Rangan, V. B. (2015). Early age properties of low-calcium fly ash geopolymer concrete suitable for ambient curing. *Procedia Engineering*, *125*, 601–607. https://doi.org/10.1016/j.proeng.2015.11.077

Nematollahi, B., & Sanjayan, J. (2014). Effect of different superplasticizers and activator combinations on workability and strength of fly ash based geopolymer. *Materials and Design*, *57*, 667–672. https://doi.org/10.1016/j.matdes.2014.01.064

NIOSH. (2017). Mining topic: Roof Support. Retrieved from https://www.cdc.gov/niosh/mining/topics/RoofSupport.html

NTI. (2019). Pumpable cribs. *NTI Mining and Tunneling Co.* Retrieved from http://ntimining.com/en/?page_id=111

Ortiz, C., & Boyce, M. C. (2015). Bioinspired structural materials. *Nature Materials*, *14*(1), 23–36. https://doi.org/10.1038/nmat4089

Pangdaeng, S., Phoo-ngernkham, T., Sata, V., & Chindaprasirt, P. (2014). Influence of curing conditions on properties of high calcium fly ash geopolymer containing Portland cement as additive. *Materials and Design*, *53*, 269–274. https://doi.org/10.1016/j.matdes.2013.07.018

Peng, S. S. (2000). Cutting through open entries require proper support. *Coal Age*, *6*, 37–40.

Pernica, D., Reis, P. N. B., Ferreira, J. A. M., & Louda, P. (2010). Effect of test conditions on the bending strength of a geopolymer- reinforced composite. *Journal of Materials Science*, *45*(3), 744–749. https://doi.org/10.1007/s10853-009-3994-6

Pokroy, B., Demensky, V., & Zolotoyabko, E. (2009). Nacre in mollusk shells as a Multi layered structure with strain gradient. *Advanced Functional Materials*, *19*(7), 1054–1059. https://doi.org/10.1002/adfm.200801201

Porcherie, O., Pershikova, E., Rimmele, G., Achtal, H., & Boubeguira, Y. (2011). Pumpable geopolymers comprising a mixing and disersing agent. https://doi.org/10.1016/j.(73)

Rangan, B. V. (2008). Fly Ash-Based Geopolymer Concrete. *Proceedings of the International Workshop on Geopolymer Cement and Concrete, December*, *2008*, 68–106. https://doi.org/10.1007/s10853-006-0523-8

Ritchie, R. O., Buehler, M. J., & Hansma, P. (2009). Built primarily from collagen molecules, mineral, (June). Retrieved from www.physicstoday.org

Rusu, V. M., Ng, C. H., Wilke, M., Tiersch, B., Fratzl, P., & Peter, M. G. (2005). Size-controlled hydroxyapatite nanoparticles as self-organized organic-inorganic composite materials. *Biomaterials*, *26*(26), 5414–5426. https://doi.org/10.1016/j.biomaterials.2005.01.051

Shadnia, R., & Zhang, L. (2017). Experimental Study of Geopolymer Synthesized with Class F Fly Ash and Low-Calcium Slag. *Journal of Materials in Civil Engineering*, *29*(10), 04017195. https://doi.org/10.1061/(ASCE)MT.1943-5533.0002065

Shen, X., Tong, H., Jiang, T., Zhu, Z., Wan, P., & Hu, J. (2007). Homogeneous chitosan/carbonate apatite/citric acid nanocomposites prepared through a novel in situ precipitation method. *Composites Science and Technology*, *67*(11–12), 2238–2245. https://doi.org/10.1016/j.compscitech.2007.01.034

Sumper, M. (2002). A phase separation model for the nanopatterning of diatom biosilica. *Science*, *295*(5564), 2430–2433. https://doi.org/10.1126/science.1070026

Sun, P., & Wu, H. C. (2008). Transition from brittle to ductile behavior of fly ash using PVA fibers. *Cement and Concrete Composites*, *30*(1), 29–36. https://doi.org/10.1016/j.cemconcomp.2007.05.008

Sun, X., Wu, Q., Zhang, J., Qing, Y., Wu, Y., & Lee, S. (2017). Rheology, curing temperature and mechanical performance of oil well cement: Combined effect of cellulose nanofibers and graphene nano-platelets. *Materials and Design*, *114*, 92–101. https://doi.org/10.1016/j.matdes.2016.10.050

Tang, Z., Kotov, N. A., Magonov, S., & Ozturk, B. (2003). Nanostructured artificial nacre. *Nature Materials*, *2*(6), 413–418. https://doi.org/10.1038/nmat906

Xie, X. L., Mai, Y. W., and Zhou, X. P. (2005). "Dispersion and alignment of carbon nanotubes in polymer matrix: A review." *Material Science and Engineering*, 49, 89-112.

Yang, Y. K., Mao, L. B., Zhou, X. P., Xie, X. L., & Mai, Y. W. (2005). Dispersion and alignment of carbon nanotubes in polymer matrix: a review - (II) alignment of carbon nanotubes in polymer matrix. *Gaofenzi Cailiao Kexue Yu Gongcheng/Polymeric Materials Science and Engineering*, *21*(6), 50–54. https://doi.org/10.1016/j.mser.2005.04.002

Yazdanbakhsh, A., Grasley, Z., Tyson, B., & Abu Al-Rub, R. K. (2010). Distribution of carbon nanofibers and nanotubes in cementitious composites. *Transportation Research Record*, 2142, 89–95. https://doi.org/10.3141/2142-13

Yu, S.-H., & Chen, S. (2011). Biomineralization: Self-Assembly Processes. *Encyclopedia of Inorganic and Bioinorganic Chemistry*, 1–24. https://doi.org/10.1002/9781119951438.eibc0318

Yunsheng, Z., Wei, S., & Zongjin, L. (2006). Impact behavior and microstructural characteristics of PVA fiber reinforced fly ash-geopolymer boards prepared by extrusion technique. *Journal of Materials Science*, *41*(10), 2787–2794. https://doi.org/10.1007/s10853-006-6293-5

Yunsheng, Z., Wei, S., Zongjin, L., Xiangming, Z., Eddie, & Chungkong, C. (2008). Impact properties of geopolymer based extrudates incorporated with fly ash and PVA short fiber. *Construction and Building Materials*, *22*(3), 370–383. https://doi.org/10.1016/j.conbuildmat.2006.08.006

Zhang, L., Ahmari, S., & Zhang, J. (2011). Synthesis and characterization of fly ash modified mine tailings-based geopolymers. *Construction and Building Materials*, *25*(9), 3773–3781. https://doi.org/10.1016/j.conbuildmat.2011.04.005

Zhang, L., Li, Y. B., Yang, A. P., Peng, X. L., Wang, X. J., & Zhang, X. (2005). Preparation and in vitro investigation of chitosan/nanohydroxyapatpite composite used as bone substitute materials. *Journal of Materials Science: Materials in Medicine*, *16*, 213–219.

Zhang, Y., Sun, W., and Li, Z. (2006). "Impact behavior and microstructural characteristics of PVA fiber reinforced fly ash-geopolymer boards prepared by extrusion technique." *J. Mater. Sci.*, 41, 2787-2794.

Zhang, Y., Sun, W., Li, Z., Zhou, X., and Chau, C. (2008). "Impact properties of geopolymer based extrudates incorporated with fly ash and PVA short fiber." *Construction and Building Materials*, 22, 370-383.

Zhao, Q., Nair, B., Rahimian, T., & Balaguru, P. (2007). Novel geopolymer based composites with enhanced ductility. *Journal of Materials Science*, *42*(9), 3131–3137. https://doi.org/10.1007/s10853-006-0527-4